# PREPARATION, CHARACTERISATION AND EVALUATION OF HYDROXYAPATITE-SODIUM ALGINATE NANOCOMPOSITES FOR APPLICATION IN ANTICANCER DRUG DELIVERY

**BY**

**Christian Chinweuba ONOYIMA**

**DEPARTMENT OF CHEMISTRY**

**AHMADU BELLO UNIVERSITY, ZARIA**

**NIGERIA**

**DECEMBER, 2016**

# PREPARATION, CHARACTERISATION AND EVALUATION OF HYDROXYAPATITE-SODIUM ALGINATE NANOCOMPOSITES FOR APPLICATION IN ANTICANCER DRUG DELIVERY

**BY**

**Christian Chinweuba ONOYIMA**

**P13SCCH9005**

**A THESIS SUBMITTED TO THE SCHOOL OF POSTGRADUATE STUDIES,**

**AHMDU BELLO UNIVERSITY, ZARIA**

**IN PARTIAL FULFILMENT OF THE REQUIREMENT FOR THE AWARD**

**OF A**

**Ph. D. DEGREE IN ANALYTICAL CHEMISTRY**

**DEPARTMENT OF CHEMISTRY,**

**FACULTY OF PHYSICAL SCIENCE,**

**AHMADU BELLO UNIVERSITY, ZARIA**

**NIGERIA**

**DECEMBER, 2016**

## DECLARATION

I declare that the work in this Thesis entitled **"Preparation, Characterizations and Evaluation of Hydroxyapatite-Sodium alginate Nanocomposites for Application in Anticancer Drug Delivery"** has been carried out by me in the Department of Chemistry. The information derived from the literature has been duly acknowledged in the text and a list of reference provided. No part of this thesis was previously presented for another degree or diploma at this or any other institution.

| **Christian Chinweuba ONOYIMA** | _____ | _____ |
|---|---|---|
| Name of Student | Signature | Date |

## CERTIFICATION

This thesis entitled **"PREPARATION, CHARACTERIZATION AND EVALUATION OF HYDROXYAPATITE-SODIUM ALGINATE NANOCOMPOSITES FOR APPLICATION IN ANTICANCER DRUG DELIVERY"** by Christian Chinweuba ONOYIMA meets the regulations governing the award of the degree of PhD in Analytical Chemistry of the Ahmadu Bello University, and is approved for its contribution to knowledge and literary presentation.

**Prof. E. B. Agbaji** _____ _____
Chairman, Supervisory Committee (Signature) Date

**Prof. V. O. Ajibola** _____ _____
Member, Supervisory Committee (Signature) Date

**Dr. F. G. Okibe** _____ _____
Member, Supervisory Committee (Signature) Date

**Prof. S. O. Idris** _____ _____
Member, Supervisory Committee (Signature) Date

**Prof. A. O. Oyewale** _____ _____
Head of Department (Signature) Date

**Prof. K. Bala** _____ _____
Dean, School of Postgraduate Studies (Signature) Date

## ACKNOWLEDGEMENT

The completion of this thesis would not have been possible without the input, guidance and sacrifice of many. I express my sincere gratitude to my supervisors: Prof. E.B Agbaji, Prof. V.O Ajibola, Prof. S.O Idris and Dr. F.G Okibe for their patience, dedication and guidance throughout this research. They are the reason for the success of this research.

My gratitude also goes to Mr. C. Ochigbo of Analytical Chemistry Laboratory, A.B.U, and all the staff of Multi-User Science Laboratory A.B.U. They were always willing to help and they made laboratory facilities readily available for this research. Mr. Umar U. Usman in Pharmaceutical Chemistry Lab., and Mr. S Isah in Chemical Engineering Lab., also made invaluable contributions to the success of this research. Thank you all.

I am also grateful to Dr. Umar M. Sani, my H.O.D at the Nigeria Police Academy, for his understanding; and to all my colleagues at the Nigeria Police Academy, I say thank you for your support.

To my brother and friend Emeka Onoyima: Thank you for always supporting me, for providing a shoulder when I needed one, and for always allowing me to share both my frustrations and excitements with you. My special thanks goes to special people in my life, whose prayers, love and support saw me through this work: my parents Chief Patrick Onoyima, and Mrs. Appolonia Onoyima, my brother Tony Nnamdi, and my sisters, Priscilla, Esther and Mabel.

Finally, I want to heartily thank my amiable and loving wife Obim, and my little daughter, Chinecherem, for their unwavering support and for bringing love and happiness to my life. Thanks for being my best friend and for bringing out the best in me – I love you.

## ABSTRACT

Chemotherapy is one of the leading means of treating cancer. However, the side effects and complications arising from the dose-dependent toxicity of anticancer drugs are often as severe as the disease itself. This research was aimed at preparation and characterization of nanocomposites from hydroxyapatite (HA) and sodium alginate (SA), and evaluation of their applications in controlled delivery of doxorubicin (DOX) and methotrexate (MTX). *In situ* preparation of hydroxyapatite-sodium alginate (HASA) nanocomposite was carried out by the wet precipitation methods. The prepared HA and the nanocomposite were characterized by Fourier Transform Infrared spectroscopy (FTIR), Scanning Electron Microscopy (SEM), X-Ray Fluorescence (XRF) and X-Ray Diffraction (XRD) analyses. Drug loading was carried out at neutral pH, while *in vitro* drug release study was carried out in synthetic body fluid (SBF) at pH 7.4 and 37$^{o}$C. Four different loading methods were investigated. Method 1 involved adsorbing the drug in already prepared nanocomposites. In method 2, the dried HA was cross-linked with SA in the drug solution using calcium chloride solution; in method 3 the hydroxyapatite was first incubated in the drug solution before the cross-linking stage; while in method 4 the freshly prepared hydroxyapatite was cross-linked with sodium alginate in the drug solution. The effect of pH of the release medium on release profile was studied using pH 3.0, pH 5.0 and pH 7.4; and drug combination study was also carried out. FTIR study showed peaks that confirmed the formation of HA as well as the formation of the composite. Image analysis revealed that the HA and the nanocomposites were of nanometre size (24.67 nm – 997.09 nm) with irregular morphologies as shown by the circularity (0.119 – 0.988) and aspect ratio (0.149 – 1). The particle size decreased with increase in SA composition from 359.46 nm for HASA-1%wt to 109.98 nm for HASA-50%wt. A similar trend was observed for crystallite size (28.39 nm – 9.47 nm) and degree of crystallinity (49.29% - 1.82%), while circularity and aspect ratio did not show any noticeable change with SA addition. XRD analysis showed the apatite phase to be composed of pure HA and carbonate-HA. Both phases were responsible for the major peaks at $2\theta = 25.88^{0}$ (d-value = 3.4394 Å), $31.77^{0}$ (d-value = 2.8144 Å), and $32.15^{0}$ (d-value = 2.7818 Å), which were assigned Miller indices of (002), (121), and (112) planes, respectively. These planes were also present in all the HASA samples. There was no notable effect on the peak positions with the addition of SA. The result of drug loading study showed that the nanocomposites have high loading efficiency for DOX, which increased with increase in SA composition reaching a

maximum value of 92.03% for HASA-50%wt, while for MTX the loading efficiency was relatively low and decreased with increase in SA composition with the highest loading efficiency of 35.24% for pure hydroxyapatite. There was sustained release of DOX by the nanocomposites with SA composition of 5%wt and above for about 57 hours, while MTX showed short release time for all the formulations with maximum release time of 5 hours for HASA-5%wt. Except for HA and HASA-1%wt, the DOX release followed first order release kinetics, with Fickian diffusion as the predominant release mechanism. Nanocomposite prepared in aqueous medium had higher loading efficiency (83.69%) compared with those prepared in organic solvents (52.46%, 47.50%, and 46.50%). The release profiles also showed that nanocomposites from aqueous medium had least burst release effect and more sustained release. The release kinetics and mechanism however, did not depend on the synthetic medium. DOX was loaded well (above 80% loading efficiency) by all the four loading methods studied, while for MTX, method 2 and 4 had better loading efficiency (39.98% and 37.10% respectively) than method 1 and 3 (10.39% and 15.21% respectively). Release study for DOX, indicated that the adsorption method had faster release rate than other methods; while for MTX, only method 4 sustained the release of the drug for about 9 hours, while other methods had high burst release effects. DOX release rate was initially faster at acidic conditions than at physiologic condition, but became slower at later release times. From the drug combination study, the release profiles for all the combination ratios showed high burst release for MTX with total release time not exceeding five hours. However for DOX, there was sustained release throughout the thirty three hours of the study. In conclusion, HASA nanocomposite was successfully prepared and characterised. Its ability to load and release the drugs depended on the nature of the drug as well as the synthetic medium and the loading method employed. The nanocomposite if prepared under optimal conditions is a potential carrier for effective delivery of DOX.

## TABLE OF CONTENTS

## LIST OF FIGURES

**Pages**

## LIST OF TABLES

## LIST OF APPENDICES

**Pages**

## LIST OF ABBREVIATIONS

A.R - Aspect ratio

AIC - Akaike Information Criteria

COD - Crystallography Open Database

DOX - Doxorubicin

EDX - Energy Dispersive X-ray

EE - Encapsulation efficiency

EPR - Enhanced Permeability and Retention

F.D - Feret diameter

FTIR - Fourier Transform Infrared Spectroscopy

FWHM - Full width at half maximum

HA - Hydroxyapatite

HASA - Hydroxyapatite-sodium alginate

IARC - International Agency for Research on Cancer

ISO - International Standard Organization

LC - Loading capacity

MDR - Multi-drug resistance

MEC - Minimum effective concentration

MSC - Model Selection Criteria

MTC - Minimum toxic concentration

MTD - Maximum tolerated dose

MTX - Methotrexate

NCI - National Cancer Institute

| | | |
|---|---|---|
| PDF | - | Powder Diffraction File |
| P-gp | - | p-glycoprotein |
| PVA | - | Poly vinyl alcohol |
| RES | - | Reticuloendothelial system |
| SA | - | Sodium alginate |
| SBF | - | Synthetic Body Fluid |
| SED | - | Spherical equivalent diameter |
| SEM | - | Scanning Electron Microscopy |
| USP | - | United State Pharmacopeia |
| WDX | - | Wavelength dispersive X-ray |

# CHAPTER ONE

## 1.0 INTRODUCTION

### 1.1 Preamble

In recent times, there has been a surge in research interest in the use of nanoparticles in several areas such as medical applications (Khotimchenko, 2001; D'Ayala *et al*, 2008; Lee and Mooney, 2012); analytics (De Vols *et al*., 2006; Antosiak-Iwariska, *et al*., 2009); cosmetics (Kailasapathy *et al*., 2002; Sugiura *et al*., 2005); optical and electronic applications (Cho *et al*., 2008). This is as a result of the unique properties possessed by nanoparticles such as high surface area to volume ratio which gives them advantages over macro and micro materials. Nanoparticles are particles with size ranging from 1 to 1000 nm (Jung *et al*., 2000). US National Cancer Institute however defined therapeutic nanoparticles as colloidal particles in the size of 1 – 100 nm (Chen, 2010).

Interestingly, one of the major promising areas of application of nanoparticles is in controlled drug delivery. As a drug delivery system, nanoparticles can entrap drugs or biomolecules onto their exterior surfaces. They could show controlled release properties due to the biodegradability, pH, and/or temperature sensibility of the materials; and they can improve the effectiveness of drugs and reduce side effects (Devanand *et al*., 2011).

Marques *et al*. (2014), stated that the most popular drug delivery systems are based on polymers and ceramics and their nanocomposites. Extensive applications of polymers in drug delivery have also been realized because polymers offer unique properties which, so far, have not been attained by any other materials.

Sodium alginate is a naturally occurring, water soluble linear polysaccharide polymer extracted from brown sea weed and is composed of alternating blocks of 1-4 linked α-L-guluronic acid and β-D-mannuronic acid residues (Kato *et al*., 2003). It is widely used for drug delivery and tissue engineering applications due to its many unique properties such as biocompatibility, biodegradability, low toxicity, non-immunogenicity, water solubility, relatively low cost, gelling ability and stabilizing properties (Aggarwal *et al*., 2012). According to Sun and Tan (2013), alginate based microcapsules and scaffolds have shown minimal or negligible cytotoxicity and are histocompatible. The polymer based carriers can protect drugs from degradation and may improve plasma half time to ensure transport and release of drugs.

However, ionically cross-linked alginate hydrogel has limited drug loading efficiency which limits its applications (Pongjanyakul *et al*., 2010; Ruvinov *et al*., 2010**).** Other major disadvantages of alginate beads are their fast disintegration, and their high porosity, which result in burst release. In order to improve drug entrapment efficiency and modulate drug release, water insoluble materials (e.g. hydroxyapatite and clay) can be incorporated to the alginate matrix (Pongjanyakul *et al*., 2010).

Hydroxyapatite (HA) is a calcium phosphate salt. It is the main component of vertebrate hard tissues such as bone and teeth in the form of nanometer-sized needle-like crystals of approximately 5-20 nm width by 60 nm length (Ferraz *et al.,* 2004). In recent years, synthetic nano-HA has been widely used in biomaterials such as drug delivery, in orthopedic as well as dental applications. This is as a result of its excellent useful properties such as biocompatibility, bioactivity and osteo-conductivity. It is also non-toxic, non-inflammatory, and non-immunogenic (Mateus *et al*., 2008). HA/polymer nanocomposites have attracted much attention since such

nanocomposites lead to improved properties (Khaled *et al*., 2014) such as sustained drug delivery (Raj *et al.*, 2013).

Sustained drug delivery involves releasing the drug into the target site over a prolonged period of time. It is characterized by releasing the drug in a controlled fashion to maintain an appropriate therapeutic plasma concentration for a long period of time, while controlled release involves providing the drug only where and when it is needed (Devanand *et al.*, 2011). Conventional form of drug delivery is not target specific and release of drug to the target site is not sustained (Raj *et al*., 2013).

Most drug carriers are associated with the problem of burst releases (Hasan *et al*., 2007). According to Martinho *et al*. (2011), burst releases lead to a significant and unpredictable toxicity for potent drugs and in treatment of chronic diseases. One of such diseases is cancer. Cancer is mainly treated by chemotherapy. The success of chemotherapy depends on the selection of an optimum carrier system. These carriers include nanoparticles, nanotubes, nanorods, dendrimers, liposomes, microspheres and so forth (Kakde *et al*., 2011). The aim of an ideal cancer chemotherapy is to deliver the correct amount of drug at controlled rate for sufficiently long time (sustained release) to the site of action (tumour cells) while minimizing contact with normal cells.

In order to endow nanosystems with long circulation properties, new technologies aimed at the surface modification of their physicochemical features have been developed. In particular, stealth nanocarriers can be obtained by polymeric coating (Salmaso *et al*., 2013). It is now recognised that long circulating nanocarriers, "stealth" systems, can be obtained by surface coating with hydrophilic polymers that prevent the opsonisation process (Moghimi *et al*., 2001; Yan *et al*.,

2005). Stealth nanocarriers are invisible to the biological system involved in clearance of particles from the bloodstream, namely the reticuloendothelial systems (RES) and Kupffer cells. Conventional chemotherapy with anticancer drugs has no tumour selectivity and is randomly distributed in the body; resulting in severe side effects associated with anticancer drugs with low therapeutic index (Kakde *et al*., 2011). Researchers have tried to develop therapeutic agent with tumour specific antibody or ligand. However, Matsumure and Maeda, (1986), reported that macromolecular drug delivery system with prolonged blood circulation can accumulate by passive retention mechanism in tumours even in the absence of targeting ligands. This is referred to as the Enhanced Permeability and Retention Effect (EPR effect). Due to the leaky vasculature and low lymphatic drainage, solid tumours present erratic fluid molecular transport dynamics. These features can yield specific accumulation of colloidal anticancer drug delivery systems into the tumour tissues by the EPR effect. The pore sizes in solid tumour vasculature vary from 100 nm to 760 nm, which is much larger than that of the normal tissue where the gaps are usually less than 6 nm (Drummond *et al*., 1999).

Nanocomposite is a composition having dispersed material that has one or more dimensions, such as length, width, and thickness in the nanometre size range (Roul *et al*., 2013). The final properties of the nanocomposite are very often not a simple addition of the properties of the independent components, but a unique result from synergistic effect (Hood *et al*., 2014).

It has been shown that the drug loading efficiency and controlled release behaviour can be enhanced because of the synergistic effect between biopolymer and inorganic materials (Devanand *et al*., 2011). Venkatesan *et al*. (2011), carried out a study on chitosan modified HA nanocomposite loaded with celecoxib. The anticancer nanocomposite showed high entrapment efficiency and sustained release profile. HA is a good biocompatible material, but when used as a

carrier in pure form, the impregnated drug can elute only for a short period (Krisanapiboon *et al*., 2006). *In vitro* drug release study by Raj *et al*., (2013) showed that normal HA showed a burst release in the initial stage. However, coating of HA by polyvinyl alcohol (PVA) showed sustained release of about 70% of the drug in 7 days 12 hours. Addition of cloisite nanoparticles to poly (ethylene-co-vinyl acetate) resulted in slower release of dexamethasone (Cypes *et al*., 2003), while modification of SA with hydrophobic poly (butyl methacrylate) led to the prolonged release of the model drug as compared with unmodified alginate gels (Yao *et al*., 2010). By controlling the release kinetics of drugs, one can not only optimize the therapeutic effects of the drugs, but also influence their biological activity (Jana *et al*., 2013).

**1.2 Statement of the Problem**

According to Martinho *et al*. (2011), sustained drug delivery is most useful in treatment of chronic diseases such as cancers. Globally, cancer remains the second most common cause of death (only exceeded by heart diseases) despite the advances in prevention, early detection and protocols of treatment (Marques *et al*., 2014). In 2012, the International Agency for Research on Cancer (IARC) gave an estimated 14.1 million new cancer cases and 8.2 million cancer related deaths, compared with 12.7 million and 7.6 million respectively in 2008 (Ferlay *et al*., 2013). A report by World Health Organization (WHO) has shown that cancer related mortality is still on the increase globally including in Nigeria. Between August 2014 and 2016, 3.4 million people have died from cancer globally out of which 36, 000 are from Nigeria alone.

Although cancer treatment is mainly based on surgery, radiotherapy and chemotherapy, chemotherapy is one of the most important treatments currently available among the various approaches. The present status of chemotherapy is far from being satisfactory. Its efficacy is

limited and patients suffer from serious side effects, some of which are life-threatening (Marques *et al*., 2014).

Methotrexate (4-amino-10-methylfolic acid) is a hydrophilic anticancer drug widely used for treatment of a number of diseases such as leukaemia, lymphomas, osteosarcoma, and rheumatoid arthritis (Nerves *et al*, 2009). Despite its importance, its use is limited by dose-dependent toxicity ranging from malaise, asthenia, to gastrointestinal and hepatic toxicity, and pancytopenia which can be fatal (Khan *et al*., 2010). MTX efficacy is also limited by its short plasma half-life (Yousefi *et al*., 2010).

Doxorubicin (DOX), on the other hand, is commonly used in the treatment of a number of diverse malignant tumours like acute leukaemia, non-Hodgkin's and Hodgkin's lymphoma and several solid tumours. However, the side effects of dose – dependent cardiotoxicity, myelosuppression as well as large distribution volume and low life time represent the limitations of its clinical use (Asadishad *et al*., 2010).

### 1.3 Justification of the Research

Despite advancement in cancer research, cancer related morbidity and mortality is still increasing. The situation is even worse in developing countries, where access to radiotherapy and some costly chemotherapy is limited; and according to Boyle and Levin (2008), most people in developing countries have no access to cancer screening and early diagnosis. It is also known that the available drugs have dose-limiting toxicity which limits their use. There is, therefore, need to fabricate drug delivery materials that are biodegradable, cheap and readily available and capable of exploiting the EPR effect to reduce wastage and dose-limiting toxicity associated with anticancer drugs.

Since the discovery of the EPR effect by Maeda *et al.* (1986), research interest on cancer has focused on exploitation of this phenomenon. For any material to make use of the EPR effect, it must have size in the range of 100 nm – 760 nm (the pore size in solid tumour vasculature, (Drummond *et al*., 1999), possess stealth characteristics, and provide sustained release profile. To this end, nanocomposite comprising a hydrophilic polymer and inorganic particles like HA is a promising material. It has been shown that the drug loading efficiency and controlled release behaviour can be enhanced because of the synergistic effect between biopolymer and inorganic materials (Devanand *et al*., 2011). The stealth characteristics can be provided by SA (because of its hydrophilicity); and research has shown that incorporating HA with a biopolymer prolongs the release of encapsulated drug (Raj *et al.*, 2013).

Although numerous researches have been carried out on encapsulation of DOX and MTX for drug delivery application, to the best of our knowledge, the use of HASA for this application has not been investigated.

## 1.4 Aim and Objectives

### 1.4.1 Aim of the Study

The aim of this study is to prepare and characterize HASA nanocomposite and to evaluate its application in delivery of two anticancer drugs - DOX and MTX.

### 1.4.2 Objectives of the study

i. To prepare HA nanoparticles and HASA nanocomposite and characterize them using XRD, XRF, SEM, and FTIR.
ii. Drug loading and *in vitro* drug release study of the HA and the HASA nanocomposite.
iii. Determination of release kinetics and release mechanism for the drug delivery system.

iv. To investigate the effects of different solvents used in the synthesis of the nanocomposites on drug loading and release profile.

v. To investigate the effects of drug loading methods on the drug release behavior.

vi. To investigate the effect of pH of the release medium on drug release profiles.

vii. To study co-delivery of the two drugs - DOX and MTX, by the nanocomposite in order to evaluate its suitability for combination therapy.

# CHAPTER TWO

## 2.0 LITERATURE REVIEW

### 2.1 Drug Delivery System

Drug delivery system refers to the technology used to present the drug to the desired body site for release and absorption. To distinguish the term from conventional dosage form, the term modified-release drug delivery system is often used. Drug release modified dosage is formulated to achieve better therapeutic effect and better patient compliance than the conventional dosage forms (Shargel *et al*, 2012). This is achieved by altering the mechanism or rate of release of the drug substance.

According to Dixit *et al*. (2013), because of their ability to overcome drawbacks of conventional dosage forms, these modified-release forms are increasingly replacing the conventional dosage forms. Some categories of modified release delivery system are: sustained-release, delayed-release, and targeted-release drug delivery systems.

Targeted release drug delivery system is a system that selectively delivers drugs only to the required physiological sites, organs or cells, while reducing/avoiding delivery to the unwanted sites. Targeted delivery systems lead to improved therapeutic index and reduced side effects (Masayuk, 2005).

Delayed release drug delivery system is a drug carrier that releases the drug at a time other than immediately after administration. This system is mostly associated with oral dosage forms (Shargel *et al.*, 2012).

2.1.1 Sustained drug delivery systems

Dixit *et al,* (2013) cited the work of Israel Liposwki in 1938 who patented a research work on sustained drug delivery system, which is probably the earliest work in this area. Sustained release drug delivery system is a delivery system designed to achieve prolonged therapeutic effect by continuously releasing the therapeutic agent over an extended period of time after administration of single dose (Patnaik *et al,* 2013). The term is used interchangeably with 'prolonged release', 'slow release', 'sustained action', 'prolonged action', and 'extended release'.

Sustained release drug delivery systems alter the pharmacodynamics and pharmacokinetics of the drug by modifying the rate at which the drug is being released into the system (Dixit *et al,* 2013). This leads to several advantages over conventional dosage forms, which include the following: improved patient compliance as a result of less frequent drug administration, reduction in fluctuation of plasma drug levels, maximal utilization of the drug, reduction in health care costs, and reduction in dose-dependent toxicity (Patnaik *et al,* 2013).

Conventional dosage forms result in fluctuation of drug concentration giving rise to peak and valley patterns. This leads to drug concentrations sharply rising above toxic level (maximum tolerated dose (MTD) or minimum toxic concentration (MTC) and within a short time falling below the minimum effective concentration (MEC). Figure 2.1 illustrates the comparison between the sustained drug release and conventional dosage forms.

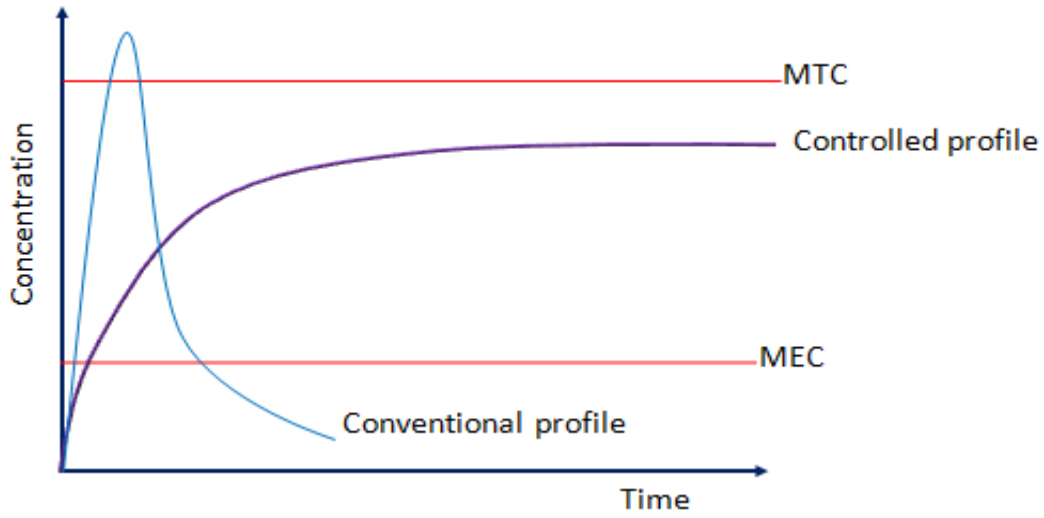


**Figure 2.1**: Schematic representation of conventional drug release profile and controlled release profile

## 2.2 Materials for Drug Delivery

### 2.2.1 Hydroxyapatite

In the 1980s, Brown and Chow (1983) and LeGeros *et al*., (1982) discovered a calcium phosphate salt known as hydroxyapatite (HA), with the formulae $Ca_{10}(PO_4)_6(OH)_2$. It is a member of the apatite mineral group with general formula $M_{10}(XO_4)_6Z_2$, where M = $Ca^{2+}$, $Sr^{2+}$, $Ba^{2+}$, $Pb^{2+}$, and so forth; $XO_4$ = $PO_4^{3-}$, $VO_4^{3-}$, $SiO_4^{3-}$, $AsO_4^{3-}$, $CO_3^{2-}$; Z = $OH^-$, $Cl^-$, $F^-$, (Byrappa and Yoshimura, 2001). Approximately 70% of natural bone is composed of HA particles (HA) and the remaining 30% is an organic matrix (mainly collagen type). Hence, it is considered attractive in biomedicine as it is naturally present in human body.

The important characteristics that determine the success of HA as biomaterials include phase composition, purity, crystallinity, specific surface area, particle size, particle size distribution, and morphology (Venkatesan *et al*., 2011). Abidi and Murtaza, (2013) reported that amorphous

HA obtained at lower temperature is metabolically more active than the fully developed crystalline HA which is insoluble in physiological environment.

HA/polymer nanocomposites have attracted much attention since such nanocomposite lead to improved properties (Khaled *et al*., 2014) as a result of improvement in the surface functionality of the apatite (Venkatesan *et al.*, 2011). Such improvement has led to wide applications of HA polymer nanocomposite in many areas such as in drug delivery system (Raj *et al*., 2013).

### 2.2.2 Polymers

Polymers have been successfully employed in drug delivery systems. According to Agrawal (2014), the polymers for drug delivery are classified based on the following characteristics:

i. Origin: It can be synthetic, natural or a combination of both. Synthetic and naturally occurring polymer used in drug delivery systems occur in the form of matrix devices, hydrogels, microspheres, nanoparticles/nanocomposites, films and sponges (Chasin and Langer, 1990).
ii. Chemical nature: It can be polyesters, polysaccharides, polyanhydrides, protein-based, and so forth.
iii. Solubility: Based on nature of water-polymer interactions, polymers for drug delivery can be classified as either hydrophilic or hydrophobic.
iv. Based on degradability: Polymers can be classified as biodegradable or non-biodegradable. Biodegradable polymers can be defined as polymers that are degradable *in vivo*, either enzymatically or non-enzymatically (Joshi and Patel, 2012).

Biodegradable polymers have been employed extensively in drug delivery more than non-biodegradable polymers. This is because for biodegradable polymers, there is no need for

subsequent removal by surgical operation as the polymers can degrade into non-toxic by-products (Park *et a*l, 2005).

The mode of degradation of polymers can dictate the release rate of the encapsulated drug; for example, polyanhydrides and polyorthoesters degrade at the surface, resulting in a release rate that is proportional to the surface area of the drug delivery system (Joshi and Patel, 2012). Factors that influence the biodegradation kinetics of the selected polymer are: the chemical structure, size, shape, chain defects, ion exchange, ionic strength, pH, morphology (amorphous, semi crystalline, crystalline, micro-structure, residual stress), mechanisms of degradation (enzymatic, hydrolysis, microbial), molecular weight distribution, processing condition and sterilization process, annealing and storage history, route of administration, and site of action (Badri *et al*., 2014). However Priya *et al*. (2013) stated that majority of polymers used in controlled drug delivery undergo bulk erosion.

Polymers are used in drug delivery because they have the ability to successfully encapsulate drugs, avoid degradation of the drug, and enhance specificity to the diseased cell, leading also to improved efficacy and reduced toxicity of the chemotherapeutic agent (Allermann *et al*., 1993). Some drugs are unstable in certain environments such as in plasma or in acidic conditions, such drugs can be protected using polymeric carrier (Vilar *et al*., 2012). Use of polymeric drug delivery system can also result in controlled and sustained delivery; and enables improved drug pharmacokinetics (absorption, distribution, metabolism, and excretion) (Badri *et al*., 2014).

Polymeric nanoparticles have multiple functionalities and can be manipulated without the loss of desired properties. This principle has been applied in the improvement of nanoparticles in cancer therapy through the attachment of tumour specific moieties (e.g. antibodies or receptor ligands).

Polymeric nanoparticles also have passive tumour-targeting properties which lead to enhanced drug efficacy and reduced side effects of the chemotherapeutic drugs (van Vlerken and Amiji, 2006).

Although polymers have been successfully used in drug delivery systems, they are not without challenges. One of the major challenges is that polymers are generally heterogeneous in nature. This heterogeneity makes each polymer-drug to differ in molecular weight, drug loading and subsequent conformation. It also makes it difficult for the delivery material to be synthesised and characterised in a reproducible manner (Agrawal, 2014).

*2.2.2.1 Sodium alginate (SA)*

The first published description of alginates was made by a British Chemist, E. C Stanford, with a patent dated 12th January 1881 (Viswanathan and Nallamuthu, 2014). Alginate was then believed to be composed of D-manuronate, until Fischer and Dorfel identified the L-guluronate residue (Fischer and Dörfel, 1955). It is now known to be a linear copolymer composed of blocks of 1, 4-linked $\beta - D -$manuronate (M) and $\alpha - L$ - guluronate (G) residues (Lee and Mooney, 2012). The blocks are composed of consecutive G residues (GGGG), consecutive M residues (MMMM) and alternating M and G residues (GMGMGM).

+

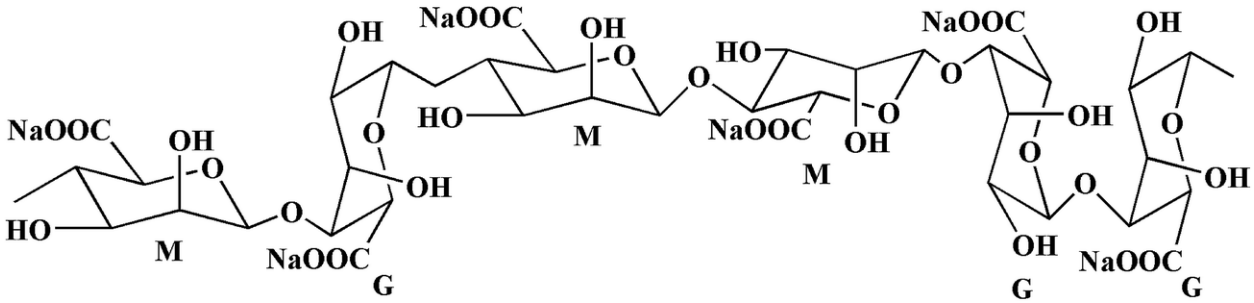

**Figure 2.2:** Structure of sodium alginate

SA is extracted from brown sea weeds. Its major biological functions in the plants include prevention from desiccation, maintaining the integrity of the cell wall, providing mechanical strength and flexibility of the plant tissue. The variability in the chemical structure of the alginates depends on the source of isolation. For example, alginates prepared from *L. hyperborea* kelp contain the highest content of $\alpha - L -$ guluronic acid residues while alginate from *A. nodosum* and *L. japonica* have low content of $\alpha - L$-guluronic acid blocks (Sachan *et al*., 2009).

The properties of the alginate are affected by such factors as the ratio of the M to G blocks (i.e. M/G ratio), sequence of the blocks, length of the G-blocks, and molecular weight (George and Abraham, 2006). For example, reactivity with calcium, causing gel formation is a direct function of the average length of the G blocks occurring in the polymer chain, i.e. the strength and stability of the gel depend on the content of the G-blocks (Skaugrud *et al*., 1999). Although SA has been certified as biocompatible and non-toxic, it has been reported that alginates with high M- content were more immunogenic than high G-alginates (Otterlei *et al*., 1991).

SA has molecular weight that range between 32,000 and 400,000 g/mol. It dissolves in water to form a viscous solution. The viscosity increases with a decrease in pH, reaching a maximum around pH 3 - 3.5 (Lee and Mooney, 2012).

One of the most interesting characteristics of SA is its ability to form gels in the presence of polyvalent cations. The most commonly used cross-linker, $Ca^{2+}$, preferentially interacts with the G blocks due to structurally favourable chelation sites (Ahirrao *et al*., 2015).

Ionically cross-linked alginates degrade by removal of the cross-linking ion (e.g. $Ca^{2+}$). As $Ca^{2+}$ ions are removed, the cross-linking decreases and the gels are destabilized blocks **(**Sachan *et al*., 2009). In mammal, this process occurs by exchange reactions with monovalent cations such as sodium ions, and can lead to leakage of entrapped material and solubilisation of high molecular weight alginate polymers (Lee and Mooney, 2012).

SA has found applications in many areas because of its excellent characteristics such as biocompatibility, biodegradability, non-toxicity, non-immunogenicity, water solubility, relatively low cost, gelling ability, stabilizing properties. According to Liew *et al*, (2006) it can be used as thickening, gel forming and colloidal stabilizing agent in the food and beverage industries. Khanedan *et al*., (2011) stated that it is used to increase the shelf life of frozen food during storage; according to Viswanathan and Nallamuthu (2014), it can also be consumed as a beverage for lowering blood sugar levels; and used as additives for textile dyes. It can also be used for treatment of tannery waste water (Marwa *et al*., 2013); synthesis of green silver nanoparticles (Balavandy *et al*., 2015).

In biomedical and pharmaceutical field, alginate has been widely exploited in many controlled drug delivery applications, protein delivery (Lee and Lee, 2009; Wells and Sheardown 2009; Chan and Neufeld, 2010); wound dressing (Balakrishnan *et al*., 2006; Murakami *et al*., 2010); cell culture (Wang et al., 2003; Bidarra et al., 2010) tissue engineering and cell delivery (Skaugrud *et al* 1999; Thornton *et al*., 2004; Silva *et al*., 2008).

According to Fattah *et al*., (1998) and Kikuchi *et al*., (1999), the characteristics/properties of alginate that make it suitable for controlled drug delivery include the following:

i. It is readily available and relatively cheap

ii. It is haemo - compatible and does not accumulate in any organ of the human body.

iii. It is biodegradable and hence needs no surgical removal after the drug is exhausted.

iv. It is soluble in water which eliminates the use of toxic organic solvents.

v. Its ability to be formulated at low temperature makes it ideal for sensitive drugs which are destroyed at high temperature.

vi. It can be cross - linked into insoluble gel for sustained/extended released of some drugs.

vii. According to WHO, there is no limitation for daily consumption of alginate by man (Yu *et al*., 2001).

SA has the ability to delay the dissolution of drugs from tablets, capsules, and aqueous suspensions, and has been applied in the preparation of sustained release formulations (Priya *et al*., 2013). Alginate gels can be orally administered or injected into the body in a minimally invasive manner (Lee and Mooney, 2012). Alginate beads of Ibuprofen prepared by Mallick *et al*., (2013) showed potential for sustained oral delivery of the drug. Also SA micro beads containing ciprofloxacin hydrochloride has good surface and size to be utilized as a dosage form for sustained release of the drug from the matrix through erosion (Patel *et al*., 2014). Similar study for the use of SA for sustained drug delivery were conducted by Harish *et al.*, (2010) using selbutamol drug, and Rajesh *et al* (2003) using theophylline drug.

The ability of SA to successfully prolong the release of diclofenac sodium, a non-steroidal anti-inflammatory agent, was investigated by Chowdhury *et al*., (2011); the result indicated that the efficiency and the sustained release characteristics depended on the polymer amount and the cross-linking agent used. Similar results were reported by Karakoti *et al*. (2014), where the release property and drug release rate of SA impregnated diclofenac sodium depends on the concentration of the biopolymer. They concluded that the polymer concentration can be altered

to achieve the desired drug release rate. Similarly, Menson and Sajeeth (2013), showed that polymer-drug ratio influences the particle size, swelling index, cumulative percentage release and drug entrapment efficiency.

Several researchers have also investigated the application of alginate nanoparticles for intravenous sustained release of drugs. Saraei *et al*., (2013) developed alginate nanoparticles with high loading capacity (over 70%) and sustained release profile that could be used as carrier drugs and vaccine delivery. The SA nanosphere formulated by Sangeetha *et al*., (2010) also showed satisfactory release characteristics.

Alginate gel has been used for the controlled and localized delivery of antineoplastic agents. Multiple drugs can be loaded into the alginate gels and delivered simultaneously or sequentially, depending on the chemical nature of the drug and its mode of incorporation. For example, study by Bouhadir *et al*., (2001) showed that MTX was rapidly released by diffusion (it has no reaction with the alginate).

Alginate microsphere can control the release rate of low molecular weight drugs (Stanislavov *et al*., 2014), and because of their hydrophilicity, can contribute to longer *in vivo* circulation times and higher encapsulation of water soluble biomolecules (Madan *et al*., 1997; Liew *et al*., 2006). The release mechanisms of drug encapsulated by alginates are mainly through diffusion, and sometimes due to erosion mechanism (Takka *et al*., 1998).

## 2.3 Nanocomposites

According to Roul *et al*. (2013), nanocomposite is a composition having a dispersed material that has one or more dimensions, such as length, width and thickness in the nanometre size range. Although this definition was widely used in literature, the term has also been used

interchangeably with the terms ‘hybrid nanocomposites,’ ‘nanohybrids’, ‘hybrid materials’ and ‘nanostructural composites’. The definition given above is in agreement with the IUPAC Gold Book, which defines nanocomposite as ‘a composition in which at least one of the phase domains has at least one dimension of the order of nanometres’. On the other hand, hybrid material is defined by the same source as ‘material composed of an intimate mixture of inorganic components, organic components, or both types of components, where the components usually interpenetrate on scale of less than 1μm (IUPAC, 1997).

The distinction between these terms has been relatively diffuse. Makishima (2004), defined hybrid materials as ‘mixture of two or more materials with newly formed chemical bonds'; while nanocomposite was defined as sub-micron mixture of similar kinds of materials. Makishima further stated that the difference between hybrids and nanohybrids was not so obvious and that nanocomposites include both hybrids and nanohybrids.

The components of nanocomposites can be organic, inorganic or both. In polymer-inorganic nanocomposite, the inorganic minerals such as HA, silica, metal oxides or calcium phosphate are incorporated into polymer matrices, to impact bioactivity, leading to nanocomposites with desired properties (Rajkumar *et al*., 2010). The novel property of the nanocomposite is as a result of physical or covalent interaction with the polymer chain (Goenka *et al.*, 2014).

### 2.3.1 Synthetic strategies for polymer-inorganic nanocomposites

Polymer-inorganic nanocomposites have been prepared by a variety of synthetic methods. For convenience, these methods can be grouped into four synthetic techniques.

#### *2.3.1.1 Ex situ formation of the components*

This is a strategy whereby both components are separately synthesized before bringing them together as a nanocomposite. These components are usually brought together by blending methods, which can either be solution blending, emulsion blending or melt blending. In solution blending, the preformed inorganic nanoparticles are dispersed in polymer solution by stirring for a long time (Cong *et al*., 2007). To stabilize the dispersed phase in the continuous polymer phase, it is imperative to incorporate surfactants molecules; a process known as emulsion blending. Melt blending on the other hand, was adopted to reduce/prevent aggregation of nanoparticles. It involves first surface modification of the nanoparticles followed by uniformly dispersing the modified nanoparticles into the molten form of the polymer (Wang and Hong, 2011).

These methods can also be classified based on the force of attachment as either covalent attachment or non-covalent (physical) attachment. In covalent attachment, the surfaces of the inorganic nanoparticles are usually functionalized to enable chemical reaction with the polymer chain (Hood *et al*., 2014). Non covalent attachment makes use of electrostatic interaction between the charged inorganic particles and the charged polymer. The most popular technique here is the layer-by-layer technique (LbL). LbL technique can be used in the formation of functional particles for use in drug delivery applications (Sukhorukov *et al*., 1998). It involves repeated addition of one charged species into a concentrated suspension of the oppositely charged species.

*2.3.1.2 In situ precipitation of the inorganic component on polymer structure*

In this technique, the inorganic precursors are mixed with the polymer solution or polymer particles. In the first case, polymers are used as structuring agents. Hydrophilic polymers in

solution act as controlling agents in the precipitation of inorganic particles from aqueous solution, a process commonly referred to as "polymer-assisted" (Taubert *et al*., 2002; Schweizer, and Taubert, 2007; Muñoz-Espí *et al*., 2008).

The polymer is used as soft template for the precipitation of the inorganic particles. The occlusion of the inorganic particles into the polymer during precipitation results in formation of materials with crystalline properties different from the bulk (Hood *et al*., 2010).

Inorganic nanoparticles can also be precipitated on the surface of polymer particles (instead of polymer solution as in the first case). In general, the advantage of in situ precipitation of nanocomposite on polymer structure is its ability to significantly reduce particles aggregation through particles stabilization by the polymer chain functional group. The major disadvantage however, is that the properties of the formed nanocomposite can be affected by the unreacted precursors (Moffitt and Eisenberg, 1995).

*2.3.1.3 In situ polymerization in the presence of ex-situ formed inorganic nanoparticles*

This technique involves polymerization in the presence of inorganic nanoparticles. The inorganic nanoparticles are mixed together with the organic monomers. Polymerization takes place under suitable conditions like the provision of water, initiator and oxidant (Wang and Hong, 2011).
There are many different polymerization methods used in the synthesis of nanocomposite. One of them involves the use of considerable amount of surfactant. This method is called emulsion polymerization (Landfester, 2009). Surfactants are necessary to stabilize the dispersed phase from the continuous phase. It is also possible to avoid the use of surfactant and stabilize the droplets and particles by means of inorganic particles placed at the interface. This process is known as Pickering emulsion (Schrade *et al*., 2013).

*2.3.1.4 In situ formation of both the polymer and the inorganic components*

This technique is often referred as "one pot method". The inorganic precursors and organic monomers are mixed together with the addition of water, catalyst, initiator and/or oxidant, leading to simultaneous polymerization and precipitation of the inorganic nanoparticles (Wang and Hong, 2011).

The major setback to this technique is that the condition for polymerization and inorganic precipitation are mostly very different. Only few works were reported on this synthetic approach, such as work by Fukui and Fujimoto, (2012); and Hamberger *et al*., (2013).

2.3.2 Methods of characterization of nanocomposites

*2.3.2.1. X-Ray diffraction (XRD)*

In 1912, William Lawrence Bragg and his son William Henry Bragg discovered that when an incident beam of monochromatic x-rays interact with a target material, there is scattering of these x-rays from atoms within the target material. The scattered x-rays undergo constructive and destructive interference. This is the process of diffraction. The diffracted x-rays contain information about the atoms of the target materials which caused the diffraction (Bragg, 1913). This forms the basis of x-ray diffraction analysis.

Constructive interference (also called in-phase diffraction) occurs at specific angles (often called Bragg's angles) and produce signals (peaks). For constructive interference to occur, the difference in path length of the diffracted beams must be equal to integral multiples of the wavelength of the x-ray radiation. This statement is known as Bragg's Law, and is stated as follows (Fultz and Howe, 2013):

$$n\lambda = 2d\sin\theta \quad (2.1)$$

where n is integer determined by the order of diffraction, $\lambda$ is wavelength of x-rays, d is spacing between the planes in the atomic lattice, and $\theta$ is angle between the incident rays and the scattering planes.

The angles at which x-rays are diffracted depend on the spacing between the planes in the atomic lattice. In order words, the space between diffracting planes of atoms (d-spacing) determines peak positions, whereas the peak intensities is determined by what atoms are in diffracting planes. Powder diffraction data are usually presented as a diffraction pattern in which the diffracted intensity I is shown as a function of the scattering angle $2\theta$ (Suryanarayana and Norton, 1998).

X – Ray Diffraction is a non-destructive analytical technique which has been widely used in phase identification of materials, microstructural analysis, degree of crystallinity, resolution and refinement of crystallite structure, determination and characterization of the preferred crystallographic orientation, and so forth.

Diffraction from different planes of atoms produces a diffraction pattern, which contains information about the atomic arrangement within the crystal. This information can be used to identify all the phases if a sample is a mixture of crystalline phases (Müller *et al*., 2005). Phase determination/identification can be performed by a comparison of a set of d-spacing and intensities with a database file like Powder Diffraction File (PDF)) (PDF, 2010).

The observation that the peak broadening is due to instrumental and sample effect can be used to calculate the crystallite size and the strain of the material (Rehani *et al*., 2006).

$$\beta_o = \beta_i + \beta_r \quad (2.2)$$

where $\beta_0$ is the observed peak broadening, $\beta_i$ is the instrumental broadening, $\beta_r$ is the broadening due to crystallite size and lattice strain.

Four different methods are used for estimation of crystallite size and strain using the peak broadening effect. These methods include: Scherrer method, Williamson-Hall method, Size-Strain plot method and Warren-Averbach method.

Scherrer method assumes that the strain broadening is negligible and that the observed broadening is due to the finite size of the crystal, where for very small crystals the intensity of x-ray at close to, but not exactly, the Bragg's condition is not zero (Meier, 2005). The Scherrer equation can be stated as follows:

$$D = \frac{0.89\lambda}{\beta cos\theta} \quad (2.3)$$

Where D is the average crystallite size, λ is the wavelength of the incident radiation, β is the corrected full width at half maximum (FWHM) (corrected for instrumental broadening), and $\theta$ is the diffraction angle. The strongest diffraction peak can be used to calculate the crystallite size.

Using the Williamson-Hall method, both size and microstrain can be calculated. Microstrain is due to imperfections within the crystalline lattice. According to Meier, (2005) the broadening effect of strain is related to Bragg's angle by the equation:

$$\beta_{strain} = \varepsilon tan\theta \quad (2.4)$$

because sample broadening is due to both size and strain,

$$\beta_{strain + size} = \beta_{size} + \beta_{strain} \quad (2.5)$$

from Scherrer equation (2.3), $\beta_{size} = \frac{K\lambda}{Dcos\theta}$

hence, $\beta_{strain + size} = \varepsilon tan\theta + \frac{K\lambda}{Dcos\theta}$ (2.6)

multiplying both sides by $cos\theta$,

$\beta cos\theta = \frac{K\lambda}{D} + \varepsilon sin\theta$ (2.7)

A plot of $\beta cos\theta$ against $sin\theta$ gives the slope as the strain (ε), while the intercept at the y axis is $\frac{K\lambda}{D}$. Hence, size can be calculated from the intercept and strain from the slope.

Warren-Averbach method uses both the peak width and shape to estimate the crystallite size distribution as well as lattice microstrain. This method is based on Fourier deconvolution of the measured peaks together with the instrumental broadening which gives the true diffraction profile (Akbari *et al*., 2011).

In Size-Strain Plot method, the strain aspect is represented by Gaussian functions while the crystallite size by Lorentian functions (Prabhu *et al*., 2014).

$(d\beta cos\theta)^2 = \frac{K}{D}(d^2\beta cos\theta) + (\frac{\varepsilon}{2})^2$ (2.8)

K is a constant which depends on the shape of the particles (for spherical particles, K = ¾).

*2.3.2.2 Scanning electron microscope (SEM)*

The scanning electron microscope uses electrons to form an image. A beam of high energy electrons, produced from a tungsten filament (known as electron gun) is focused on the sample, which impinges on the sample and interacts with the atoms of the sample producing signals that reveal information about the sample, based on external morphology, chemical composition,

crystalline structure, particle size and orientation of materials making up the sample (Nixon, 1971).

The interaction of the beam of electrons with the sample produces secondary electrons, backscattered electrons, characteristic X-Rays, Auger electrons, and transmitted electrons. These emitted particles can be collected with appropriate detector to yield valuable information about the material. The most widely used signal produced by the interaction of the primary electron beam with the sample is the secondary electron emission (Wang, 2004).

When the primary beam of electrons strikes the sample surface, they cause ionization of sample atoms, and loosely bound electrons are emitted. These are referred to as secondary electrons. Since the energy of the secondary electrons is very small, only those generated at the top of the surface of the sample are emitted outside the sample. Thus secondary electrons are very sensitive to the surface and are used to observe the external morphology/topography of the material (Goldstein *et al.*, 2003).

When the primary beam causes the ejection of inner shell electrons from the atom of the sample, an outer shell electron falls into the inner shell to re-establish the proper charge balance, leading to emission of characteristic x-rays. Because these x-rays are characteristic of the atomic structure of the element from which they are emitted, these are used to elucidate the elemental composition of the sample. An in-built spectrometer called Energy Dispersive X-ray (EDX) is used. The Energy Dispersive x-ray detector measures the number of emitted x-rays versus their energy (Zhou *et al*., 2005).

Incident electrons that are elastically scattered through an angle of more than $90^{o}$ are called Backscattered electrons (BSE). BSE are sometimes called reflected electrons. They escape from

the surface with energy greater than 50 eV (higher than that of Secondary electrons), hence contains information from a relatively deep region of the sample. As the atomic number of the constituent atoms in the sample increase (becomes larger), BSE yield becomes larger. For this reason, areas that consist of heavy atoms appear relatively bright in the BSE image. Thus this image is suitable for observing compositional difference in a material (Goldstein *et al*., 2003).

Auger electrons are produced as a result of excess energy produced when an outer shell electron fills in the inner shell vacancy created by electron knocked out by the primary electron beam. These electrons have characteristic energy, and can therefore be used to provide chemical information. Auger electrons have low energy and are emitted only near the surface, hence are used in surface analysis (Goldstein *et al*., 2003).

The SEM is capable of producing high resolution images of a sample surface. SEM images have great depth of field yielding a characteristic three dimensional appearance useful for understanding the surface structure of a sample.

*2.3.2.3 Fourier transform-infrared spectroscopy (FTIR)*

Infrared spectroscopy is the study of interaction of infrared radiation with matter as a function of photon frequency. It works on the principle that molecules have specific frequencies at which they rotate or vibrate corresponding to discrete energy levels (Colthrup *et al*., 1990).

The origin of many characteristic frequencies that can be assigned to particular combination of atoms within a molecule can be explained using the basic model of the simple harmonic oscillator. According to Coates (2000), the fundamental vibration frequency of a molecule can be expressed using a simple statement of Hooke's Law:

$$\nu = \frac{1}{2\pi c}\sqrt{\frac{k}{\mu}} \quad (2.9)$$

where ν is the fundamental vibration frequency, k is the force constant, and μ is the reduced mass. The reduced mass is given as:

$$\mu = \frac{m_1 m_2}{m_1 + m_2} \quad (2.10)$$

where $m_1$ and $m_2$ are the components masses for the bond under consideration. This equation provides a theoretical link between the bond strength and the frequency of vibration. The values obtained for stretching vibrations using this equation agrees reasonably with the experimental values observed for the fundamentals (Coates, 2000).

When a beam of infrared radiation is passed through a sample, molecules absorb infrared radiation at certain wavelength and frequencies corresponding to the vibration characteristics of their chemical bonds. Measuring the transmitted radiation as a function of frequency produces a spectrum which can be used to identify functional groups and compounds as well as for quantitative analysis applying Beer-Lambert's Law.

A well-known mathematical technique called the Fourier transform can be used for decoding the individual frequencies. Fourier transformation is done by connecting to the computer system. Alternatively, this can be done using a dispersive instrument which changes in wavelength over time. The Fourier transform infrared spectroscopy (FTIR) is based on the idea of the interference of radiation between two beams to yield an interferogram. The three basic components of an FTIR system are: a radiation source, an interferometer, and a detector (Stuart, 2004).

The radiation source is a glowing black body which emits infrared energy. For the mid-infrared region, a Globar or Nernst source is used. The interferometer produces interference signals, which contain infrared spectral information generated after passing through a sample. The most commonly used interferometer is Michelson interferometer. For the detector in the mid-infrared region, a pyroelectric device incorporating deuterium tryglycine sulphate in a temperature resistant alkali halide window is more common (Stuart, 2004).

The infrared spectrum is displayed either in a transmittance, or absorbance mode. The transmittance spectra provide better contrast between intensities of strong and weak bands because transmittance ranges from 0 to 100%T whereas absorbance ranges from infinity to zero. However, the absorbance mode is preferred for quantitative work. Transmittance (T) is the ratio of radiant power (I) transmitted by the sample to the radiant power ($I_0$) incident on the sample. Absorbance (A), is the logarithm to the base 10 of the reciprocal of the transmittance.

$$A = \log_{10}(\frac{1}{T}) = -\log_{10}T = -\log_{10}(\frac{I}{I_0}) \quad (2.11)$$

FTIR can be used to analyse solid, liquid, and gaseous samples. The most commonly used methods for preparing solid samples in transmission infrared spectroscopy are the alkali halide method and the mull method. The commonly used alkali halide is potassium bromide (KBr), which is completely transparent in the mid-infrared region. The solid sample and the KBr are mixed and ground with an agate mortar and pestle, and then subjected to high pressure to produce a clear transparent disc. The mull method involves suspending the powdered sample in one or two drops of mulling agent which are further ground to obtain a smooth paste. The most commonly used mulling agent is Nujol (liquid paraffin) (Chalmers *et al*., 2002).

Infrared spectroscopy is most useful in providing information about the presence or absence of specific functional groups. The mid-infrared region from 4000 $cm^{-1}$ to 400 $cm^{-1}$ is used. The infrared absorption in this region can be summarized into four different parts according to Nakamoto, (2002).

i. The region from 4000 to 2500$cm^{-1}$ corresponding to absorptions caused by N-H, C-H, and O-H single bond stretching motions. N-H and O-H single bonds absorb in the 3300 to 3600 $cm^{-1}$ range whereas C-H bond stretching occurs near 3000 $cm^{-1}$.
ii. The region from 2500 to 2000 $cm^{-1}$ is where triple bond stretching occurs. Both nitriles (R-C≡N) and alkynes (-C≡C-) show absorption here.
iii. The region from 2000 to 1500 $cm^{-1}$ is where double bonds of all kinds absorb (C=O, C=N, C=C). Carbonyl groups generally absorb in the range 1680 to 1750 $cm^{-1}$ and alkenes stretching normally occur in a narrow range from 1640 to 1680 $cm^{-1}$.
iv. The region from 1500 to 400 $cm^{-1}$ is called the fingerprint region. This is a complex area showing many bands overlapping each other. C-C, C-O, C-N, C-X single vibrations occur here. The complexity limits its use to that of a fingerprint.

For a molecule to show infrared absorption, the electric dipole moment of the molecules must change during the vibration. Such molecules are said to be infrared-active. The intensity of the band depends on the magnitude of the dipole moment associated with the bond in question.

*2.3.2.4 X-ray fluorescence (XRF)*

X – Ray Fluorescence Spectroscopy (XRF) is a non-destructive analytical technique used for elemental analysis of materials. In XRF analysis, a material is exposed to x-ray of high energy produced by a source which can be an x-ray tube, a synchrotron or a radioactive material. As the

x-ray hits an inner shell electron in the atom of the sample, energy is absorbed by the atom which, if high enough, will knock out a core electron from its atomic orbital. An electron from an outer shell then drops into the vacant orbital to fill the hole left behind. The energy difference between the inner and outer shell is balanced by the emission of x-ray fluorescence which can be detected by a fluorescence detector (Jenkins, 2000; Brouwer, 2010).

The energy needed to eject an inner electron is characteristic of each element, and so is the energy emitted by the transition. The relation between the emission energy and the atomic number is described by an empirical law known as Moseley's law (Jenkins, 2000):

$$E_m = R_H (Z - \sigma)^2 \left(\frac{1}{n^2} - \frac{1}{m^2}\right) \quad (2.12)$$

Where $R_H$ is the Rydberg constant, $Z$ is the atomic number and $\sigma$ is the screening constant of atom. Every element has its own characteristic radiation which is its fingerprint.

Not all initial vacancies created by incoming radiation produce fluorescent photons. Emission of Auger electron is another process that can take place. Both processes have Z-dependent probabilities that are complementary; the Auger yield is high for light elements and fluorescent yield is high for heavy elements. The fluorescent yield is the ratio of the emitted fluorescent photons to the number of initial vacancies. Because it is low for the very light elements, it is difficult to measure these elements (Brouwer, 2010).

XRF are used for both quantitative and qualitative elemental analysis of organic and inorganic compounds and materials. Basically two types of XRF instruments are used: the wavelength dispersive (WDX) and the energy dispersive spectrometer (EDX). The two differ in the way x-ray spectra emitted by the sample are detected. In wavelength dispersive spectrometers, the

fluorescent spectrum is dispersed into discrete wavelength using a dispersion device, while in energy dispersive spectrometers, the entire fluorescent spectrum is measured directly using a solid detector which is then processed using a multichannel analyser to obtain the information on an energy scale (the pulse height of the detector signal is proportional to the energy of the x-ray photon) (Jenssens *et al.*, 2000).

These x-rays can be detected and displayed as a spectrum on intensity against energy or wavelength ($2\theta$). The positions of the peaks identify which elements are present in the sample, while the peak height can be used to determine how much of each element is present in the sample. The intensity (peak height) of the x-ray fluorescent radiation is proportional to the element concentration (Jenssens *et al*., 2000).

Energy dispersive x-ray fluorescent (EDX) can be used for a wide range of elements from sodium to uranium, while for wavelength dispersive x-ray fluorescent, the range is even wider: from beryllium to uranium.

## 2.4 Drug Loading Methods

The ability of a drug delivery system to successfully load or encapsulate the chemotherapeutic agent indicates to a large extent its success as a delivery system. High drug loading capacity reduces the amount of matrix required for administration, and also reduces wastage of the chemotherapeutic agent. Therefore, care must be taken to select the delivery system, loading method and conditions that ensure maximum loading capacity. There are basically two methods of drug loading – incorporation method and adsorption method.

### 2.4.1 Incorporation method

In this method, drug is incorporated during the formation of nanocomposites. Incorporation method has the advantage of higher loading capacity than the adsorption method (Ueda *et al*., 1998). The method also achieves better protection against environmental factors and more control over the encapsulation process (i.e. it is easier to reproduce) (Bennet and Kim, 2014). The major disadvantage, however, is that the preparation conditions for the nanocomposite can compromise the integrity of the drug, hence not suitable for labile drugs and proteins.

Incorporation method is applied to both polymer-polymer composite and polymer-inorganic composite. In the case of polymer-inorganic composites, this method is mostly applied where the ex-situ preparation condition technique is used. This is probably due to incompatibility of the in situ preparation conditions with the drug. Roul *et al*. (2013), however incorporated ofloxacin during the in situ formation of HA in SA solution.

There are different ways of incorporating drugs into a nanocomposite. One of these is emulsion methods – double emulsion or single emulsion. Preparation of rimfapicin loaded chitosan-poly lactic was carried out by incorporation method following the water-in-oil-water (w/o/w) double emulsion technique (Rajan and Raj, 2013). w/o/w double emulsion was also used to synthesise 5-flurouracil-polylactic acid-montmorillonite nanocomposite (Seema and Datta, 2013). Double emulsion involves two steps; first formation of primary w/o emulsion and then the secondary w/o/w emulsion. The primary emulsion is stabilized by a hydrophobic surfactant while the secondary emulsion by a hydrophilic surfactant (Mora-Huertasa *et al*., 2010). Single emulsion has also been successfully used to encapsulate drugs into nanocomposites (Hua *et al*., 2010; Javid *et al* 2014).

In another approach known as solvent evaporation method, the drug solution is mixed with a solution containing the components and the solvent evaporated. This has been used to load/incorporate ofloxacin on gelatine/montmorillonite cloisite 30B nanocomposite (Sahoo *et al*., 2011); synthesize paclitaxel loaded gelatin/montmorillonite nanocomposite (Das *et al*., 2011); encapsulate curcumin onto chitosan-alginate/cloisite 30B nanocomposite (Malesu *et al*., 2011); load curcumin onto chitosan-polyvinyl alcohol/cloisite 30B nanocomposite (Parida *et al*., 2011); load curcumin onto starch-chitosan/montmorillonite nanocomposite (Mohanty *et al*., 2015).

Solvent evaporation method can leave free drug on the surface of the nanocomposite. In an approach to remove this shortcoming in a procedure for preparation of celecoxib-loaded HA-chitosan nanocomposite, celecoxib was first dissolved in ethanol and then added to the dispersion of HA in chitosan solution. The mixture was centrifuged and re-dispersed in ethanol to remove free celecoxib (Venkatesan *et al*., 2011).

A different approach was followed by Iliescu *et al*., (2011) in the preparation of carboplatin-mmt-alginate nanocomposite. The first step involved formation of carboplatin-mmt hybrid. This is followed by addition of carboplatin-mmt hybrid powder containing $CaCl_2$ to the alginate solution (ionotropic gelation) to form carboplatin-montmorillonite-alginate nanocomposite. Similar technique was applied in the preparation of irinotecan-montmorillonite-alginate nanocomposite (Iliescu *et al*., 2014).

### 2.4.2 Adsorption/absorption method

This method involves adsorbing the drug on the nanocomposites/nanoparticles after the formation of the nanoparticles. The formed nanoparticles are stirred and incubated in a

concentrated solution of the drug, after which the drug-bound nanoparticles is recovered and dried (Soppimatha *et al*., 2001; Peer *et al.*, 2007; Sahoo and Nayak, 2013).

Various procedures have been reported in literature. In a study by Prasath *et al* (2011), loading of amoxicillin into polycaprolactone/polyethylene-HA nanocomposite was carried out by incubating the nanocomposite in the antibiotic solution at 37$^{o}$C for 48 hours, after which the drug-loaded nanocomposite was recovered and air-dried. Similar approach was followed by Zhao *et al*., (2007) to synthesize DOX-chitosan-alginate multilayer microcapsules. The microcapsule-drug solution was incubated at 37$^{o}$C for 12 hours, although the drying method was not reported. Adsorption of bovine serum albumin onto poly (2-hydroxyethyl methylacrylate) grafted hydroxyapatite (PHEMA-g-HAP) was also carried out by shaking and incubating at 37$^{o}$C for 24 hours (Bach *et al*., 2012).

While some researchers omitted the incubation step, (Liu *et al*., 2006; Chahatray *et al*., 2013; Sahoo and Nayak, 2013), others incubated the nanocomposite-drug solution at room temperature for varying periods of time (Sivakumar and Rao, 2002; Raj *et al*., 2013; Alimardan *et al*., 2014). Unlike other reported works, Sivakumar and Rao (2002), however, carried out adsorption of gentamicin onto coralline HA/gelatine nanocomposite in a phosphate buffer saline at pH 7.4. Other drying methods reported in literature include freeze-drying (Venkatasubbu *et al*., 2011) and vacuum oven drying (Alimardan *et al*., 2014).

As mentioned earlier, the adsorption method of drug loading has lower drug loading capacity compared with the incorporation method. Surface adsorption has been given as one of the major causes of high burst release in drug delivery systems (Huang and Brazel, 2001). However, the method also has several advantages. It is simple to use and does not affect the stability of the

drug. Again, vital information can be obtained from the adsorption isotherm of the nanocomposite-drug delivery system which can be used to get the best possible formulation, the drug binding capacity onto the surface of nanocomposite, and the amount of drug adsorbed (Soppimatha *et al*., 2001).

## 2.5 Drug Release Mechanisms and Kinetic Models

### 2.5.1 Drug release mechanisms

Release mechanisms refer to the ways through which drug molecules are transported or released from the carrier system to the surrounding medium. The knowledge of release mechanisms and the physicochemical processes that influence drug release is important for the development of effective controlled drug delivery systems.

Based on release of active agents from delivery systems, mechanisms of controlled drug release can be classified as diffusion, erosion/degradation and swelling controlled delivery systems. More than one mechanism is often involved at a given time or different mechanisms may dominate at different stages of the drug delivery process (Siegel and Rathbone, 2012).

#### *2.5.1.1 Diffusion controlled mechanism*

Karimi (2011), defined diffusion as the process by which penetrants are moved from one part of the system to another as a result of random molecular motion. Numerous models of diffusion in polymer-based systems are based on Fick's first law which governs steady state diffusion. The equation is stated:

$$J = -D\frac{\partial c}{\partial x} \qquad (2.13)$$

Where J is the flux which gives the quantity of penetrant diffusing across unit area of medium per unit time, D is the diffusion coefficient, c the concentration, and x the distance, and $\frac{\partial c}{\partial x}$ is the gradient of the concentration along the axis (Comyn, 1985).

Fickian diffusion release occurs by the usual molecular diffusion of the drug due to a chemical potential gradient. The filled polymers with nanoparticles have lower diffusion coefficient than unfilled ones. Geometrical dimension, size distribution and amount of fillers as well as its level of dispersion into polymer matrix are important factors controlling the rate of mass transfer through the filled polymer especially nanocomposites (Karimi, 2011).

Hydrophilic matrix shows a typical time dependent profile by which the dissolution medium penetrate into the dosage form and the polymeric material swells and drug molecules start to move out from the system through diffusion (Landgraf *et al*., 2005).

The most widely used model to describe diffusion controlled drug release systems is the Higuchi models (Higuchi, 1961). Although drug release may follow mixed mechanisms, in diffusion controlled mechanism diffusion is the rate limiting step (Huang and Brazel, 2001).

*2.5.1.2 Erosion/degradation controlled mechanism*

In this mechanism, drug release is by polymer degradation or erosion. Degradation describes the polymer chain/bond cleavage reaction which is a chemical process, whereas erosion refers to loss of polymer material (chemical and physical processes) (Kanjickal and Lopina, 2004).

Erosion can either be surface (heterogeneous) or bulk (homogeneous) erosion. Polymer systems with highly reactive functional groups undergo faster degradation than diffusion of water into it, leading to surface erosion (heterogeneous), while degradation of polymer with less reactive

groups (e.g. poly (lacitide-co-glycolide) (PLGA)) is much slower than diffusion of water into it, leading to bulk or homogeneous erosion (Kanjickal and Lopina, 2004). Factors influencing the biodegradation kinetics of the selected polymers are the chemical structure, size, shape, chain defects, ion exchange, ionic strength, pH, morphology (amorphous, semi-crystalline, crystalline, microstructure and residual stress), mechanism of degradation (enzymatic, hydrolysis or microbial) molecular weight distribution, route of administration, and site of action (Badri *et al*., 2014). If degradation is relatively rapid, then the swelling state of the network may change during the release process, and a complex interplay between swelling and diffusion will determine the release kinetics (Siegel and Rathbone, 2012).

Drug release mechanism for biodegradable material (e.g. SA, polylactic acid (PLA) and PLGA) are mainly through bulk erosion (Biondi *et al*., 2008). However, it has been shown that the release rate from such materials are not simply driven by degradation in earlier stage, the concentration gradient and shape of the device seem to have more profound impact on the release rate, while in the later stage, degradation becomes the dominant driving force (Biondi *et al*., 2008).

Furthermore, polysaccharides also undergo dissolution in aqueous medium as result of solvent penetration effect, polymer swelling and polymer chain disentanglement and relaxation. For this reason, release mechanism for polysaccharide-based materials could be driven by diffusion and/or erosion (Bonacucina *et al*., 2009). In general, water soluble drugs are mainly released by diffusion, while self-erosion is the principal release mechanism for low water soluble drugs (Singhvi and Singh, 2011).

#### *2.5.1.3 Swelling controlled mechanism*

Swelling controlled systems consist of water soluble drugs dispersed in glassy polymer matrix. During swelling, there is uptake of water by a polymer system which leads to increase in volume and formation of gel layer in which the dissolved drug can be transported due to increased mobility of the polymeric chain. The drug release kinetics for this system can be modified by the gel layer thickness and the rate at which it is formed (Kanjickal and Lopina, 2004). As the proportion of the polymer increases, the gel formed reduces diffusion of the drug and delays erosion of the matrix (Ford *et al.*, 1985).

Swelling dynamics are often complex and a variety of temporal release patterns are observed under swelling controlled system (Siegel and Rathbone, 2012).

### 2.5.2 Drug release models

In 1897, Noyes and Whitney developed an equation which formed the fundamental evaluation of the kinetics of drug release. This equation is known as Noyes-Whitney's Rule, and is stated as (Noyes and Whitney, 1987):

$$\frac{dM}{dt} = KS\,(C_s - C_t) \qquad (2.14)$$

Where M is the mass the transferred with respect to time, t, by dissolution from the solid particles of instantaneous surface, S, under the effect of prevailing concentration driven force ($C_s$- $C_t$), where $C_t$ is the concentration at time t, and $C_s$ is the equilibrium solubility of the solvent at the expected temperature. The rate of dissolution $\frac{dM}{dt}$ is the amount dissolved per unit area per unit time.

Using the Noyes-Whitney Rule, it can be seen that the rate of dissolution can be modified by altering the particle size, and the surface area of the solid. The rate of dissolution can also be changed by choosing a suitable polymorphs of the delivery system as crystalline forms dissolve slower than amorphous (Noyes and Whitney, 1987). The drug release kinetics is influenced by the nature of the drug such as its polymorphic form, crystallinity, particle size, solubility, and its amount in pharmaceutical dosage form (Singhvi and Singh, 2011).

According to Dash *et al.* (2010), and Shaikh *et al.* (2015), mathematical modelling in drug delivery system is important for the following reasons:

i. It helps to predict *in vivo* performance from the in vitro data by rational development of controlled release formulations.
ii. Mathematical modelling enables the prediction and optimization of release kinetics before the release system is realized.
iii. It enables new drug delivery systems to be designed using the general release expression.
iv. It enables the determination of physical mechanism of drug transport from the release data.
v. It enables prediction of the effect of particles parameters, for example, shape, size and composition on the overall release rate.
vi. It ensures improvement of therapeutic efficacy by modification of the release profile.
vii. It helps in the reduction on the amount of time required for drug design experiments.

The following models are commonly used to evaluate drug release data: zero order model, first order model, Higuchi model, Korsmeyer-Peppas model (power law), and Hixson – Crowell's model.

*2.5.2.1 Zero order release model*

The zero order release model describes the system where drug release rate is independent of its concentration. It releases the same amount of drug per unit time without depending on the initial concentration of drug (Dash *et al*., 2010; Singhvi and Singh, 2011; Yadav *et al.*, 2013).

The zero order equation is stated as:

$$Q_t = Q_0 + K_0 t \quad (2.15)$$

Where $Q_t$ is the quantity released at time t, $Q_0$ is the initial quantity of drug and $K_0$ is the zero order release constant. A plot of $Q_t$ versus t gives a straight line that passes through the origin. Controlled delivery systems that can provide zero order drug delivery have the potential for maximizing efficiency while minimizing dose frequency and toxicity (Yadav *et al.*, 2013).

*2.5.2.2 First order release model*

This was first applied for drug dissolution studies by Gibaldi and Feldman in 1967 and later by Wagner in 1969 as reported by Chime *et al*., (2013). A system in which the release rate is proportionally dependent on concentration is described as first order system. A first order equation is given as:

$$\text{Log } C = \text{Log}C_0 - \frac{Kt}{2.303} \quad (2.16)$$

where C is the concentration at time t, and $C_0$ is the initial concentration, and K is the first order constant. A plot Log C Vs t gives the slope as $\frac{k}{2.3.3}$ and y intercept as $\text{Log}C_{0.}$

*2.5.2.3. Higuchi model*

Higuchi model is used to study the release of both hydrophilic and hydrophobic drugs from semi solid and/or solid matrices. It was proposed and first used by Higuchi to describe the dissolution of drugs in ointments suspensions (Higuchi, 1961). Its use however, has been extended to other types of dissolution from other pharmaceutical dosage forms. The Higuchi equation is given as:

$$Q = A\sqrt{D(2C - C_s)C_s}t \quad (2.17)$$

Where Q is the amount of drug released in time t, A is the area of the matrix, D is the diffusivity of the drug (diffusion coefficient), $C_s$ is the drug solubility in the matrix media.

Where the drug concentration in the matrix is lower than its solubility and release occurs through pores in the matrix.

$$Q = \sqrt{\frac{D\delta}{\tau}(2C - \delta C_s)C_s t} \quad (2.18)$$

$\delta$ is the porosity of the matrix and $\tau$ is the tortuisity of the matrix.

A simplified Higuchi model is given as:

$$Q = K_H\sqrt{t} \quad (2.19)$$

$$\text{Log } Q = \text{Log}K_H + \frac{1}{2}\text{Log}t$$

where $K_H$ is called Higuchi constant.

According to Dash *et al*. (2010), Higuchi model is based on the following assumptions:

i. Initial drug concentration in the matrix is much higher than drug solubility.
ii. Drug diffusion takes place only in one dimension (edge effect must be neglected).
iii. Drug particles are much smaller than system thickness.
iv. Matrix swelling and dissolution are negligible.

v. Drug diffusivity is constant.

vi. Perfect sink conditions are always attained in release environment.

The classical Higuchi equation was derived under pseudo-steady state assumptions which are not valid for most controlled drug delivery systems; however due to its extreme simplicity, Higuchi equation is often used to analyse experimental drug release data, to get a rough idea of the underlying release mechanism (Siepmann and Peppas, 2001).

In addition to the Higuchi classical equation, proportionality between the fraction of drug released and square root of time can also be derived from Fick's second law of diffusion. Because diffusion is the dominant mechanism in both cases, a proportionality between the cumulative amount of drug released and square root of time is commonly regarded as an indicator of diffusion controlled release. Diffusion controlled process dominates when the slope of the graph of log Q versus Log t approaches 0.5 (Siepmann and Peppas, 2001).

*2.5.2.4 Korsmeyer-Peppas model*

The Korsmeyer-Peppas model, also known as power law, is more comprehensive than the Higuchi equation, but still very simple and semi empirical equation to describe drug release from polymeric systems. It was Korsmeyer and Peppas who first gave an introduction into the use and limitation of this law (Peppas, 1985; Peppas and Korsmeyer, 1986).

The Korsmeyer-Peppas equation is given as:

$$\frac{M_t}{M_\infty} = Kt^n \qquad (2.20)$$

$$\log\frac{M_t}{M_\infty} = \log K + n\log t$$

where $M_t$ is the amount of drug released at time t, and $M_\infty$ is the amount of drug loaded. The value of the exponent n is used to indicate the type of release mechanism, where K is a constant which depends on diffusion coefficient and thickness of the film (Siepmann and Peppas, 2001).

From Equation 2.20, when n becomes 1, the drug release is independent of time corresponding to zero order release kinetics. Zero order release kinetics is referred to as case 11 transport in polymer science. Case 11 transport indicates swelling-controlled drug release. When n = 0.5, the equation coincides with the Higuchi equation indicating diffusion controlled drug release. Values of n between 0.5 and 1.0 indicate superposition of both phenomena (anomalous transport). These values are for slab geometry and vary slightly for spheres and cylinders as can be shown in the table below (Ritger and Peppas, 1987; Siepmann *et al*., 1999):

Table 2.1: Exponent n of the Korsmeyer-Peppas law and drug release mechanisms from delivery systems of different geometry

| Exponent (n) | | | Drug release mechanism |
|---|---|---|---|
| Thin film | Cylinder | Sphere | |
| 0.5 | 0.45 | 0.43 | Fickian diffusion |
| 0.5<n<1.0 | 0.45<n<0.89 | 0.43<n<0.85 | Anomalous transport |
| 1 | 0.89 | 0.85 | Case 11 transport |

In order to find out mechanism of drug release from polymeric system, 60% of drug release data is fitted into Korsmeyer-Peppas model (Dash *et al*., 2010).

*2.5.2.5 Hixson-Crowell model*

Hixson-Crowell model assumes that the release rate is limited by the dissolution rate of the drug particles and not by the diffusion of the drug through the drug carrier. Consequently, in the model Hixson and Crowell (1931) recognized that the particles regular area is proportional to the cube root of its volume and proposed the following equation model:

$$W_t^{\frac{1}{3}} = W_0^{\frac{1}{3}} - Kt \qquad (2.21)$$

Where $W_t$ is the weight (mg) of the drug released at time t, $W_0$ is the initial amount (mg) in the release material, and K is a constant.

*2.5.2.5 Hopfenberg model*

This model correlates the release of drug from eroding surface of polymers and polymer-based materials. Surface area remains constant during the degrading process. Assumption of this model is that the rate limiting step of release of drug is the erosion of the matrix itself and that time dependent diffusion resistance internal or external to the eroding matrix do not influence it.

$$\frac{M_t}{M_\infty} = 1 - [1 - \frac{K_0 t}{C_0 a_0}]^n \qquad (2.22)$$

Where $M_t$ is the amount of drug released at time t, $M_\infty$ is the amount of drug loaded, $K_0$ is the erosion rate constant, $C_0$ is the initial concentration of the drug in the matrix, $a_0$ is the initial radius of the particle and n denotes the geometry (Shaikh *et al*., 2015)

Other mathematical models used in drug release study include, Weibul model, Gompertz model, Ritger-Peppas model, Baker Landsdale model.

## 2.6 Cancer Therapeutics

### 2.6.1 Cancers

Cancer was first described in an Egyptian Papyrus sometimes around 1600 BC (Wu *et al*., 2006). Normal cells grow and divide to form new cells based on the body's need while old cells die and are replaced by new cells (National Cancer Institute, 2015). However, according to Kakde *et al*. (2011), some chemical agents known generally as carcinogens, or infectious organisms can trigger uncontrolled/unregulated cell growth, leading to a situation known as cancer.

The cancer-causing agents affect two classes of genes the proto-oncogene and tumour suppressor gene. The proto-oncogene is a gene that code for protein that stimulates cell division. Cancer-causing agents convert this gene to the mutated form known as oncogene, which does not have the code for protein that stimulates cell division. Tumour suppressor genes, on the other hand, lose their ability to inhibit cell division. There is abnormal growth of cells due to these losses of normal cell functions (control over cell cycle and normal DNA replication) (Kakde *et al*., 2011).

Cancer progresses in different stages. The uncontrolled growth of cells leads to formation of primary tumours, then secretion of various growth factors which induces abnormal growth of blood vessels (angiogenesis), which subsequently gives way to spread of cancer cells (metastasis) to other distant part of the body where they establish secondary tumour sites (Kakde *et al*., 2011).

Many cancers form solid tumours, which are an abnormal mass of tissues. Solid tumours may be benign (not cancer), or malignant (cancer). Cancers of the blood such as leukaemia generally do not form solid tumours. Examples of solid tumours are sarcoma, carcinoma, and lymphomas. These are named based on type of cells that form them (NCI, 2015).

### 2.6.2 Enhanced permeability and retention effect (EPR)

Active targeting to tumour tissues involves either the use of tumour associated antigens (antigens that present in both normal and cancer cells, but predominate in cancer cells), or tumour specific antigens (antigens that can only be found in tumour tissues). Upon binding of the ligand, the ligand-receptor complex is internalized via receptor mediated endocytosis (Bertrand *et al*., 2013). Progress with this approach was relatively slow, until Maeda *et al.*, (1986) discovered the phenomenon of Enhanced Permeability and Retention Effect (EPR Effect).

Solid tumours possess unique pathological characteristics absent in normal tissues. Prominent among these peculiarities of tumour tissues are leaky (wide fenestrations) and irregular vasculature, decreased or absence of lymphatic drainage, high proportion of proliferating endothelial cells, cytokine-rich and hypoxic environment. Matsumera and Maeda (1986), discovered that due to the leaky vasculature and low lymphatic drainage, macromolecular drug delivery system can preferentially accumulate by passive retention mechanism in tumours even in the absence of targeting ligands. This is referred to as enhanced permeability and retention effect (EPR effect).

The pore size in solid tumour vasculature vary from 100 nm to 760 nm, which is much larger than that of the normal tissue where the gaps are usually less than 6 nm (Drummond *et al*., 1999). Experiments using liposome of different mean sizes suggest that the threshold vesicle size

for extravasations into tumour is ~ 400 nm (Yuan, 1995). This is in conformity with the result by Hobb's *et al* (1998). However, Couvreur and Vanthier (2006) reported that particles with size <200 nm are more effective.

Since the discovery of EPR effect, much progress has been made in the development of drug delivery system for tumour tissues and then tumour cells. This is because EPR effects tend to limit the drug only to tumour sites. In the words of Maeda *et al*., (2009) "traditional low-molecular weight anticancer drugs have very little tumour selectivity, and most such drugs are widely distributed to normal organs and tissues as well as tumours. Consequently, these anticancer drugs provide insufficient therapeutic benefits and cause severe systemic toxicity, a so-called dose-limited toxicity." This problem can be avoided by development of tumour selective anti-cancer agents (Maeda *et al*., 2013).

One of the major advantages of EPR based therapy over active targeting is the more universality of the EPR based approach, as it can be applied to wider tumour spectrum. In addition, epitopes of different tumours may be unidentified at early stage of diagnosis, a situation which limits the design of active-targeted therapy (Maeda *et al*., 2012).

Various researchers have confirmed evidence of EPR effect in solid tumours (Matsumura and Maeda, 1986; Maeda *et al*., 2009; Maeda and Matsumura, 2011; Rajora *et al*., 2014). It has also been shown that EPR effect is influenced by such factors as presence/absence of lymphatic, size, type, and location of tumour, patient characteristics such as age, gender, and body weight (Duncan *et al*., 2013). To ensure improved drug delivery in clinical setting, the delivery system is often augmented with some identified permeability factors that facilitate extravasations such as bradykinin, NO, and prostaglandins (Maeda *et al*., 2012).

### 2.6.3 Stealth characteristics

In order to fully exploit the EPR effect, the nano-vehicle should be able to have prolonged circulation in the blood stream (Salmaso and Caliceti, 2013). However, following intravenous injection, nanoparticles can be rapidly cleared from the blood by the mononuclear phagocytic system (also known as the reticuloendothelial system, (RES)) (Man *et al*., 2012). Clearance by the RES is preceded by opsonisation. The particle size, hydrophobicity, surface charge and composition of the system influence the clearance profile of the system by the RES of the body (Kakde *et al.,* 2011). This is because in the blood stream, opsonins interact with nanoparticles by Van der Waal's, electrostatic, ionic, and hydrophobic/hydrophilic forces. Hydrophobic and charged particles undergo higher opsonisation compared with hydrophilic and neutrally charged particles (Carstensen *et al,* 1992; Roser *et al*., 1998).

In order to endow nanosystems with long circulation properties, new technologies aimed at the surface modification of their physicochemical features have been developed. These are called stealth nanocarriers. The ability of nanoparticles to evade immune recognition so as to enhance their circulation time in vivo and thereby their chance of reaching the target is called 'stealth characteristics' (Encyclopaedia of Nanoscience and Nanotechnology, 2005). Stealth nanocarriers can be obtained by polymeric coating (Salmaso and Caliceti, 2013). It is now recognized that long circulating nanocarriers, "stealth" systems, can be obtained by surface coating with hydrophilic polymers that prevent the opsonisation process (Moghimi *et al*., 2001; Yan *et al*., 2005). Stealth nanocarriers are invisible to the biological system involved in clearance of particles from the bloodstream, namely the RES and Kupffer cells.

### 2.6.4 Multidrug resistance

One of the biggest challenges in cancer treatment with chemotherapy is the acquisition of drug resistance by the cancer cells. Cancer cells often develop multiple resistances to different functionally unrelated drugs. This is known as multi-drug resistance (Gottesman, 2002). Cancer multi-drug resistance is defined as the cross resistance or insensitivity of cancer cells to the cytostatic or cytotoxic actions of various anticancer drugs, which are structurally or functionally unrelated and have different molecular targets (Gottesman, 1993).

The two mechanisms involved in cancer drug resistance are classified as cellular and non-cellular mechanisms. The non-cellular mechanism can occur in one or more of the following ways: reduced access of the drug to tumour cells due to poorly vascularised nature of tumour regions; ionization of basic drugs in acidic environment of the tumour which prevent their diffusion across cellular membrane (the pH around tumour tissues in the body is more acidic (~5.5 – 6.5), relative to physiological pH which is 7.4 (Magadala *et al*., 2008); reduced extravasations of drug molecules due to high vascular pressure and low microvascular pressure of the tumour site (Kakde *et al*., 2011).

Cellular mechanism involves a plasma membrane protein known as p-glycoprotein (P-gp). P-gp which is over-expressed in tumour tissues is capable of binding to the drug molecules, forms trans-membrane channels and pumps the drug molecules out of the cell using energy of the ATP hydrolysis (Kakde *et al*., 2011). In addition, after repeated treatments, surviving cancer cells can undergo some genetic mutation leading to acquisition of resistance to the drug.

The most common mechanism of multi-drug resistance is the over-expression of the drug efflux pump (P-gp) (Hu and Zhang, 2009). Krishna and Mayer (2000), has proposed co-administration

of P-gp inhibitor with nanoparticles encapsulated anticancer drugs as a way of preventing P-gp mediated multi-drug resistance. Another approach is the use of combination therapy. Combination chemotherapy is the administration of multiple agents that have different mechanism of action. The multiple agents used must work synergistically (Kogashiwa and Kohno, 2013). The compounds having the ability to reverse resistance against anticancer drugs are called MDR inhibitor, chemosensitizer, or MDR modulators (Kellen, 2003).

### 2.6.5 Overview of the anticancer drugs –DOX and MTX

Doxorubicin hydrochloride, an anthracycline derivative isolated from Streptomyces *Peucetius Var. Caesius,* is a highly effective anti-neoplastic agent. Doxorubicin hydrochloride is successfully used, mostly against ovarian cancer, Multiple Myeloma and Kaposi Sarcoma, The mechanism of action of Doxorubicin hydrochloride was that it interact with DNA by intercalation and inhibition of macro-molecular biosynthesis, this inhibits the progression of the enzyme topoisomerase-II, which relaxes super coils in DNA transcription. The main side effects of this drug are cardiac toxicity, Infusion reactions and Myelosupression (Konda *et al*., 2013)

Methotrexate (MTX) is a chemotherapy agent and immune system suppressant. It is used to treat cancer, autoimmune diseases, ectopic pregnancy, and for medical abortions. Type of cancers it is used for include breast cancer, leukemia, lung cancer, lymphoma, and osteosarcoma. MTX is an antimetabolite of the antifolate type. It affects cancer by competitively inhibiting synthesis dihydrofolate reducase, which consequently inhibits the synthesis of DNA, RNA, thymidylates, and proteins. Despite its importance, its use is limited by dose-dependent toxicity ranging from malaise, asthenia, to gastrointestinal and hepatic toxicity, and pancytopenia which can be fatal (Khan *et al*., 2010). MTX efficacy is also limited by its short plasma half-life (Yousefi *et al*., 2010).

Table 2.2: Physicochemical properties of DOX and MTX

| Property | MTX | DOX-HCl |
|---|---|---|
| Molecular formula | $C_{20}H_{22}N_8O_5$ | $C_{27}H_{29}NO_4$ |
| Molecular weight | 454.447 g/mol | 579.98 g/mol |
| Color | Yellow to orange | Orange red |
| Nature | Hydrated (8-10%) | Hygroscopic |
| Crystalline/amorphous | Crystalline powder | Crystalline powder |
| Melting point | 180°C to 189°C | 204°C – 205°C |
| pH | pH 7.0 - 7.9 in sterile solution | 0.5% solution has pH 4.0 to 5.5 |
| Odour | Odourless | Odourless |
| Stability | stable if solution is not strongly acidic or basic | Stable in solution having pH range 3.0 - 6.5 |

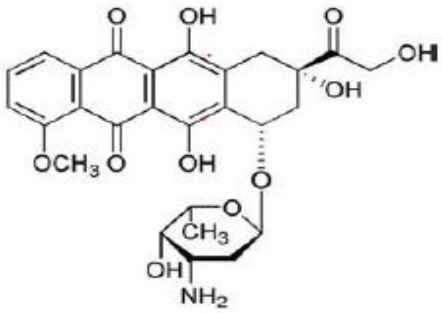

DOX

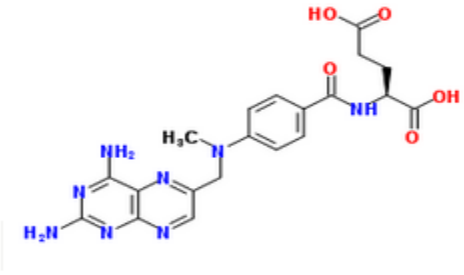

MTX

# CHAPTER THREE

## 3.0 MATERIALS AND METHODS

### 3.1 Materials

Distilled water was used for the preparation of all the solutions used in this work. SA was obtained from Fisher Scientific Company, USA, while the drugs DOX HCl and MTX were from Zuvius Lifescience Ltd and Pharma Aid respectively. All other reagents were of analytical grade and were used without further purification.

### 3.2. Preparation of Hydroxyapatite (HA)

3.2.1. Preparation of reagents

*3.2.1.1 Preparation of 0.06M diammonium hydrogen phosphate ($(NH_4)_2HPO_4$)*

Solution of diammonium hydrogen phosphate (0.06M) was prepared by carefully weighing 7.924 g of the diammonium hydrogen phosphate into a beaker. Distilled water was added with continuous stirring for complete dissolution. The solution was then quantitatively transferred into a 1 $dm^3$ volumetric flask, and made up to the mark using distilled water.

*3.2.1.2 Preparation of 0.1M calcium nitrate tetrahydrate ($(Ca(NO_3)_2.4H_2O)$)*

In order to prepare 0.1M calcium nitrate tetrahydrate, 23.615 g of the salt was carefully weighed into a 200 $cm^3$ beaker and dissolved completely with distilled water. The solution was quantitatively transferred into a 1 $dm^3$ volumetric flask and made up to the mark with distilled water.

*3.2.2 Procedure*

The moles of the calcium and phosphate precursors were chosen so as to maintain a Ca/P mole ratio of 1.67, the stoichiometric amount of HA **(**$Ca_{10}(PO_4)_6(OH)_2$). Aqueous solution of calcium nitrate tetrahydrate ($Ca(NO_3)_2.4H_2O$) (0.1M) (200 $cm^3$) was measured into a beaker and set on a magnetic stirrer. The prepared Diammonium hydrogen phosphate solution ($(NH_4)_2HPO_4$) (0.06M) (200 $cm^3$) was transfered into a burette. The phosphate solution was added drop by drop to the calcium nitrate solution with continuous stirring for 24 h after the phosphate addition**.** The pH was maintained at approximately 10.5 throughout the experiment using sodium hydroxide (1M). The suspension was then stored for 24 h at room temperature for aging, after which the precipitate was separated by centrifugation, and subsequently washed with distilled water thrice. The resulting gel-like paste was dried at 60$^oC$ for 24 h and then ground using agate mortar to obtain fine powder (Chandrasekar *et al*., 2013).

**3.3. Preparation of HASA Nanocomposites**

3.3.1 Preparation of reagents

*3.3.1.1 Preparation of sodium alginate (SA) solutions*

SA dissolves slowly in water. To prepare 1%wt of SA, 20 mg of SA was weighed in a 200 $cm^3$ beaker, and 100 $cm^3$ of distilled water added onto it. The mixture was stirred vigorously using magnetic stirrer for about 30 minutes for complete dissolution of SA. Exactly 110 mg, 520 mg, 1.04 g, and 2.14 g of the alginate were subsequently measured in order to prepare approximately 5%wt, 20%wt, 33%wt and 50%wt of the alginate in the nanocomposite (note: weight of HA synthesised using the concentration of the precursors stated in section 3.3.2 was approximately 2.14 g)

3.3.2 Procedure (first synthetic route)

The *in-situ* preparation of HA in the presence of SA was done according to the method by Rajkumar *et al.,* (2010**)** with some modifications. The calcium solution (200 $cm^3$) was added in drops to a separately prepared 100 $cm^3$ of SA solution (1%wt) while stirring vigorously. This mixture was set on a magnetic stirrer, and 200 $cm^3$ of 0.06M diammonium hydrogen phosphate solution ($(NH_4)_2HPO_4$) added into it drop by drop with continuous stirring. The stirring was continued for 24 h. The pH was maintained at approximately 10.5 throughout the experiment using 1 M sodium hydroxide. The suspension was then stored for 24h at room temperature for aging, after which the precipitate was separated by centrifugation, and subsequently washed with distilled water thrice. The resulting gel-like paste was dried at 60$^oC$ for 24 h and then ground using agate mortar to obtain fine powder (Chandrasekar *et al*., 2013).

The same procedure was repeated using varying quantities of SA (5%wt, 20%wt, 33%wt, and 50%wt).

3.3.3 Procedure (second synthetic route)

To investigate the effect of order of polymer addition, the procedure in section 3.3.2 was repeated but with first adding SA to the phosphate solution before drop-wise addition to the calcium solution. The prepared phosphate solution (200 $cm^3$ of 0.06M) was added in drop-wise manner to a 100 $cm^3$ separately prepared SA solution (1%wt) while stirring vigorously. The mixture was added drop by drop to 200 $cm^3$ aqueous solution of calcium nitrate tetrahydrate ($Ca(NO_3)_2.4H_2O$) (0.1M) prepared earlier with continuous stirring for 24 h**.** The pH was maintained at approximately 10.5 throughout the experiment using 1M sodium hydroxide solution. The suspension was then stored for 24h at room temperature for aging, after which the

precipitate was separated by centrifugation, and subsequently washed with distilled water thrice. The resulting gel-like paste was dried at 60$^{o}$C for 24 h and then ground using agate mortar to obtain fine powders. The procedure was repeated using varying quantities of SA (5% wt, 20% wt, 33% wt, and 50% wt).

## 3.4 Material Characterizations

### 3.4.1 Fourier transforms infrared spectroscopy (FTIR)

FT-IR analysis was conducted to identify the functional groups of the free and the drug-loaded HA and HASA samples. Infrared spectra in the wavenumber range of 650-4000 $cm^{-1}$ were recorded with Cary 630 Agilent Fourier Transform Infrared Spectrometer. The analyses were carried out with 8 scans at 16 $cm^{-1}$ resolution, applying transmittance method. The machine was operated in accordance with the manufacturers specifications

### 3.4.2 Scanning electron microscopy (SEM).

The HA and the nanocomposites containing different concentrations of SA were characterized using Scanning Electron Microscope (SEM) (PHENOM WORLD SEM Machine). The powdered samples were placed on standard aluminium specimen mounts (pin type) with double-sided adhesive electrically conductive carbon tape. The specimen mounts were then coated with 60% gold and 40% palladium for 30 seconds with 45 mA current in a sputter coater. The coated samples were then observed on the SEM using an accelerating voltage of 20 kV at a tilt angle of 30$^{o}$.

### 3.4.3 Image analysis

Image analysis of the particles was carried out using ImageJ software. The scale bar was used to convert the pixel unit of the image to nanometer units. The bandpass-filtered image was set to the lower and upper threshold values, segmenting the image into particles and background. The SEM micrograph was then binarised using watershed segmentation. The 'set measurement' was used to select relevant parameters for measurement; and the analysis was limited to threshold area, excluding particles on edges and structures with aberrant morphology.

An image analysis system could describe non-spherical particles using the Feret diameter, perimeter, projected area, spherical equivalent diameter, circularity and aspect ratio (ISO 9276-6: (2008):

Feret diameter: this is the longest distance between any two points along the particle boundary.

$$\text{Spherical equivalent diameter (SED)} = \sqrt{\frac{4A}{\pi}} \tag{3.1}$$

This is the diameter of a circle with the same area as the particle. Where A is the area of the particle.

$$\text{Perimeter (P)} = \frac{\pi}{N}\sum_{N}^{\pi} l_{\alpha}\, dL \tag{3.2}$$

This is the Cauchy-Crafton equation with $l$ as the number of intercepts formed by a series of parallel lines, with spacing dL, exploring N directions from $\alpha$ to $\pi$.

$$\text{Circularity (C)} = \sqrt{\frac{4\pi A}{P^2}} \tag{3.3}$$

where A is the area and P the perimeter of the particle. The values range from 0 to 1, the closer it is to unity the more spherical the particles. In order words, the further away from a perfectly round and smooth circle that a particle becomes, the lower the circularity value.

$$\text{Aspect ratio (A.R)} = \frac{\text{minor axis}}{\text{major axis}} \quad (3.4)$$

A.R is a dimensionless quantity and has been scaled by ISO 9276-6 (2008) to always be in the range $0 \geq A.R \leq 1$. Symmetric particles have high aspect ratio.

### 3.4.4 X-Ray powder diffraction analysis

The X-ray powder diffraction (XRD) patterns were measured on X-ray diffractometer Rigaku Ultima IV (reflection mode, Brag-Brentano arrangement, CuKα1 radiation) in ambient atmosphere under constant conditions (40 kV, 40 mA). The scanning range was $10^o - 70^o$, with scanning step of 0.02. The phases were identified by matching the patterns with Crystallography Open Database (COD-Inorg REV173445), and using FullProf program for Rietveld refinement.

The crystallite size was calculated using Scherrer equation (Equation 2.3). The strongest diffraction peak was used to calculate the crystallite size.

Microstrain was estimated using the Williamson-Hall method (Equation 2.7), while the degree of crystallinity ($X_c$) was calculated using the equation:

$$X_c = \left(\frac{0.24}{\beta}\right)^3 \quad (3.5)$$

The specific surface area (S) was calculated with the equation:

$$S = \frac{6\ x\ 10^3}{D\ x\ \rho} \quad (3.6)$$

Where $\rho$ is the theoretical density.

3.4.5 X-Ray fluorescence analysis

Elemental Analysis was carried out to ascertain the Ca/P ratio present in the nano-HA. The Energy Dispersive X-Ray Fluorescence was used for the analysis.

**3.5 Drug Loading Study**

3.5.1 Preparation of drug solutions

DOX: Lyophilized DOX HCl powder was used to prepare the solution. In order to prepare 2 mg/cm$^3$ of the drug, 100 mg of the powder was completely dissolved in 50 cm$^3$ beaker and quantitatively transferred to 50 cm$^3$ volumetric flask and then made up to mark with distilled water. The solution was used immediately after preparation.

MTX: Each vial of MTX injection BP contains 50 mg/2 cm$^3$ of MTX. To prepare 2 mg/cm$^3$, two vials containing a total of 100 mg of MTX were quantitatively transferred into a 50 cm$^3$ volumetric flask, and made up to mark. The solution was used immediately after preparation.

3.5.2 Preparation of drug-loaded hydroxyapatite

Drug loading was done according to the method by Raj *et al.*, (2013). In order to load the drugs on HA particles, 100 mg of the HA was added to 10 cm$^3$ of the drug solution (2 mg/ml) and stirred using magnetic stirrer for 40 min. Then the solution was left undisturbed overnight. The suspension was then centrifuged (2000 rpm, 5 min) and the supernatant and precipitate were separated. The amount of drug loaded was determined by finding the difference in the concentrations in the aqueous solution before and after loading. The drug encapsulation efficiency (EE) and loading capacity (LC) were evaluated by measuring the absorbance of the

supernatant using UV spectrophotometer. The wavelength of maximum absorbance ($\lambda_{max}$) for DOX (290 nm) and MTX (419 nm) were obtained by scanning a solution of the drugs with a UV spectrophotometer within the wavelength range of 200 nm to 600 nm. A series of standards were prepared which were used to construct a calibration curve.

The EE and LC of the nanoparticles were calculated according to the equations (Papadimitriou, *et al*., 2008):

$$E.E = \frac{W_t - W_f}{W_t} \quad (3.7)$$

$$L.C = \frac{W_t - W_f}{W_n} \quad (3.8)$$

Where $W_t$ represents the total amount (mg) of the drug; $W_f$ is the amount (mg) of free drug in the supernatant; and $W_n$ is the weight (mg) of the particles. All measurements was performed in triplicate and the mean value reported.

3.5.3 Preparation of drug-loaded HASA nanocomposites

Drug loading into HASA nanocomposites was similar to the method described above for HA (section 3.5.2).

## 3.6 Evaluation of Different Drug Loading Methods

3.6.1 Preparation of reagents

*3.6.1.1 Preparation of calcium chloride dihydrate solution ($CaCl_2.2H_2O$)*

Exactly 0.5513 g of calcium chloride dihydrate ($CaCl_2.2H_2O$) was measured and transferred into a 50 $cm^3$ beaker. Distilled water was added and stirred using glass rod until it completely

dissolved. The solution was then quantitatively transferred into a 100 $cm^3$ volumetric flask and made up to mark using distilled water.

*3.6.1.2 Preparation of 10 mg/$cm^3$ of sodium alginate solution*

SA solution (10 mg/$cm^3$) was prepared by measuring 5 g of SA into a 1000 $cm^3$ beaker. The beaker was placed on a magnetic stirrer and 500 $cm^3$ of distilled water introduced into it using measuring cylinder. The mixture was stirred continuously until a clear solution was obtained.

3.6.2 Procedures

Method 1 is the adsorption method which involved adsorbing the drug in already prepared nanocomposites, while methods 2, 3, and 4 are different modifications of incorporation methods. In method 2 the dried HA was cross-linked with SA in the drug solution using calcium chloride solution; in method 3 the HA was first incubated in the drug solution before the cross-linking stage; while in method 4 the freshly prepared HA was cross-linked with SA in the drug solution.

*3.6.2.1 Method 1*

This method is the traditional adsorption method previously described in section 3.5.2. Drug loaded HASA nanocomposite was prepared by agitating ex-situ prepared HA-SA nanocomposite (100 mg) in the drug solution for 1 hour. The nanocomposite /drug solution was then incubated for 12 hours after which the mixture was centrifuged and the drug-loaded nanocomposite recovered for drug release study.

*3.6.2.2 Method 2*

HA (90 mg) was weighed into a 5 $cm^3$ drug solution (2 mg/$cm^3$). SA solution (3 $cm^3$) having concentration of 10 mg/$cm^3$ was then added into the mixture. Solution (2 $cm^3$) of $CaCl_2$ (5.513 mg/$cm^3$) was then added in drops into the mixture with vigorous shaking. The shaking was

continued for 1 hour. The drug-nanocomposite solution was then incubated for about 12 hours at room temperature, after which the drug loaded nanocomposite was recovered by centrifugation.

*3.6.2.3 Method* 3

HA (90 mg) was shaken in a 5 $cm^3$ drug solution (2 $mg/cm^3$) for 1 hour and then incubated for another 6 hours at room temperature. 3 $cm^3$ of SA (10 $mg/cm^3$) was then added with shaking followed by drop wise addition of 2 $cm^3$ $CaCl_2.2H_2O$ (5.513 $mg/cm^3$). The shaking was continued for another 1 hour. The mixture was then incubated at room temperature for 6 hours and the drug-nanocomposite recovered by centrifugation.

*3.6.2.4 Method 4*

HA was prepared following the method by Chandrasekar *et al*., (2013)**.** The freshly prepared HA was re-dispersed in a 5 $cm^3$ drug solution. 3 ml of SA solution (10 $mg/cm^3$) was then added while stirring, followed by addition of 2 $cm^3$ of $CaCl_2.2H_2O$ (5.513 $mg/cm^3$) in drops. The mixture was shaken for 1 hour and allowed to stand for 12 hours. The drug-loaded nanocomposite was recovered by centrifugation.

## 3.7 Drug Release Study

3.7.1 Preparation of synthetic body fluid (Kokubo *et al.*, 1990)

For preparing 1 litre of Synthetic Body Fluid (SBF), the first five reagents were added according to the order given on Table 3.1 to 700 $cm^3$ deionized water in a 2 litre beaker with continuous stirring using magnetic stirrer. Preparation of 1 litre SBF requires 40 $cm^3$ of 1M HCl. Before the addition of the sixth reagent, 15 $cm^3$ of 1M HCl was added to the solution. Then sixth, seventh and eight reagents were added subsequently and the temperature was raised to 37$^oC$. The

remaining 25 $cm^3$ 1M HCl solution was added in drops until the pH was adjusted to 7.4 at 37$^oC$. Deionized water was added to make it up to 1000 $cm^3$. The prepared SBF was stored in a refrigerator to avoid degradation before use.

**Table 3.1**: The composition of the reagents required to prepare 1Litre of SBF

| Order | Reagent | Amount (g) |
|---|---|---|
| 1 | Sodium chloride (NaCl) | 6.546 g |
| 2 | Sodium bicarbonate ($NaHCO_3$) | 2.268 g |
| 3 | Potassium chloride (KCl) | 0.373 g |
| 4 | Disodium hydrogen phosphate dehydrate ($Na_2HPO_4$).$2H_2O$ | 0.178 g |
| 5 | Magnesium chloride ($MgCl_2$).$6H_2O$ | 0.305 g |
| 6 | Calcium chloride dehydrate ($CaCl_2$).$2H_2O$ | 0.368 g |
| 7 | Sodium sulphate ($Na_2SO_4$) | 0.071 g |
| 8 | Tris(hydroxymethyl)aminomethane $(CH_2OH)_3CNH_2$ | 6.057 g |

3.7.2 In-vitro drug release study

The *in vitro* drug release study was carried out following a method reported by Sivakumar and Rao, (2002). In order to determine the drug release profile, 100 mg each of the drug loaded nanocomposite and drug loaded HA were introduced into a screw capped glass bottle containing 50 $cm^3$ of synthetic body fluid (SBF) medium at 37$^oC$ and pH 7.4 under sterile conditions. Aliquots of 5 $cm^3$ samples were withdrawn by a pipette at regular intervals and replaced immediately with 5 $cm^3$ of fresh SBF medium (this was accounted for when calculating the

amount released). Drug concentrations in the collected samples were measured using UV-VIS Spectrophotometer.

The quantity of the drug released at any time $Q_t$ was calculated using the equation:

$$Q_t = C_t V_T + v\sum_{i=1}^{n-1} C_{ti} \quad (3.9)$$

where $Q_t$ is the quantity of drug (mg) released at the time point t; $C_t$ is the concentration (mg/cm$^3$) at time t, $V_T$ is the total volume (cm$^3$) of the release medium, v is the volume (cm$^3$) of the sample, $\sum_{i=1}^{n-1} C_{ti}$ is the summation of C from i = 1 to n-1, and i is the nth sample. The second part of the right hand side of the equation, $v\sum_{i=1}^{n-1} C_{ti}$ is the volume correction, used to account for the amount of the drug discarded at every sampling point.

while the percent cumulative release (%$Cr_t$) at any time point t is:

$$\%Cr_t = \frac{Q_t}{Q_T} \times 100 \quad (3.10)$$

Where %$Cr_t$ is the percent cumulative release at time t (h), and $Q_T$ is the quantity of the drug (mg) encapsulated into the material.

3.7.3 Comparison of drug release profiles

A release profile is a measurement of *in vitro* drug release from a preparation in receptacle media over a period of time. Similarities between the different release profiles were investigated using model-independent approach. Pairwise procedures were followed, while similarity factor ($f_2$) and the difference factor ($f_1$) were chosen for comparison (Zhang *et al.*, 2010)

$$f_1 = \{\frac{\sum_{t=1}^{n} |R_t - T_t|}{\sum_{t=i}^{n} R_t}\} \times 100 \quad (3.11)$$

$$f_2 = 50 \text{ x } \log\{[1 + \frac{1}{n}\sum_{t=1}^{n}(R_t - T_t)^2]^{-0.5} \text{ x } 100\} \quad (3.12)$$

where n is the number of time points and $R_t$ and $T_t$ are the average percentage of drugs released in reference and test products respectively at time t. The value of $f_2$ falls between 0 and 100, and two profiles are considered to be similar when $f_2$ ranges between 50 and 100 (Zuo *et al*., 2014). $f_1$ is zero when the test and reference profiles are identical and increases proportionally with the dissimilarity between the two profiles. $f_1$ values above 15 are considered dissimilar (Moore and Flanner, 1996)**.**

In order to reduce calculation time and eliminate calculation errors, DDSolver program (excel plug-in program) was used for the calculations.

3.7.4 Drug release kinetics and mechanistic study

In order to elucidate the release kinetics and the mechanism of drug release, the data was fitted into zero order model (Equation 2.15), first order model (Equation 2.16), Higuchi model (Equation 2.19), Korsmeyer-Peppas model (Equation 2.20), Hixon-Crowel model (Equation 2.21), and Hopfenberg model (Equation 2.20). This was done using a combination of DDSolver software and excel sheet.

**3.8 Preparation of HASA Nanocomposite in Different Solvents**

It is known that solvents have substantial effect on reaction. Effect of using different solvents in the preparation of HASA was evaluated. Based on toxicity profiles, water, ethanol, ethylacetate and acetone were selected for this study.

Calcium nitrate tetrahydrate solutions (400 $cm^3$) prepared in different solvents (water, ethanol, ethylacetate, and acetone) were separately added in drop-wise manner to different SA aqueous solutions (100 $cm^3$) (50%wt) while stirring vigorously. The temperature of the one prepared in acetone solution was raised to above 37$^oC$. This mixture was set on a magnetic stirrer, and 50 $cm^3$ of 0.06 M diammonium hydrogen phosphate aqueous solution ($(NH_4)_2HPO_4$) added onto it drop by drop with continuous stirring. The stirring was continued for 24 h. The pH was maintained at approximately 10.5 throughout the experiment using 1 M sodium hydroxide. The suspension was then stored for 24 h at room temperature for aging, after which the precipitate was separated by centrifugation, and subsequently washed with distilled water three times. The resulting gel-like paste was dried at 60$^oC$ for 24 h and then ground using agate mortar to obtain fine powders. The nanocomposites were then used for drug loading and release study as previously described (section 3.5.2 and 3.7.2 respectively).

### 3.9 Investigation of the Effect of Release Medium pH on Drug Release Profiles

Before the release study was carried out, freshly synthesised synthetic body fluid media were divided into three parts and the pH adjusted to 7.4, 5.0 and 3.0 respectively using 1M HCl. Drug release studies were then carried out in each of them as previously described (section 3.7.2).

### 3.10 Drug Combination Study

Studies have shown that ratiometric dosing (controlling drug ratios following systemic administration) of anticancer drug combinations can profoundly influence therapeutic outcomes (Meyer *et al*., 2006). In this study, different drug combination ratios were used to evaluate the suitability of the nanocomposites for combination therapy. The drugs were mixed in a

combination ratio (DOX: MTX) of 16:1, 4:1, 1:1, 1:4, and 1:16. The drugs were loaded simultaneously following adsorption method described earlier (section 3.5.2).

Series of standards were prepared for both drugs and the absorbance taken at both wavelengths of maximum absorbance for DOX (290 nm) and MTX (419 nm). Calibration graphs were plotted for the two drugs at both wavelengths. This is because absorbance is additive. Drug loading and release were evaluated by taking the absorbance of the supernatant at both wavelengths and solving simultaneously to obtain the concentrations of the two drugs in the solution.

# CHAPTER FOUR

## 4.0 RESULTS

### 4.1 Fourier Transform Infra-Red (FTIR) Spectra Analysis the Free and the Drug-Loaded Samples

The spectrum of SA (Figure 4.1) exhibited peaks at 3236.3 $cm^{-1}$ attributed to O-H stretching mode, 2922.2 $cm^{-1}$ due to C-H asymmetric stretching, 1297.1 $cm^{-1}$ and 887 $cm^{-1}$ due to C-H in-plane and out-of-plane bending respectively. The peaks at 1595.3 $cm^3$ and 1405.2 $cm^3$ are due to $COO^-$ stretching vibrations, while peaks at 1103.3 $cm^{-1}$ and 1025 $cm^{-1}$ are due to C-O and C-O-C stretching vibrations. C-C stretching mode also absorbs here.

Characteristic peaks for HA were observed in the FTIR spectrum shown in Figure 4.1 and assignments of the observed peaks shown in Table 4.1. The peak at 3384.4 $cm^{-1}$ was due to O–H stretching vibration; the peak at 1640 $cm^{-1}$ attributed to O-H bending mode of absorbed water. The strong peaks at 1021.3 $cm^{-1}$ and 960 $cm^{-1}$ are due to asymmetric and symmetric stretching of $PO_4^{3-}$ respectively, while the weak peak at 2012.8 $cm^{-1}$ is due to its overtone and/or combination band. The observed peaks at 1453.7 $cm^{-1}$ and 1412.7 $cm^{-1}$ are due to asymmetric stretching mode of $CO_3^{2-}$, while the peak at 872.2 $cm^{-1}$ resulted from bending mode of $CO_3^{2-}$.

The peaks for HASA are at 3220.4 $cm^{-1}$, 2989.2 $cm^{-1}$, 1602.8 $cm^{-1}$, 1401.5 $cm^{-1}$, 1341.5 $cm^{-1}$, 1025 $cm^{-1}$ and 823.7 $cm^{-1}$.

Presented in Figure 4.2 are the FTIR spectra of drug-loaded HA and the nanocomposites while the assignment of the spectra is in Table 4.2. The results show the following peaks for MTX-loaded HA (HA-MTX): 3268.9 $cm^{-1}$ due to O-H stretching vibration overlapped with N-H

stretching mode, 1636.3 $cm^{-1}$ assigned to N-H bending mode, 1036.2 $cm^{-1}$ due to C-O stretch and $PO_4^{3-}$ from HA; MTX-loaded HA-SA (HASA-MTX) (3268.9 $cm^{-1}$, 1636.3 $cm^{-1}$, 1420.1 $cm^{-1}$, 1028.7 $cm^{-1}$); and DOX-loaded HA (HA-DOX), (2038.9 $cm^{-1}$, 1636.3 $cm^{-1}$ 1453.7 $cm^{-1}$, 1021.3 $cm^{-1}$ 875.9 $cm^{-1}$ 704.5 $cm^{-1}$). Prominent peaks for DOX-loaded HA-SA nanocomposite (HASA-DOX) spectrum (Figure 4.2) include the peaks at 3183.1 $cm^{-1}$ and 1408.9 $cm^{-1}$ due to O-H stretching vibration and in-plane bending respectively, 1595.3 $cm^{-1}$ due to $COO^-$ asymmetric stretching, and 1017.6 $cm^{-1}$ due to P-O asymmetric stretching.

### 4.2 Scanning Electron Microscope (SEM) Analysis

The scanning electron micrograph of HA at a magnification of x6000 is presented in Figure 4.3. The micrograph shows the morphology of the synthesized HA as irregularly shaped nano-sized particles. Also presented in Figures 4.4 – 4.8 are the SEM micrographs of the different formulations of the HASA nanocomposites. The micrographs show particles of irregular morphologies for all the compositions.

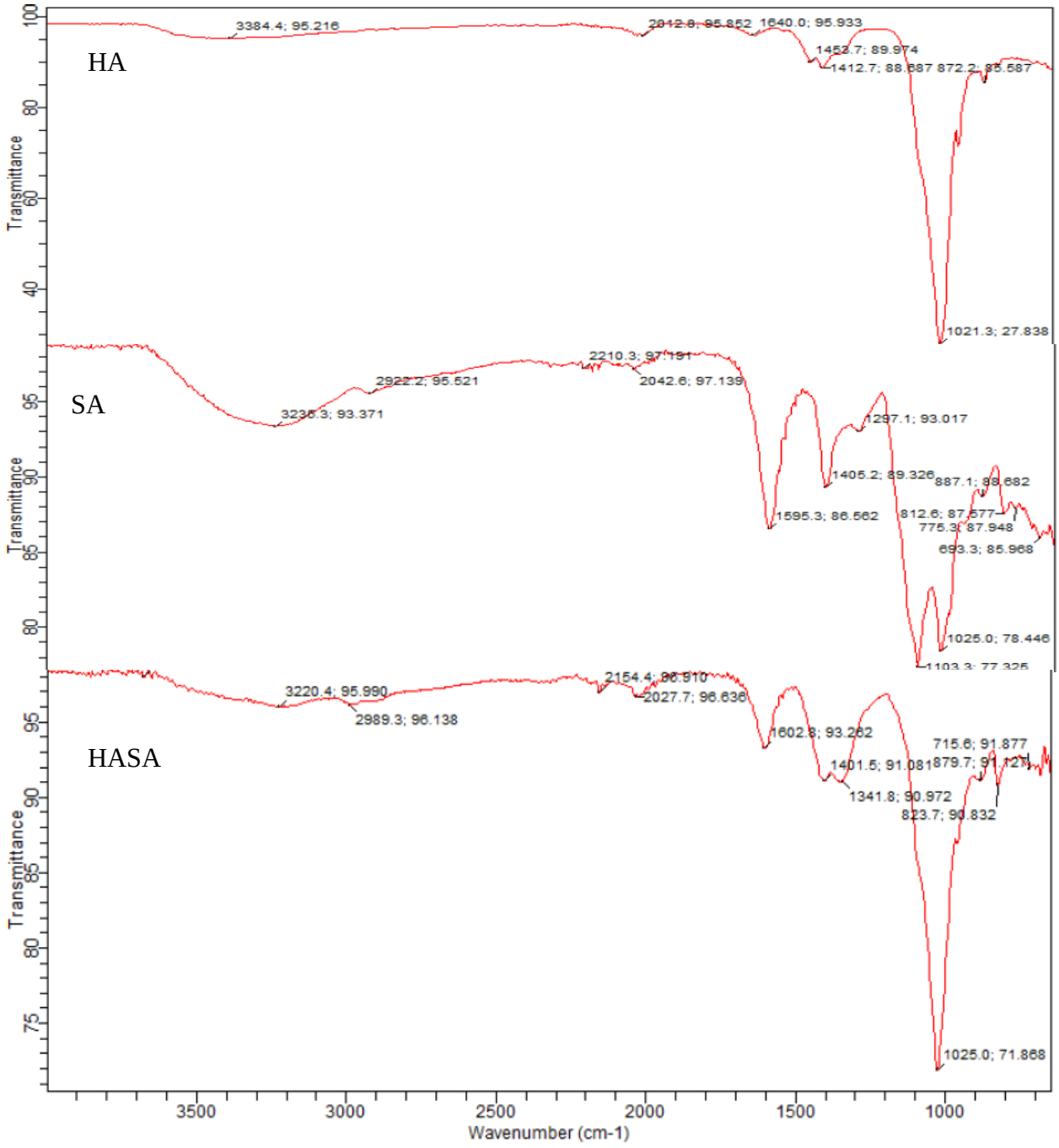


**Figure 4.1**: FTIR spectra of hydroxyapatite (HA), sodium alginate (SA), and hydroxyapatite-sodium alginate (HASA)

**Table 4.1**: Assignments of FTIR peaks of sodium alginate (SA), hydroxyapatite (HA), and hydroxyapatite-sodium alginate (HASA)

| Wavenumber ($cm^{-1}$) | Assignments |
|---|---|
| | **SA** |
| 3236.3 | O-H stretching, Hydrogen-bonded. |
| 2922.2 | Asymmetric C-H stretching |
| 2042.6 | Combination bands |
| 1595.3 | $COO^-$ stretching (asymmetric) |
| 1405.2 | $COO^-$ stretching (asymmetric) |
| 1297.1 | C-H in-plane deformation |
| 1103.3 | C-O, C-C, & C-O-C stretching |
| 1025 | C-O, C-C, & C-O-C stretching |
| 887.1 | C-H out-of-plane deformation |
| | **HA** |
| 3384.4 | O-H stretching vibration |
| 2012 | overtone and/or combinational bands of $PO_4^{3-}$ groups |
| 1640 | O-H bending mode of absorbed water |
| 1453.7 | $CO_3^{2-}$ asymmetric stretching |
| 1412.7 | $CO_3^{2-}$ asymmetric stretching |
| 1021.3 | asymmetric stretching of $PO_4^{3-}$ |
| 960 | $PO_4^{3-}$ symmetric stretching |
| 872.2 | $CO_3^{2-}$ asymmetric stretching |
| | **HASA** |
| 3220.4 | O-H stretching mode |
| 2989.3 | C-H asymmetric stretching |
| 2027.7 | overtone and/or combinational bands |
| 1602.8 | $COO^-$ stretching (asymmetric) |
| 1401.5 | $COO^-$ symmetric stretching |
| 1341.5 | COO-Ca vibrational mode |
| 1025 | C-O and $PO_4^{3-}$ asymmetric stretching |
| 823.7 | C-H bending mode |

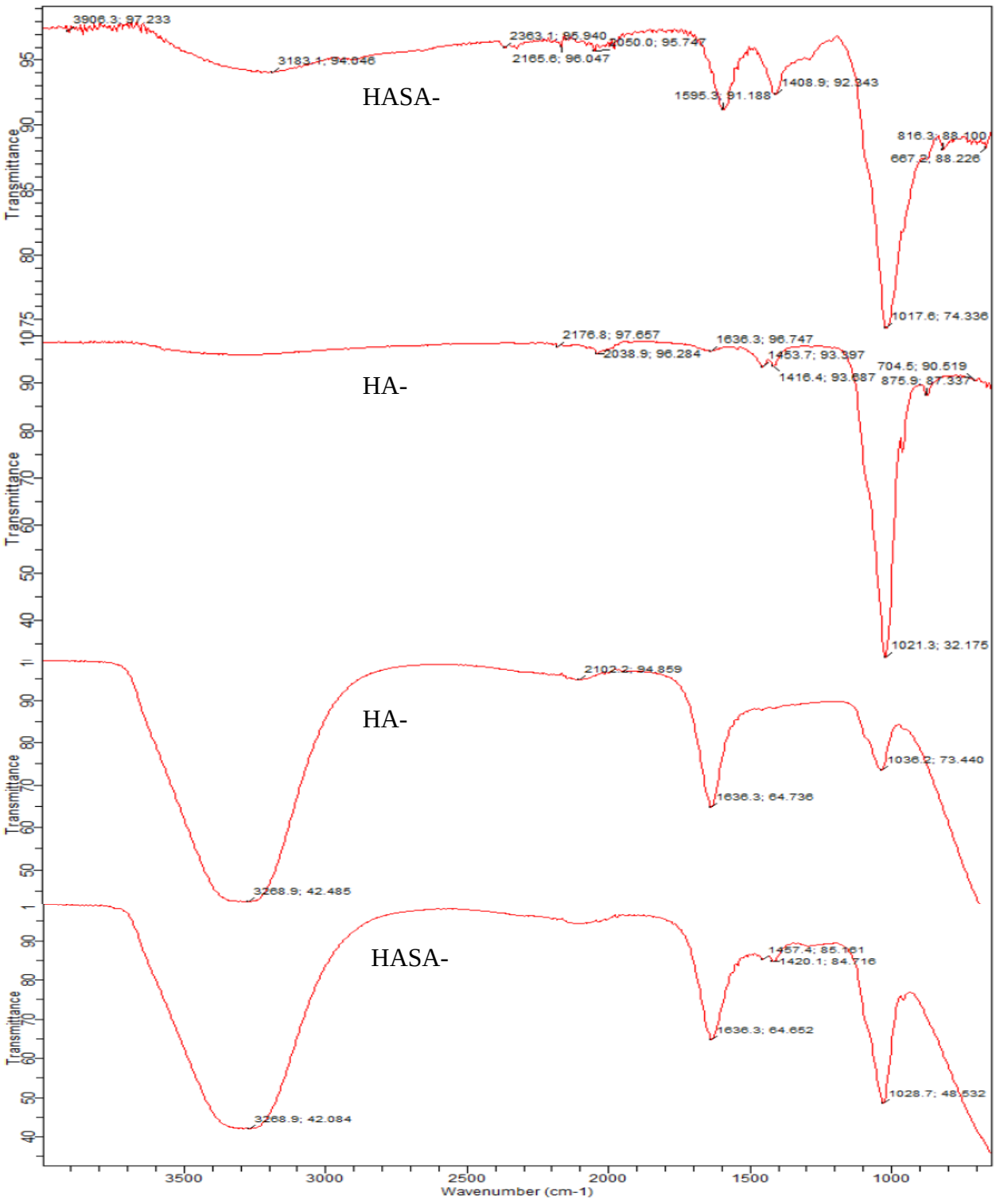


**Figure 4.2**: FTIR spectra of HASA-DOX, HA-DOX, HA-MTX, and HASA-MTX

**Table 4.2**: Assignments of FTIR peaks of drug-loaded HA and drug-loaded HASA nanocomposite

| Wavenumber ($cm^{-1}$) | Assignments |
|---|---|
| | **HA-DOX** |
| 2038.9 | overtone/combinational band |
| 1636.3 | N-H bending vibration |
| 1453.7 | CO asymmetric stretching |
| 1021.3 | asymmetric stretching of $PO_4^{3-}$ |
| 875.9 | $CO_3^{2-}$ stretching vibration |
| 704.5 | $NH_2$ out-of-plane wagging |
| | **HA-MTX** |
| 3268.9 | O-H stretching vibration/N-H stretch (3400-3250 $cm^{-1}$) |
| 1636.3 | $NH_2$ bending vibration |
| 1036.2 | C-O and $PO_4^{3-}$ stretch |
| | **HASA-DOX** |
| 3183.1 | O-H stretching vibration |
| 1595.3 | $COO^-$ asymmetric stretching |
| 1408.9 | O-H in-plane bending |
| 1017.6 | C-O and $PO_4^{3-}$ asymmetric stretching |
| | **HASA-MTX** |
| 3268.9 | O-H stretching |
| 1636.3 | $NH_2$ bending mode |
| 1420.1 | C-N stretch |
| 1028.7 | C-O and $PO_4^{3-}$ stretching vibration |

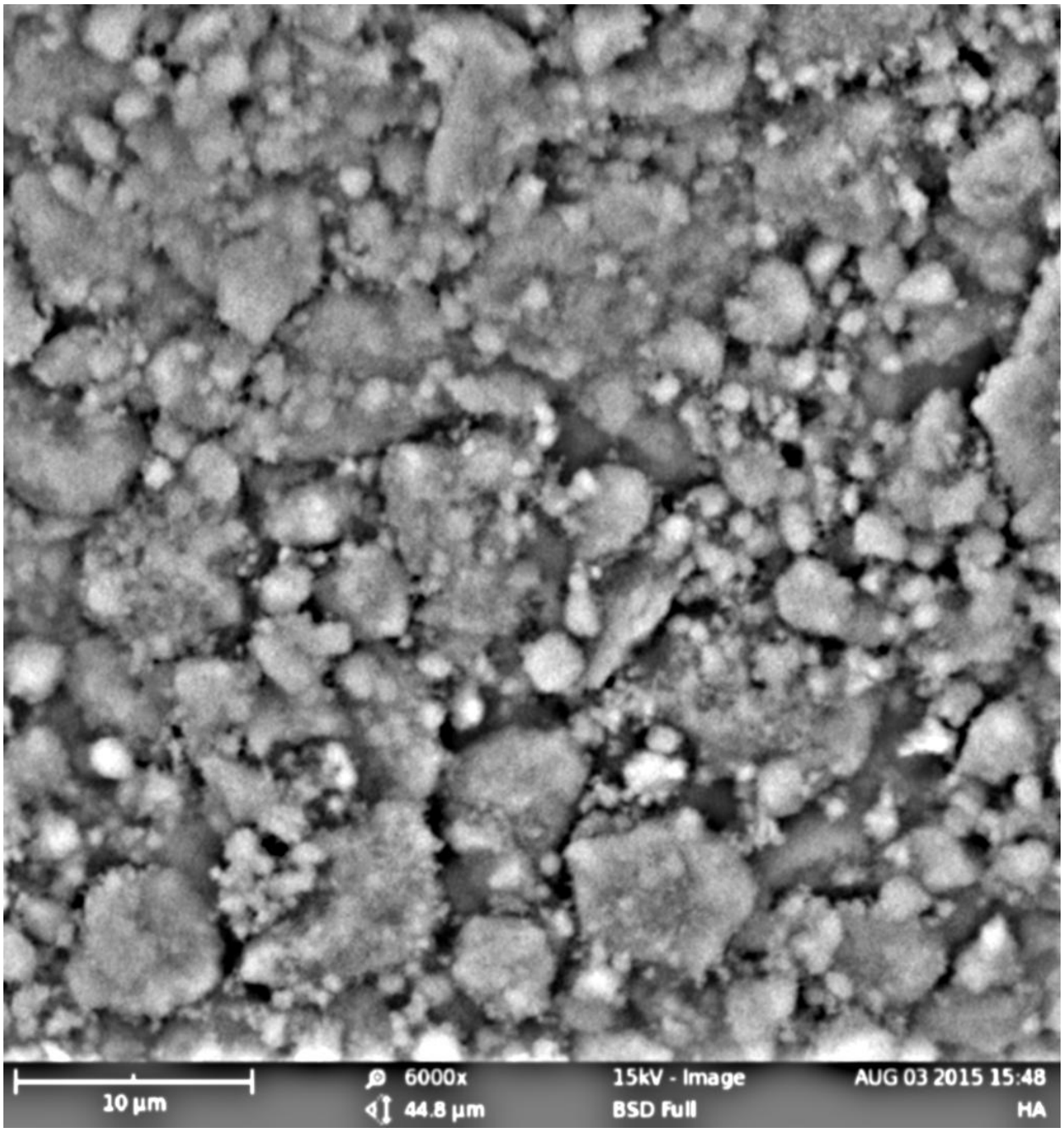


**Figure 4.3**: Scanning Electron Micrograph of hydroxyapatite (HA)

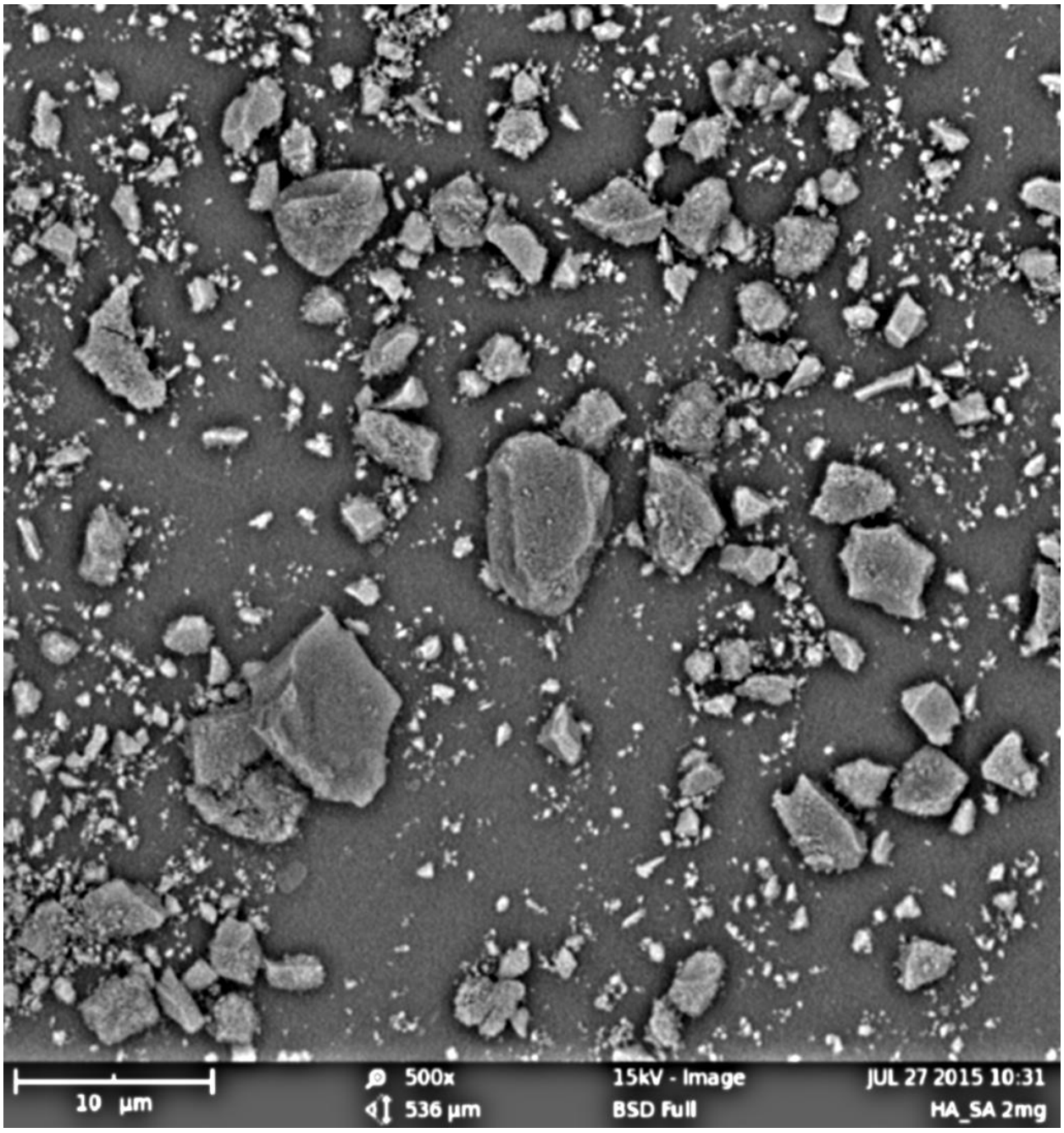


**Figure 4.4**: Scanning Electron Micrograph of HASA Nanocomposite (HASA-1%wt)

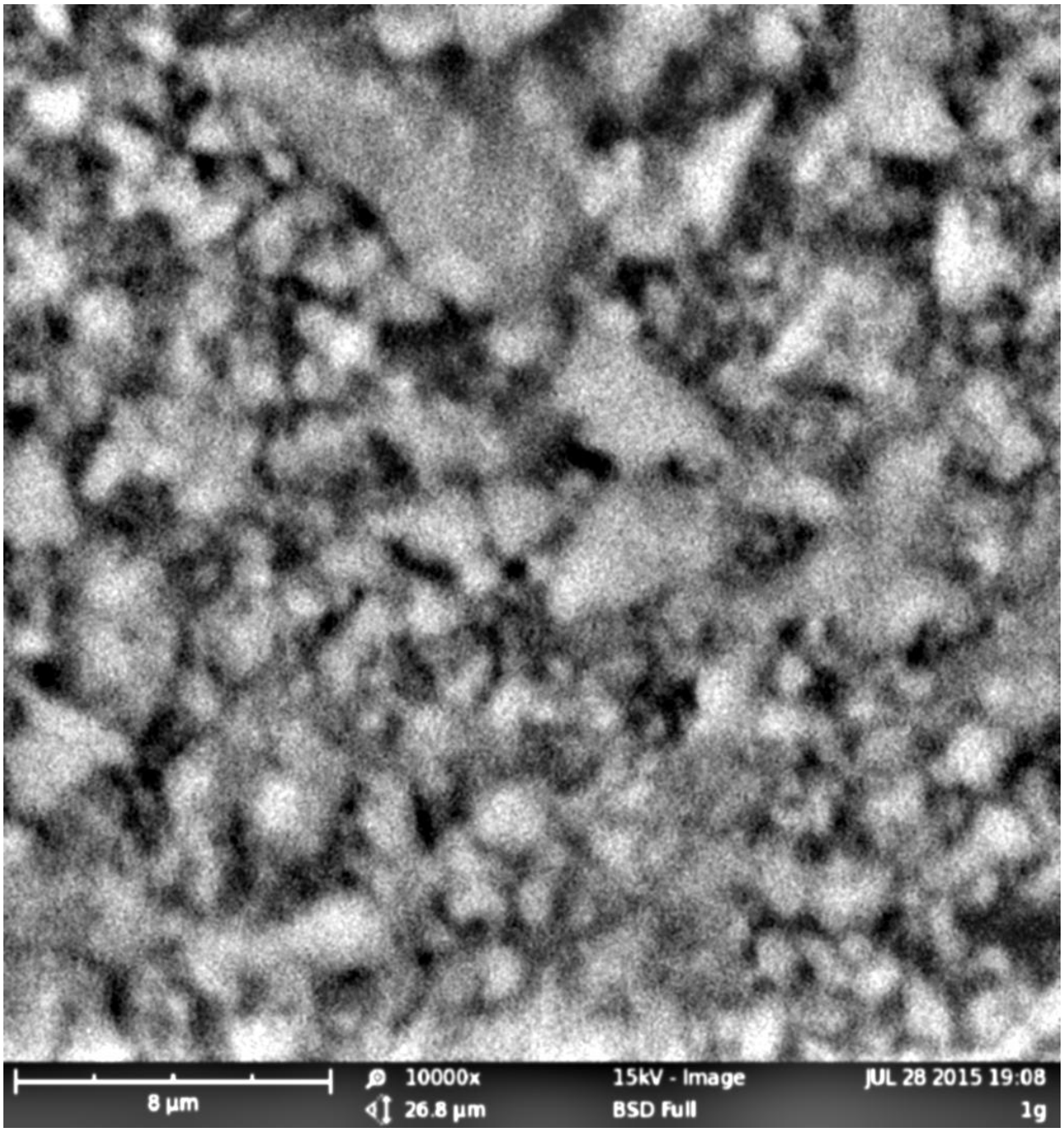


**Figure 4.5**: Scanning Electron Micrograph of HASA Nanocomposites (HASA-5%wt)

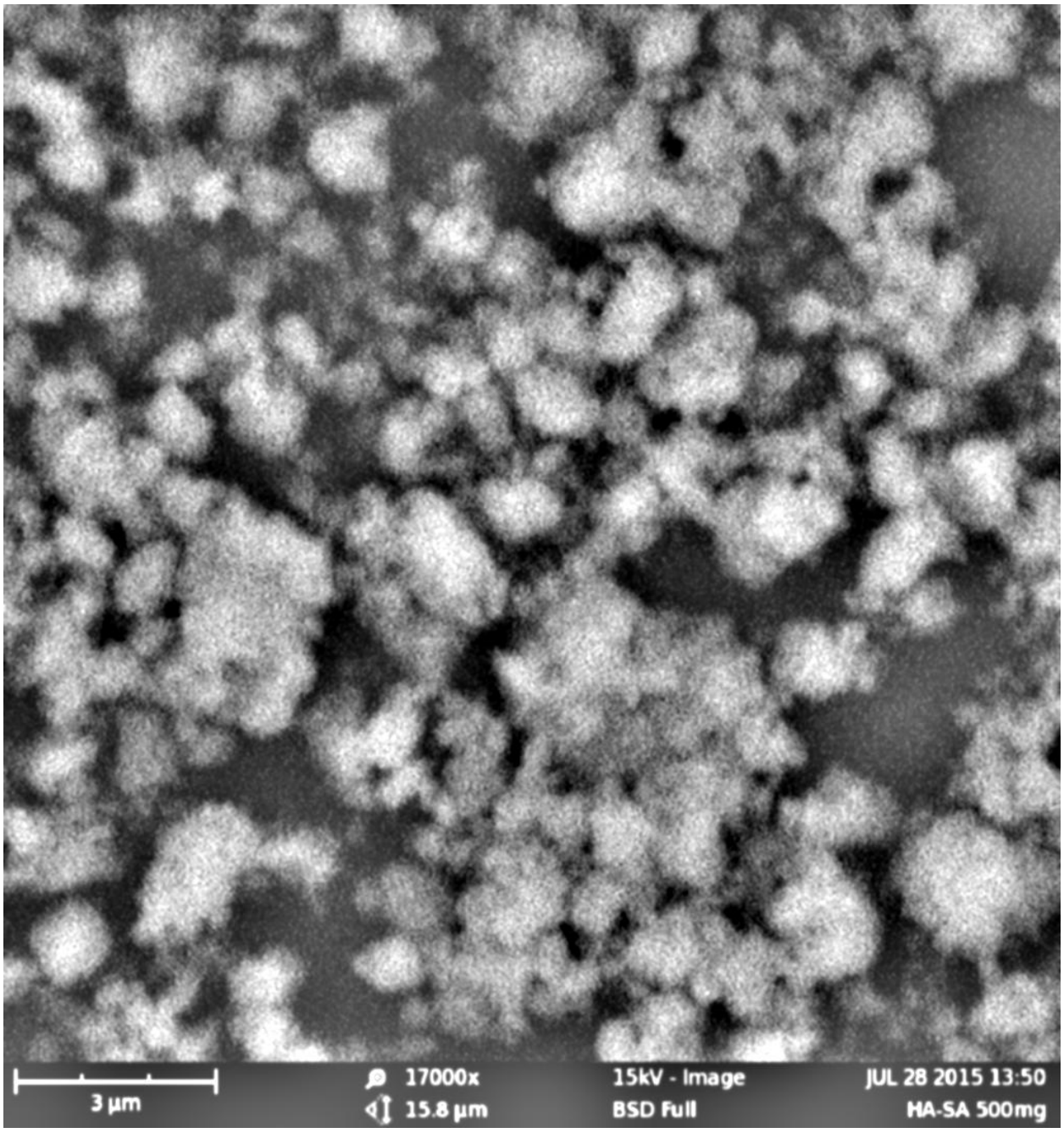


**Figure 4.6**: Scanning Electron Micrograph of HASA Nanocomposite (HASA-20%wt)

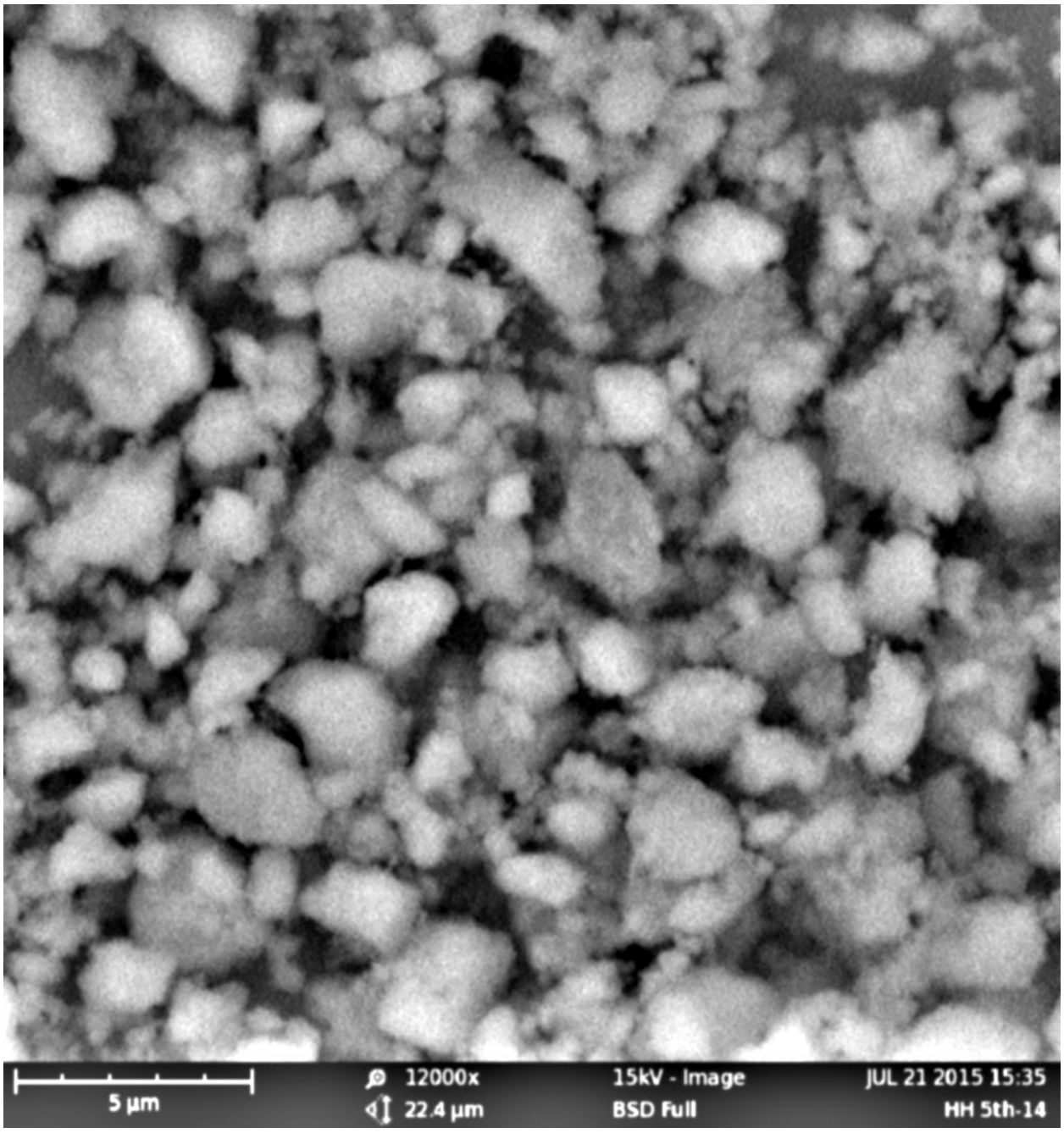


**Figure 4.7**: Scanning Electron Micrograph of HASA Nanocomposite (HASA-33%wt)

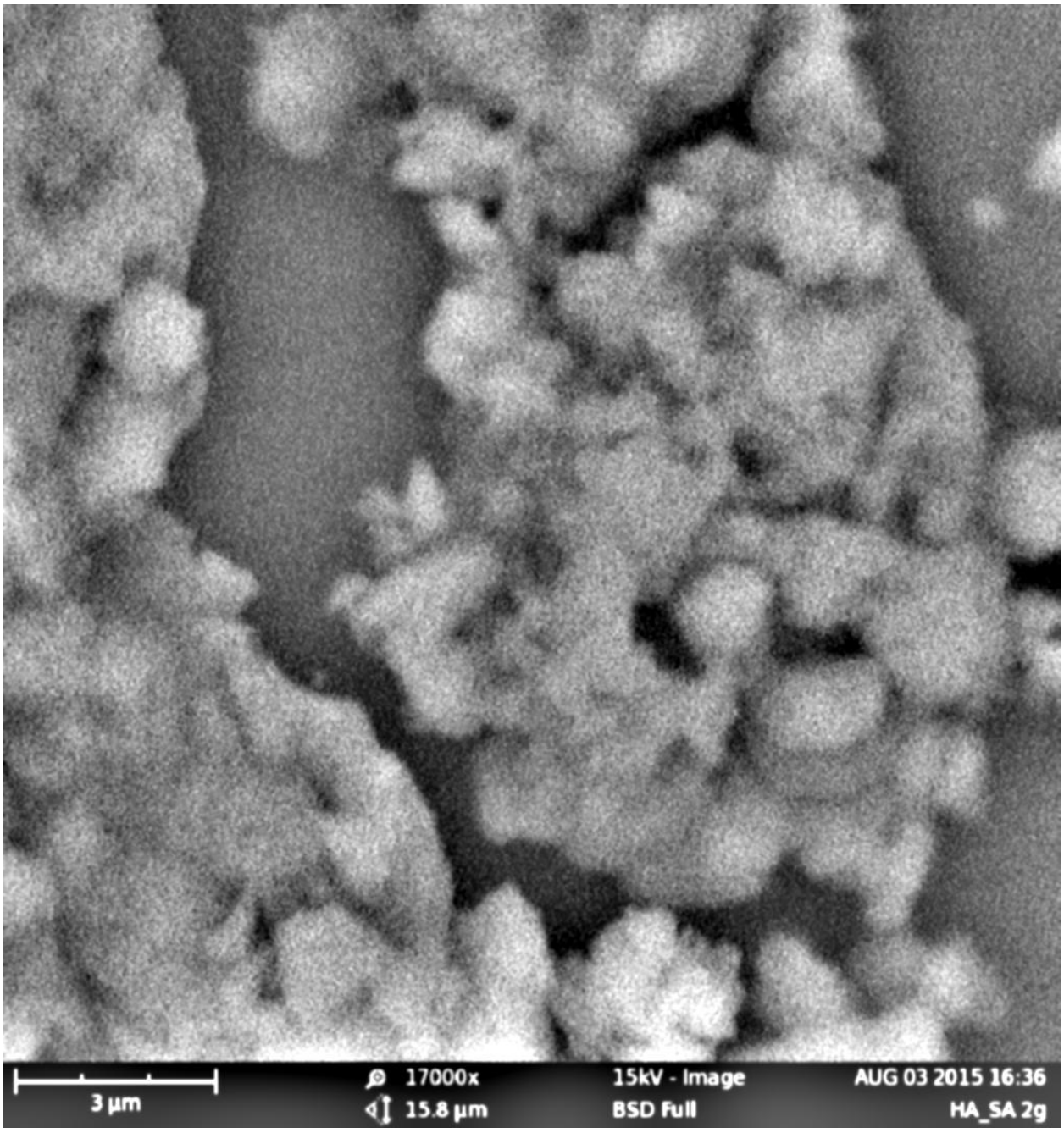


**Figure 4.8**: Scanning Electron Micrograph of HASA Nanocomposite (HASA-50%wt)

## 4.3 Image Analysis

The results of image analysis of the synthesised HA are presented in Table 4.3, while those of HASA nanocomposites (represented as HASA-1%wt, HASA-5%wt, HASA-20%wt, HASA-33%wt, and HASA-50%wt) are presented in Table 4.3 – 4.8. The Tables show the particles sizes represented as spherical equivalent diameter (SED) and the Feret diameters (F.D) for the HA and HA-SA particles. Also shown are the morphological characterizations of the particles using aspect ratio (A.R) and circularity. The statistics, D10, D50 and D90 are used to show the distributions of the parameters measured. D10 is the population representing 10% of the particles, D50 represents 50% of the particles (also called the median value), while D90 represents 90% of the particles. The Tables also display the mean, mode, standard deviation, kurtosis, skewness, range, minimum and the maximum values of the parameters. Included in the data in Table 4.3 – 4.8 is the total count, which is the total number of particles, measured for each analysis.

The particles size distribution using the SED of the synthesized HA particles presented in Figure 4.9 also shows majority of the particles falling below 200 nm size; while the effect of SA contents on the particles size (SED and F.D) and morphology (A.R and circularity) are presented in Figure 4.10. This plot was made using the median values (D50). The result shows size variation with increasing SA composition, whereas morphological variation is not prominent. The result also shows that the particles are in nanometres size range.

**Table 4.3**: Size and shape parameters of HA

| STATISTIC | SED (nm) | F.D (nm) | A.R | CIRCULARITY | PERIMETER (nm) |
|---|---|---|---|---|---|
| **D10** | 46.18 | 69.12 | 0.3798 | 0.439 | 153.08 |
| **D50(Median)** | 85.50 | 132.12 | 0.5782 | 0.703 | 320.53 |
| **D90** | 280.89 | 405.91 | 0.8017 | 0.922 | 1258.71 |
| **Standard Error** | 3.2784 | 4.59 | 0.00465 | 0.00530 | 15.68 |
| **Mean** | 127.34 | 189.58 | 0.5860 | 0.692 | 531.66 |
| **Mode** | 57.89 | 69.16 | 0.5166 | 0.857 | 236.81 |
| **Standard Deviation** | 112.66 | 157.62 | 0.1599 | 0.1822 | 538.81 |
| **Kurtosis** | 6.29 | 6.12 | -0.5472 | -1.0219 | 6.36 |
| **Skewness** | 2.34 | 2.26 | 0.1850 | -0.2282 | 2.38 |
| **Range** | 700.22 | 1071.81 | 0.7695 | 0.740 | 3258.78 |
| **Minimum** | 24.68 | 43.74 | 0.2305 | 0.248 | 87.48 |
| **Maximum** | 724.90 | 1115.54 | 1 | 0.988 | 3346.26 |
| **Count** | 1181 | 1181 | 1181 | 1181 | 1181 |

**SED=**Spherical equivalent diameter**, F.D =** Feret diameter**, A.R =** Aspect ratio

**Table 4.4**: Descriptive statistics of size and shape parameters of HASA-1%wt

| Statistic | **SED (nm)** | **F.D (nm)** | **A.R** | **Circularity** | **Perimeter (nm)** |
|---|---|---|---|---|---|
| D10 | 160.55 | 240.44 | 0.370 | 0.496 | 563.73 |
| D50(Median) | 309.41 | 462.49 | 0.577 | 0.746 | 1127.45 |
| D90 | 639.31 | 973.70 | 0.805 | 0.927 | 2761.04 |
| Mean | 359.46 | 541.63 | 0.583 | 0.727 | 1397.99 |
| Standard Error | 3.910 | 5.739 | 0.00322 | 0.00335 | 17.564 |
| Mode | 210.20 | 240.44 | 0.333 | 0.857 | 639.76 |
| Standard Deviation | 191.681 | 281.340 | 0.1577 | 0.164 | 860.970 |
| Kurtosis | 0.7789 | 0.6875 | -0.543 | -0.7001 | 1.2475 |
| Skewness | 1.1326 | 1.0895 | 0.193 | -0.3984 | 1.2865 |
| Range | 911.27 | 1443.72 | 0.785 | 0.746 | 4698.76 |
| Minimum | 85.82 | 152.07 | 0.215 | 0.242 | 304.13 |
| Maximum | 997.09 | 1595.79 | 1 | 0.988 | 5002.89 |
| Count | 2403 | 2403 | 2403 | 2403 | 2403 |

**SED=**Spherical equivalent diameter**, F.D =** Feret diameter**, A.R =** Aspect ratio

**Table 4.5**: Descriptive statistics of size and shape parameters of HASA-5%wt

| STATISTIC | SED (nm) | F.D (nm) | A.R | CIRCULARITY | PERIMETER (nm) |
|---|---|---|---|---|---|
| D10 | 104.62 | 146.63 | 0.374 | 0.430 | 343.78 |
| D50(Median) | 184.94 | 282.04 | 0.584 | 0.705 | 698.81 |
| D90 | 507.15 | 747.66 | 0.806 | 0.923 | 2262.70 |
| Mean | 250.70 | 378.23 | 0.588 | 0.694 | 1044.40 |
| Standard Error | 4.175 | 6.035 | 0.0036 | 0.00413 | 21.020 |
| Mode | 128.13 | 191.18 | 0.333 | 0.967 | 409.35 |
| Standard Dev. | 186.421 | 269.486 | 0.1610 | 0.1842 | 938.649 |
| Kurtosis | 4.7367 | 4.0104 | -0.5132 | -1.00424 | 5.8921 |
| Skewness | 2.0543 | 1.9063 | 0.1324 | -0.2566 | 2.2731 |
| Range | 1214.49 | 1785.01 | 0.803 | 0.736 | 6293.95 |
| Minimum | 52.31 | 92.74 | 0.197 | 0.252 | 185.47 |
| Maximum | 889.80 | 1877.75 | 1 | 0.988 | 6479.42 |
| Count | 1994 | 1994 | 1994 | 1994 | 1994 |

**SED=**Spherical equivalent diameter**, F.D =** Feret diameter**, A.R =** Aspect ratio

**Table 4.6**: Descriptive statistics of size and shape parameters of HASA-20%wt

| STATISTIC | SED (nm) | F.D (nm) | A.R | CIRCULARITY | PERIMETER |
|---|---|---|---|---|---|
| D10 | 49.34 | 77.32 | 0.400 | 0.444 | 171.20 |
| D50(Median) | 93.95 | 145.89 | 0.614 | 0.692 | 351.46 |
| D90 | 452.91 | 609.99 | 0.816 | 0.916 | 2009.13 |
| Mean | 172.96 | 247.73 | 0.610 | 0.684 | 728.97 |
| Standard Error | 5.821 | 7.823 | 0.00558 | 0.00626 | 27.004 |
| Mode | 67.57 | 103.74 | 0.378 | 0.857 | 214.94 |
| Standard Dev. | 165.156 | 222.009 | 0.1583 | 0.1776 | 766.18 |
| Sample Variance | 27276.44 | 49288.05 | 0.0251 | 0.0316 | 587038.7 |
| Kurtosis | 1.5080 | 1.4268 | -0.5129 | -1.091 | 1.7999 |
| Skewness | 1.5951 | 1.5529 | 0.00140 | -0.110 | 1.6525 |
| Range | 677.49 | 997.87 | 0.823 | 0.718 | 3531.19 |
| Minimum | 24.67 | 43.74 | 0.177 | 0.270 | 87.48 |
| Maximum | 702.16 | 1041.61 | 1 | 0.988 | 3618.67 |
| Count | 805 | 805 | 805 | 805 | 805 |

**SED=**Spherical equivalent diameter**, F.D =** Feret diameter**, A.R =** Aspect ratio

**Table 4.7**: Descriptive statistics of size and shape parameters of HASA-33%wt

| STATISTIC | **SED** (nm) | **F.D** (nm) | **A.R** | **CIRCULARITY** | **PERIMETER** (nm) |
|---|---|---|---|---|---|
| D10 | 60.33 | 97.65 | 0.345 | 0.335 | 210.85 |
| D50(Median) | 123.16 | 195.29 | 0.524 | 0.684 | 470.66 |
| D90 | 305.67 | 513.91 | 0.759 | 0.916 | 1610.05 |
| Mean | 161.01 | 259.81 | 0.545 | 0.656 | 733.03 |
| Standard Error | 3.515 | 6.088 | 0.00496 | 0.0067 | 22.137 |
| Mode | 69.67 | 127.31 | 0.333 | 0.857 | 228.936 |
| Standard Dev. | 112.848 | 195.500 | 0.1592 | 0.2149 | 710.809 |
| Sample Variance | 12734.77 | 38219.92 | 0.0253 | 0.0462 | 505249 |
| Kurtosis | 4.0362 | 5.2176 | -0.315 | -0.927 | 11.2570 |
| Skewness | 1.8067 | 2.0302 | 0.4090 | -0.382 | 2.7359 |
| Range | 753.38 | 1345.99 | 0.804 | 0.863 | 6274.29 |
| Minimum | 34.83 | 61.76 | 0.196 | 0.119 | 123.51 |
| Maximum | 788.21 | 1407.75 | 1 | 0.982 | 6397.80 |
| Count | 1031 | 1031 | 1031 | 1031 | 1031 |

**SED=**Spherical equivalent diameter**, F.D =** Feret diameter**, A.R =** Aspect ratio

**Table 4.8**: Descriptive statistics of size and shape parameters of HASA-50%wt

| STATISTIC | SED (nm) | F.D (nm) | A.R | CIRCULARITY | PERIMETER (nm) |
|---|---|---|---|---|---|
| D10 | 46.22 | 69.16 | 0.367 | 0.428 | 162.14 |
| D50(Median) | 81.94 | 124.67 | 0.562 | 0.711 | 307.72 |
| D90 | 182.40 | 297.05 | 0.797 | 0.922 | 859.76 |
| Mean | 109.98 | 168.12 | 0.572 | 0.694 | 465.20 |
| Standard Error | 1.992 | 2.830 | 0.0033 | 0.00387 | 10.658 |
| Mode | 60.52 | 90.17 | 0.333 | 0.857 | 184.01 |
| Standard Dev. | 96.149 | 136.597 | 0.1613 | 0.1866 | 514.459 |
| Sample Variance | 9244.65 | 18658.65 | 0.0260 | 0.0348 | 264668.4 |
| Kurtosis | 11.8340 | 10.0000 | -0.4470 | -0.870 | 15.1979 |
| Skewness | 3.2158 | 2.9210 | 0.3004 | -0.344 | 3.5702 |
| Range | 679.54 | 969 | 0.851 | 0.801 | 4420.33 |
| Minimum | 24.71 | 43.74 | 0.149 | 0.187 | 87.477 |
| Maximum | 704.25 | 1012.74 | 1 | 0.988 | 4507.803 |
| Count | 2330 | 2330 | 2330 | 2330 | 2330 |

**SED=**Spherical equivalent diameter**, F.D =** Feret diameter**, A.R =** Aspect ratio

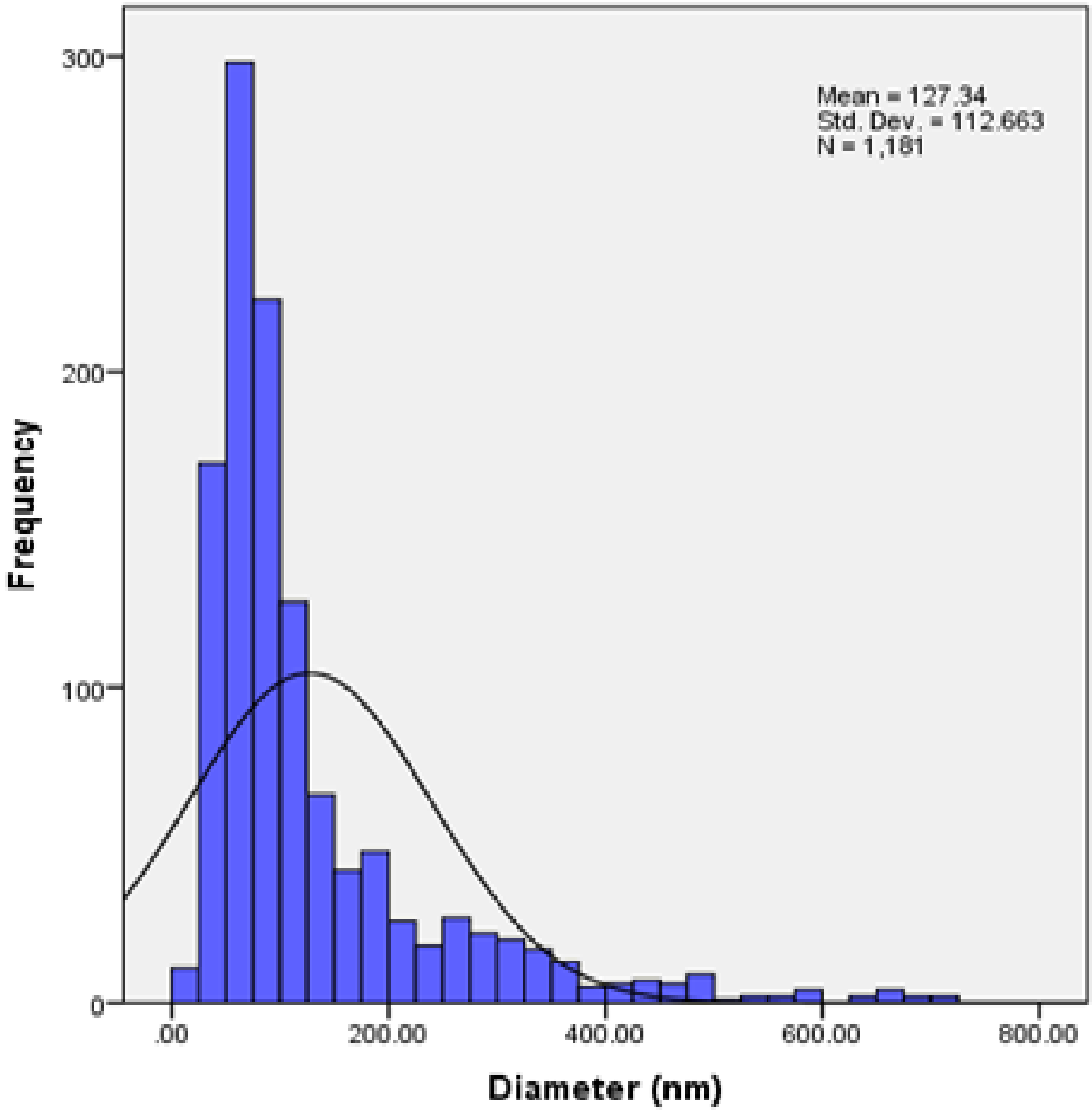


**Figure 4.9**: Particle size distribution of HA

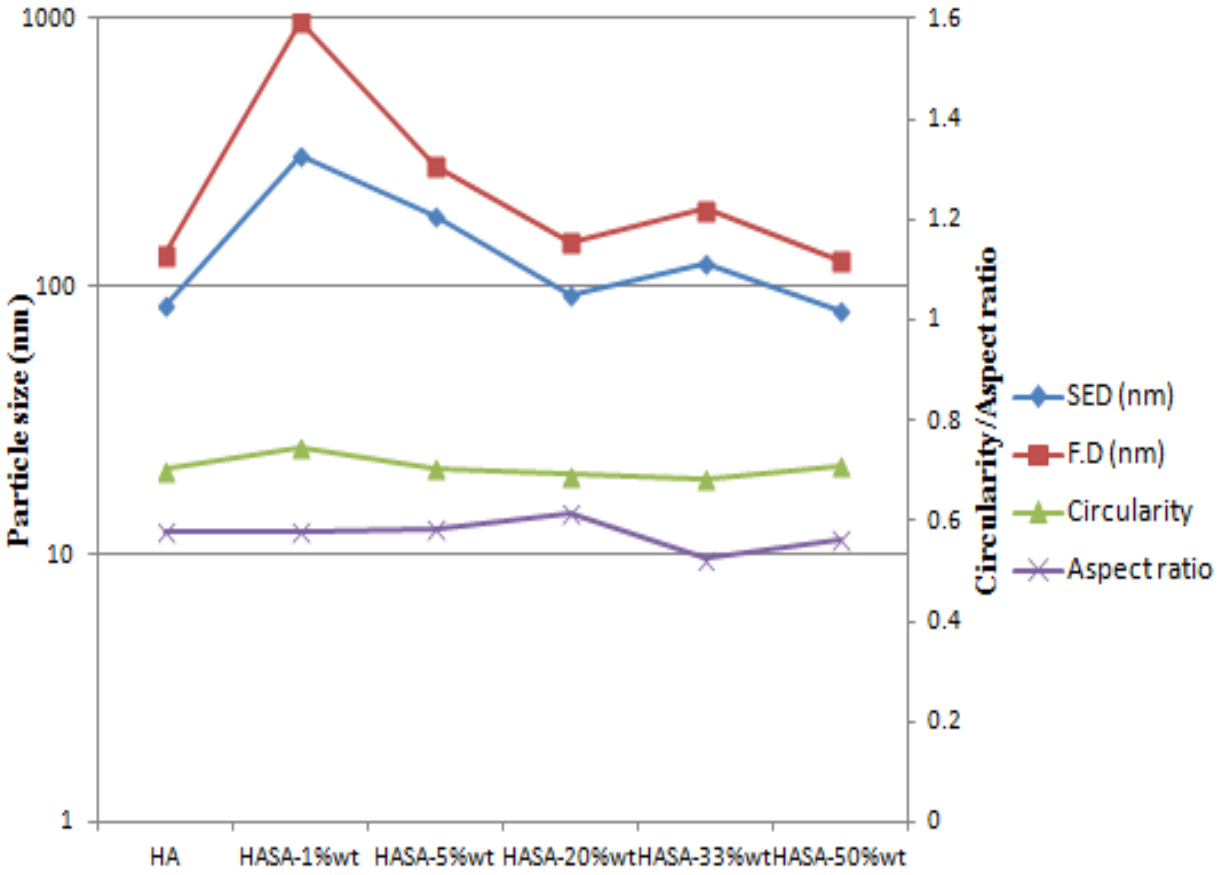


**Figure 4.10**: Variation of size and morphology of the particles with increase in composition of SA

## 4.4 X-Ray Powder Diffraction Analysis

The X-Ray Diffraction (XRD) spectrum of HA is presented in Figure 4.11, while the spectra for different compositions of HASA nanocomposites are shown in Figure 4.12. From the XRD results the degree of crystallinity and crystallite size were calculated and the crystallite size compared with the mean particle size using the SED in Figure 4.13.

Microstrain and specific surface area were also calculated for each formulation and the result is presented in Figure 4.14.

## 4.5 Energy Dispersive X-Ray Fluorescence (XRF) Analysis

Figure 4.15 is the XRF spectrum showing elemental composition of the HA. It shows the major components as calcium (Ca), phosphorus (P), and oxygen (O). In addition to these, there are also the presence of some impurities such as iron (Fe), and samarium (Sm).

## 4.6 Comparison of Nanocomposites Prepared by the two synthetic routes

Presented in Figure 4.16 are the FTIR spectra of HASA nanocomposite prepared by the first synthetic route (HASA), and HASA nanocomposite prepared by the second synthetic route (2HASA). The particle size and crystallite size of the nanocomposites prepared by the two routes are also shown in Figure 4.17. These results indicate that 2HASA has higher particle size and crystallite size for all the formulations. However, at higher SA composition (HASA-33%wt and HASA-50%wt) the crystallite sizes for both methods are very close.

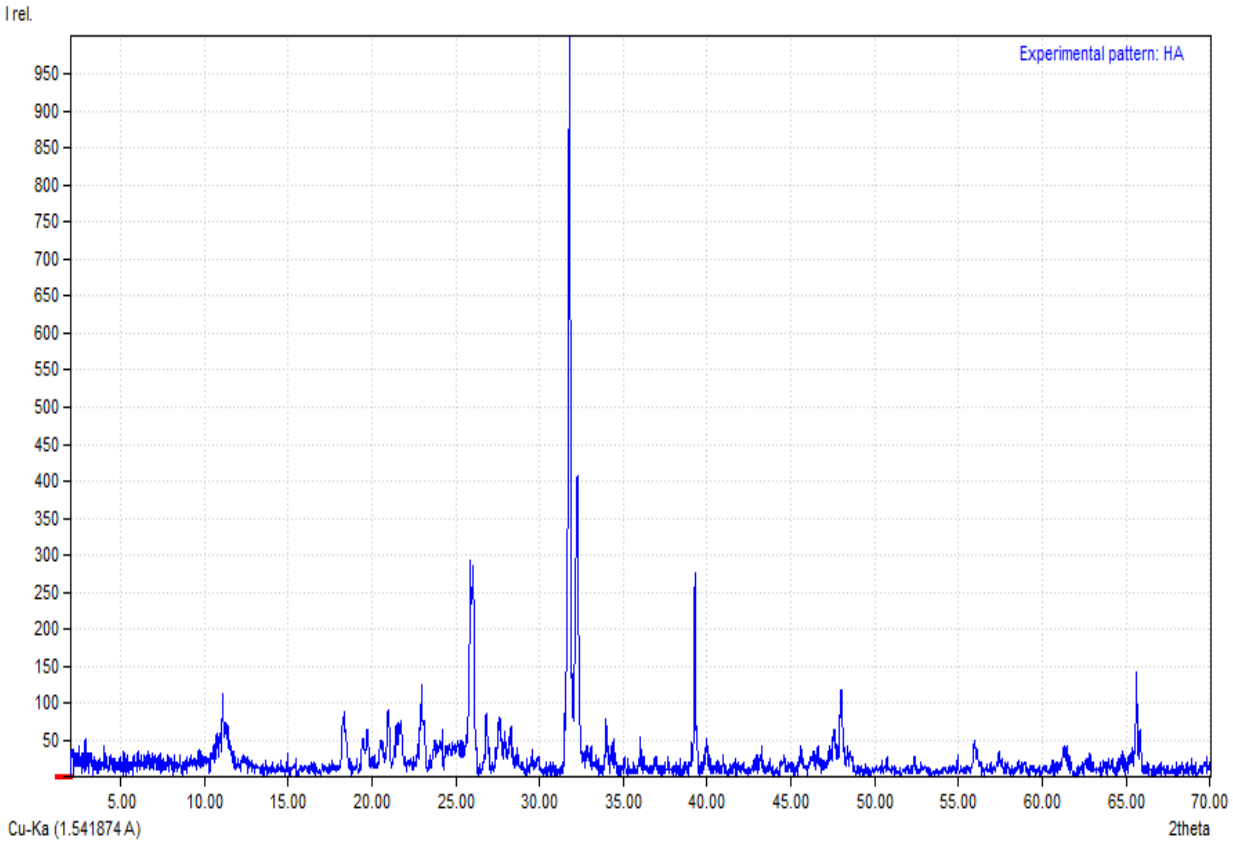


**Figure 4.11**: X-Ray Diffraction spectrum of HA

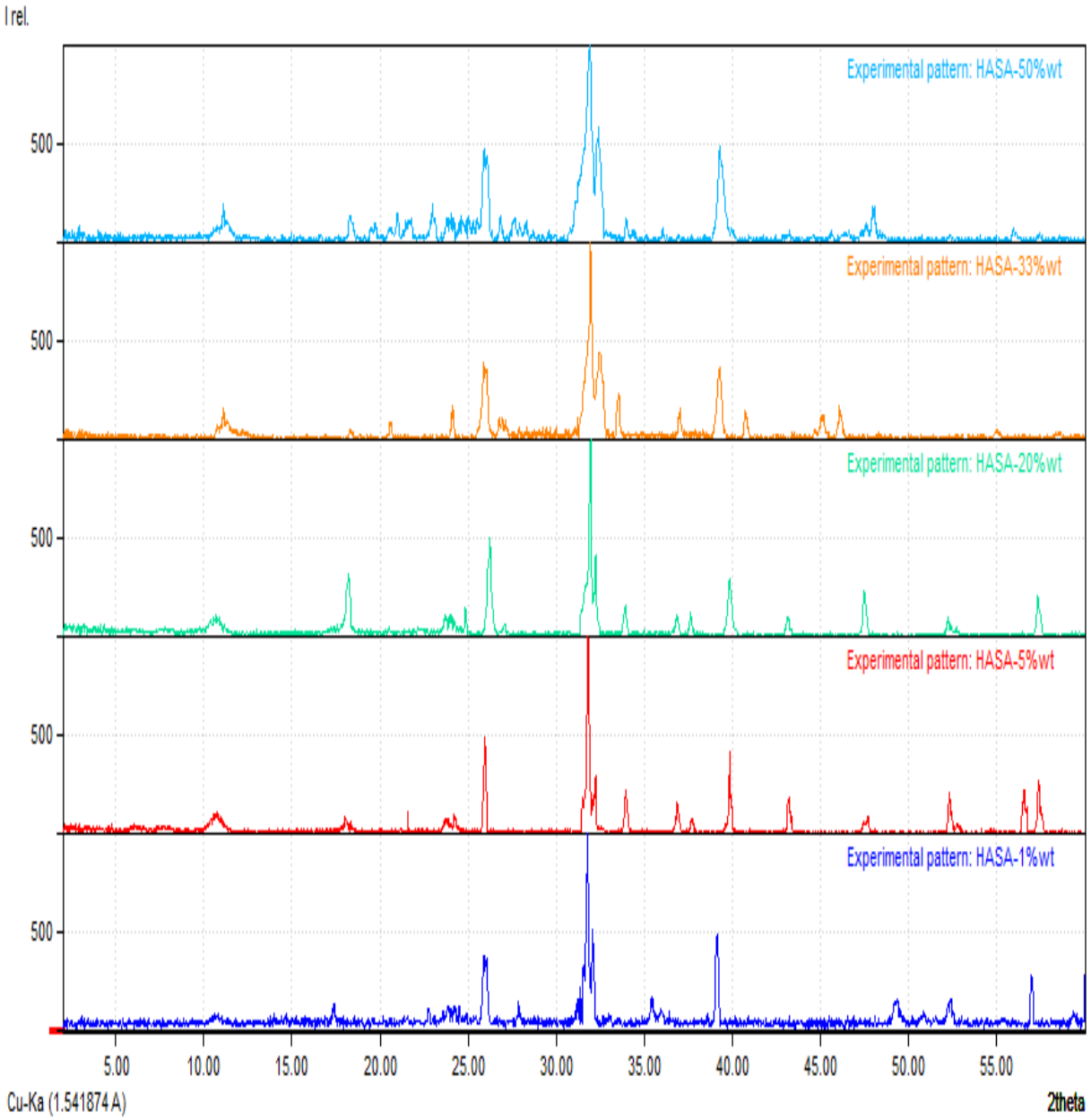


**Figure 4.12**: XRD Spectra of Different Formulations of HASA nanocomposites

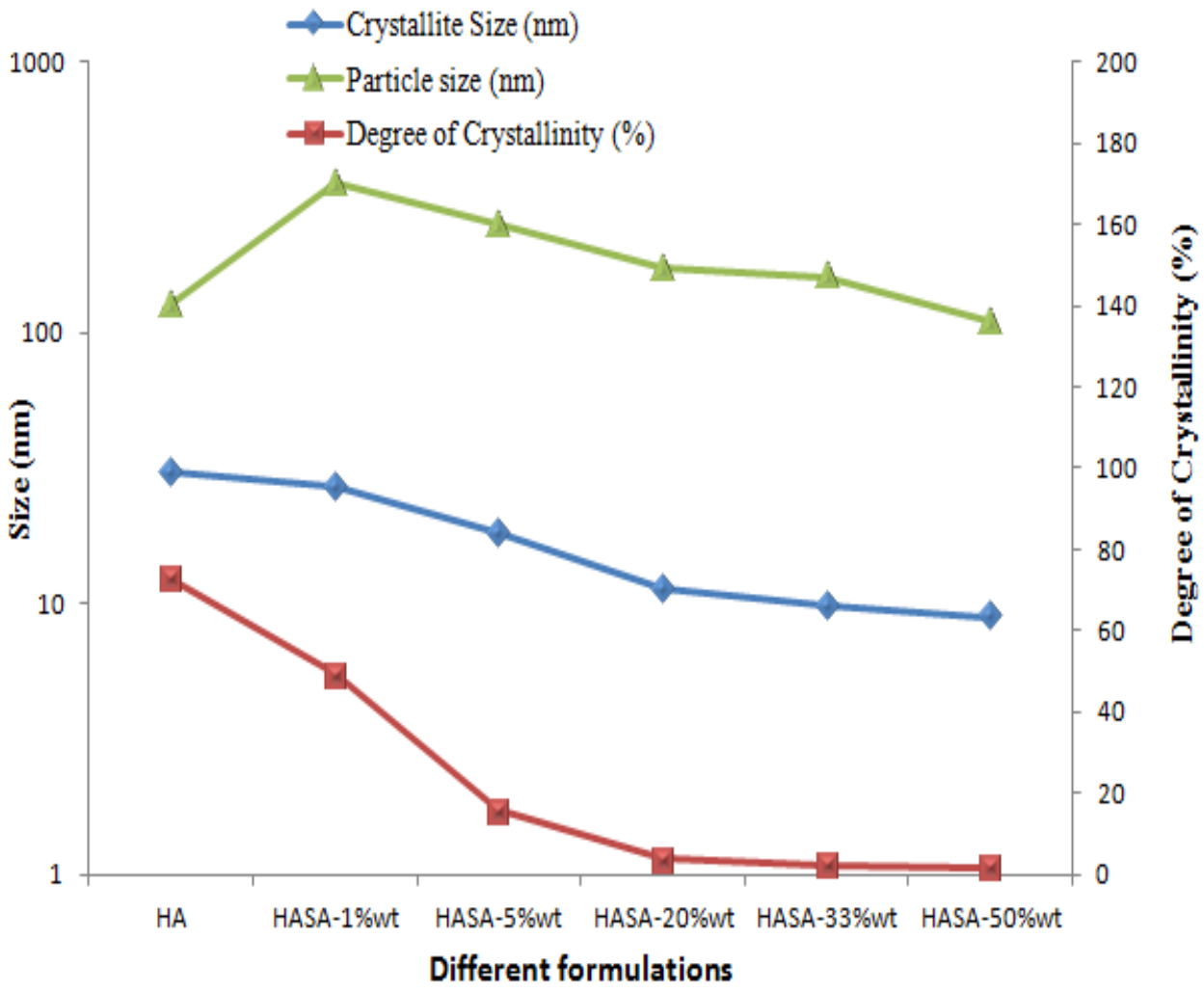


**Figure 4.13**: Effects of quantity of SA on the particle size, crystallite size and variation in crystallinity of HA

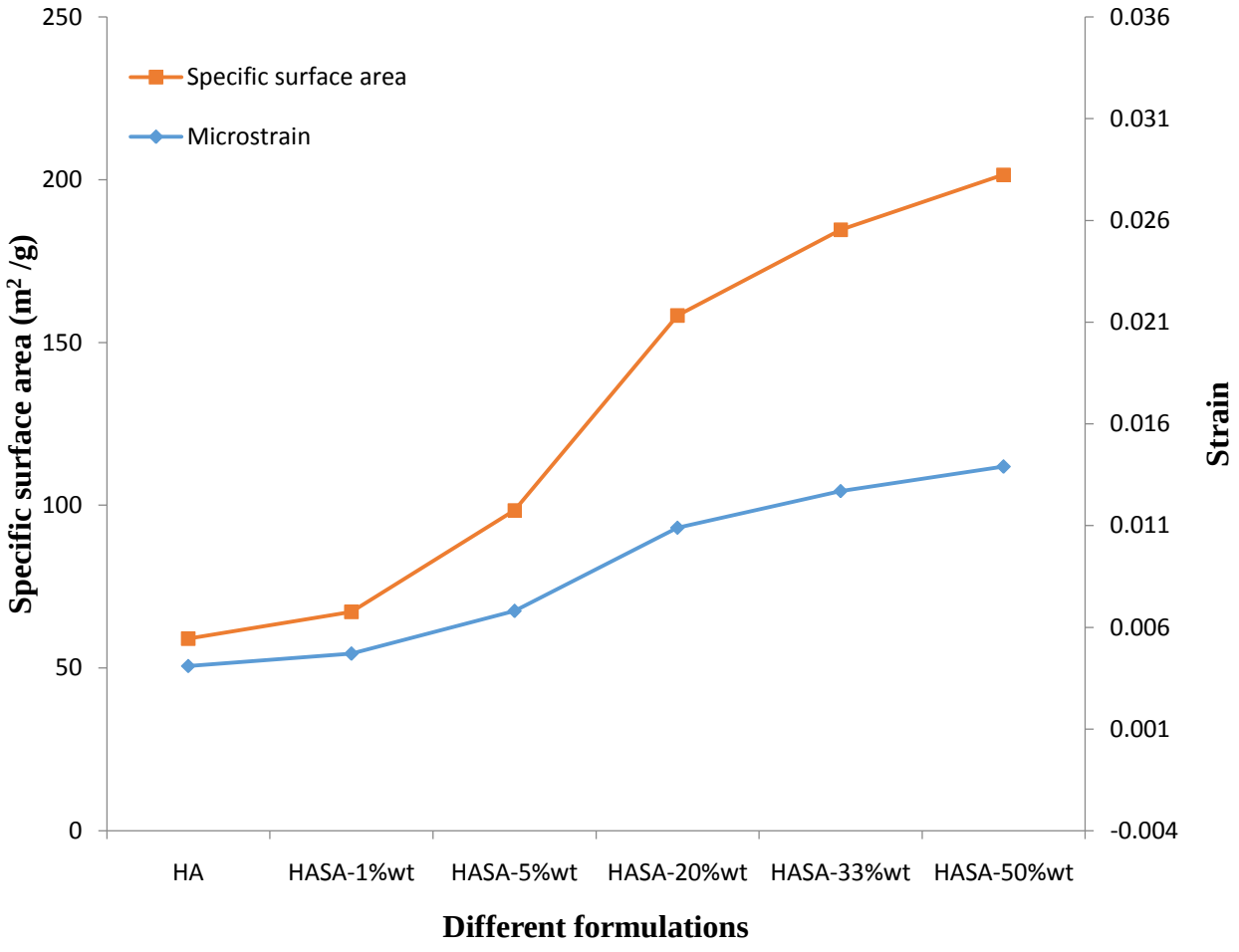


**Figure 4.14**: Variation of microstrain and specific surface area with the quantity of SA

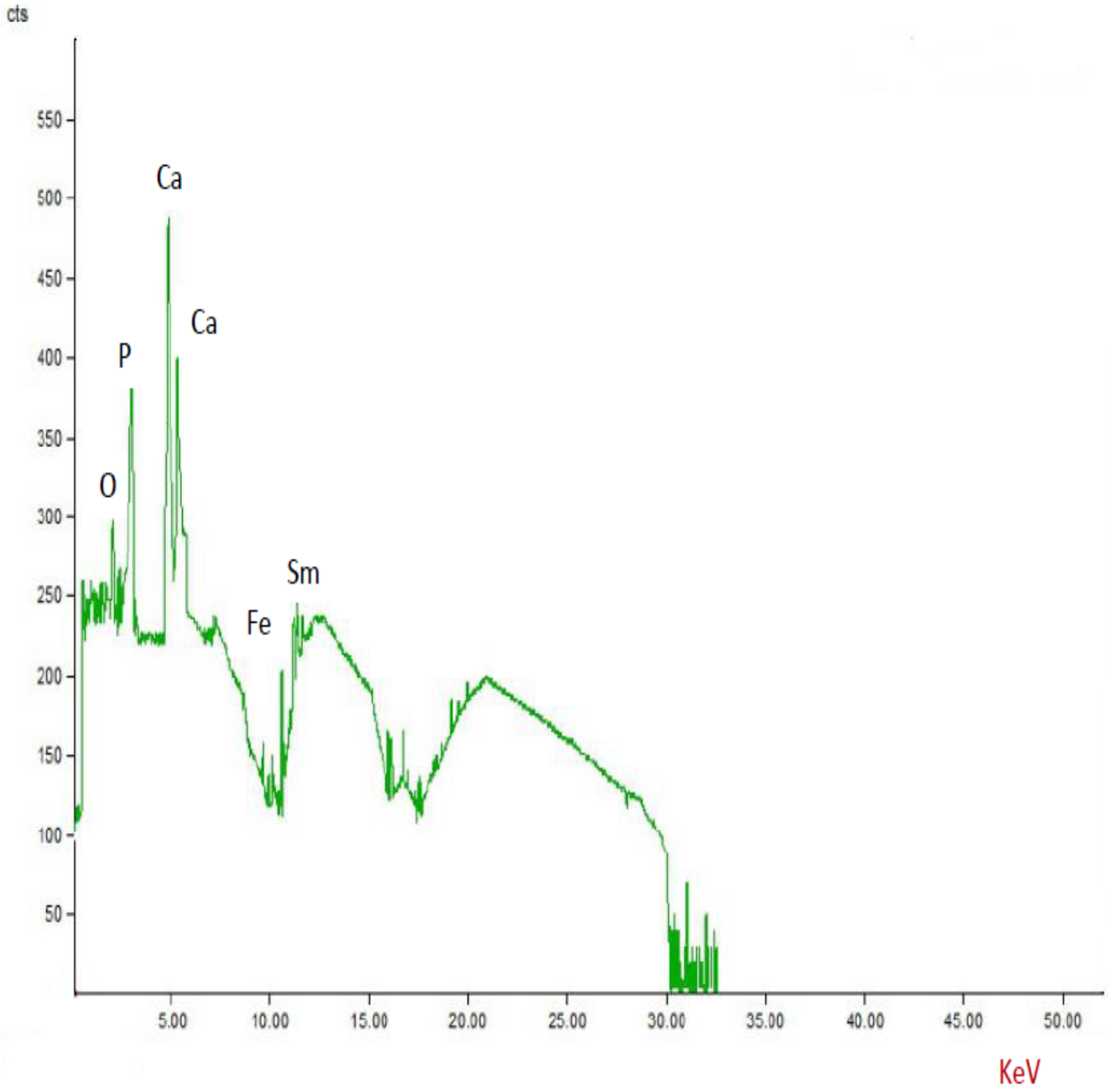


**Figure 4.15**: Energy Dispersive X-Ray Fluorescence Spectrum of HA

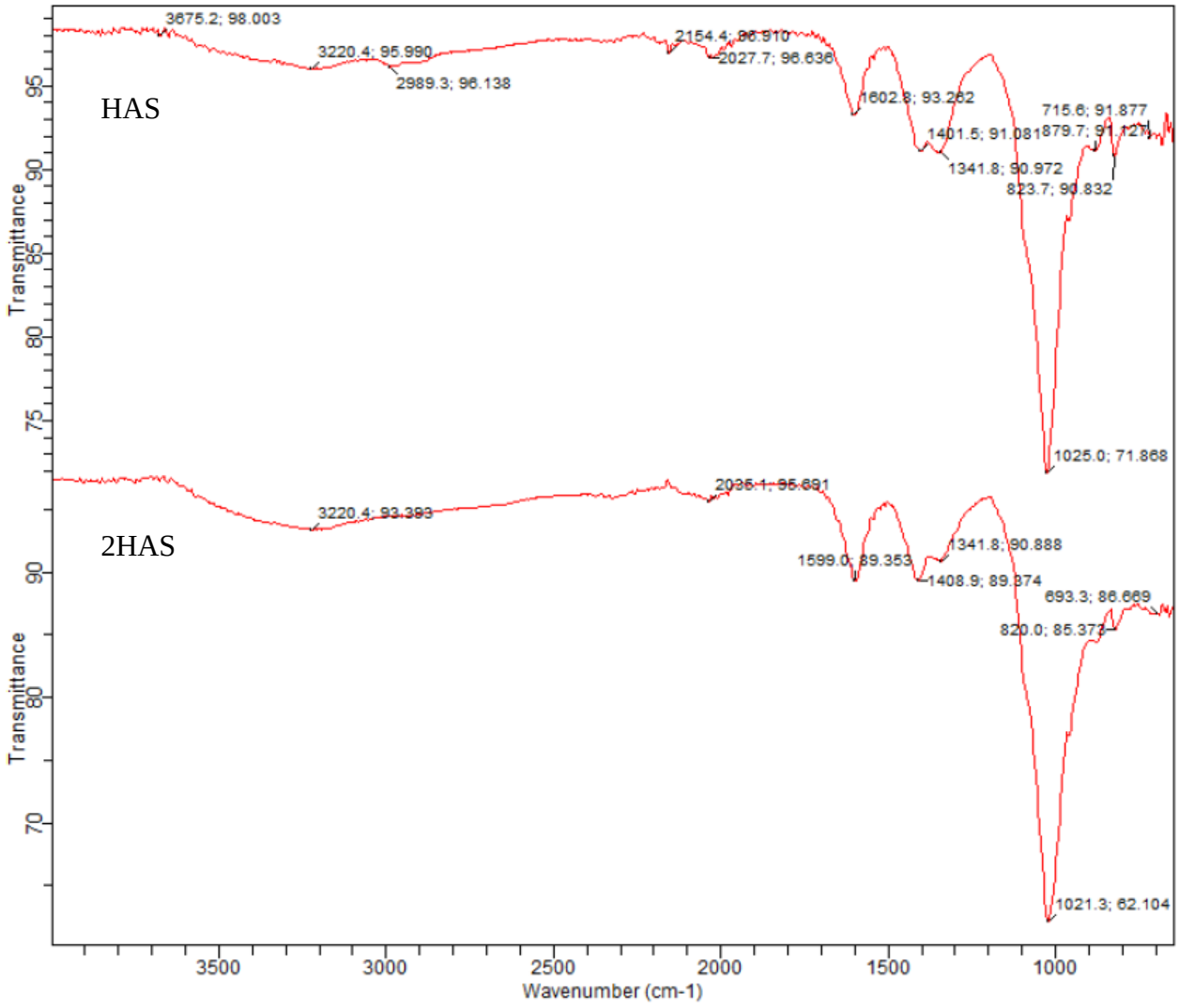


**Figure 4.16**: FTIR Spectra of HASA nanocomposite prepared by first synthetic route (HASA) and HASA nanocomposite prepared by the second synthetic route (2HASA)

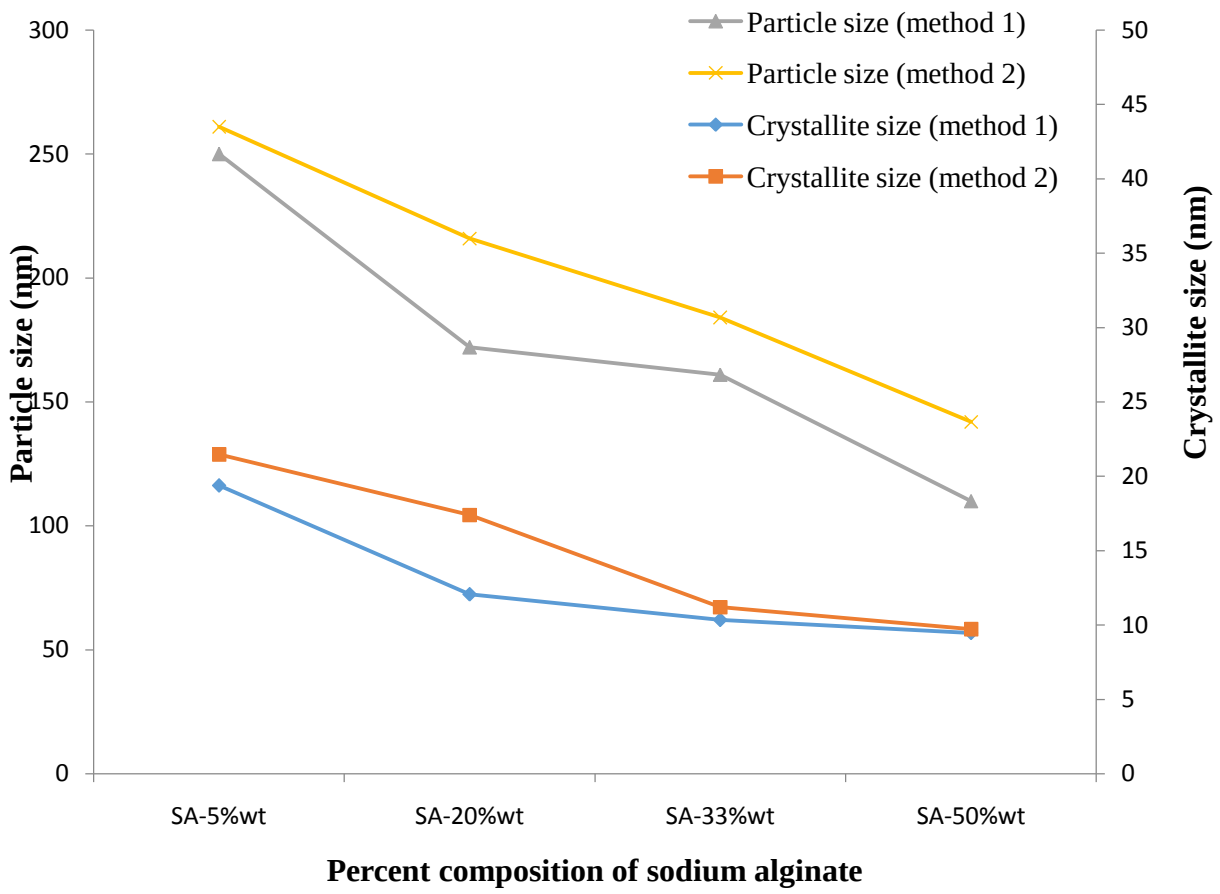


**Figure 4.17**: Comparison of the effect of synthetic route on particle size and crystallite size of nanocomposites

## 4.7 Drug Loading and Release Results

### 4.7.1. Drug loading

The percent loading efficiency of DOX onto HA and HASA nanocomposite presented as Figure 4.18 shows the following values: HA – 21.93%, HASA-1%wt – 26.29%, HASA-5%wt – 63%, HASA-20%wt – 74.92%wt, HASA-33%wt – 87.69% and HASA-50%wt – 92.03%. The result shows a direct relationship between the quantity of SA and the encapsulation efficiency of DOX. However, for MTX the results of encapsulation efficiency presented in Figure 4.18 indicate that increasing quantity of SA had negative influence on its loading efficiency. The values are as follows: HA – 35.18%, HASA-1%wt – 30.05%, HASA-5%wt – 23.15%, HASA-20%wt – 17.01%, HASA-33%wt – 17.01% and HASA-50%wt – 17.01%.

The comparison of loading efficiencies for the two synthetic routes is shown in Figure 4.19 for DOX. For nanocomposites prepared with 5%wt of SA, the loading efficiency for the first synthetic route was 63.42%% while the second synthetic route was 69.39%; for nanocomposites prepared with 20%wt of SA, the loading efficiency for the first synthetic route was 74.92%, while the second synthetic route was 88.9%; with 33%wt of SA, the loading efficiency for the first synthetic route was 87.69%, while the second synthetic route was 92.63%, and with 50%wt of SA the first synthetic route was 92.03% while the second synthetic route was 94.74%. For MTX (Figure 4.20), the loading efficiency for the first synthetic route using 5%wt SA was 23.15% while the second synthetic route was 24.89%; for nanocomposites prepared with 20%wt of SA, the loading efficiency for the first synthetic route was 17.09%, while the second synthetic route was 21.57%; with 33%wt of SA, the loading efficiency for the first synthetic route was 17.01%, while the second synthetic route was 15.02%, and with 50%wt of SA the first synthetic

route was 17.01% while the second synthetic route was 12.01%. The results of FTIR analysis of the drug loaded HA and the nanocomposites from the two methods are also presented in Figure 4.21. The spectra show similar peaks for nanocomposites synthesised from the two synthetic routes.

### 4.7.2 Drug release

Presented in Figure 4.22 are MTX release profiles from HA and HASA. The release study was conducted for 23 hours. However, after 5 hours there was no observed MTX release from any of the formulations. This means that the actual release time was less than 5 hours for all the formulations. Comparison of MTX release profile from HA and other nanocomposites (Table 4.9) showed that the release profile from HA is similar to HASA-1%wt, HASA-5%wt and HASA-20%wt

In Figure 4.23, DOX release profiles shows sustained release, which increased with increasing quantity of SA except for HA and 1%w which did not sustain the release of DOX. Comparison of DOX release profiles was carried out for all the formulations using similarity factor (f2) (Table 4.10). The results show f2 values greater than 50 for HASA-5%wt versus HASA-20%wt, HASA-20%wt versus HASA-33%wt, and HASA-33%wt versus HASA-50%wt.

Table 4.11 gives the results of model-dependent kinetic and mechanistic study of DOX release from HA and the nanocomposites. The Model Selection Criteria (MSC) values shows that DOX followed first order release kinetic, while the release exponent n from the Korsmeyer-Peppas model indicates that drug release mechanism was predominantly by Fickian diffusion.

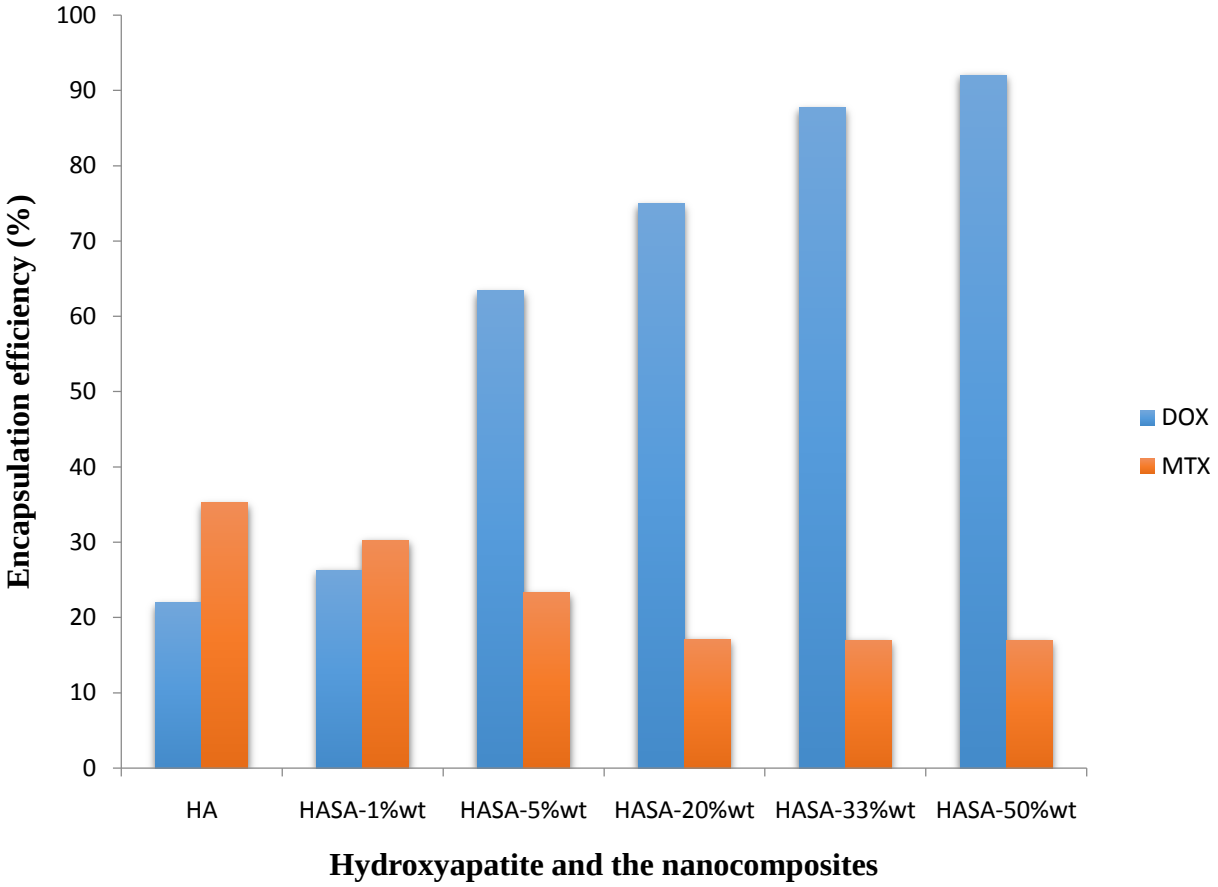


**Figure 4.18**: Loading efficiencies of DOX and MTX in HA and the nanocomposites

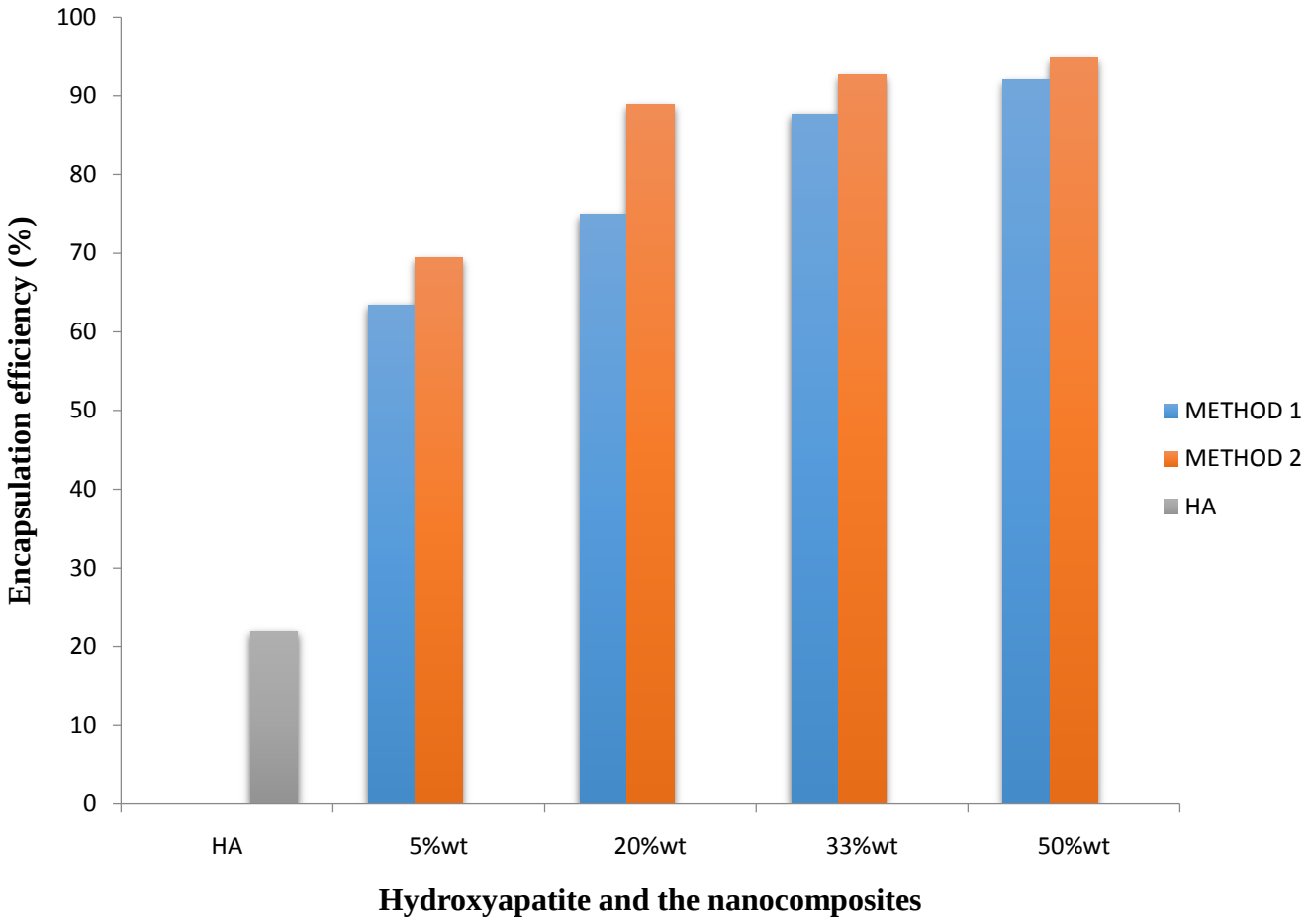


**Figure 4.19**: Comparison of loading efficiency of DOX in nanocomposites prepared by the two synthetic routes

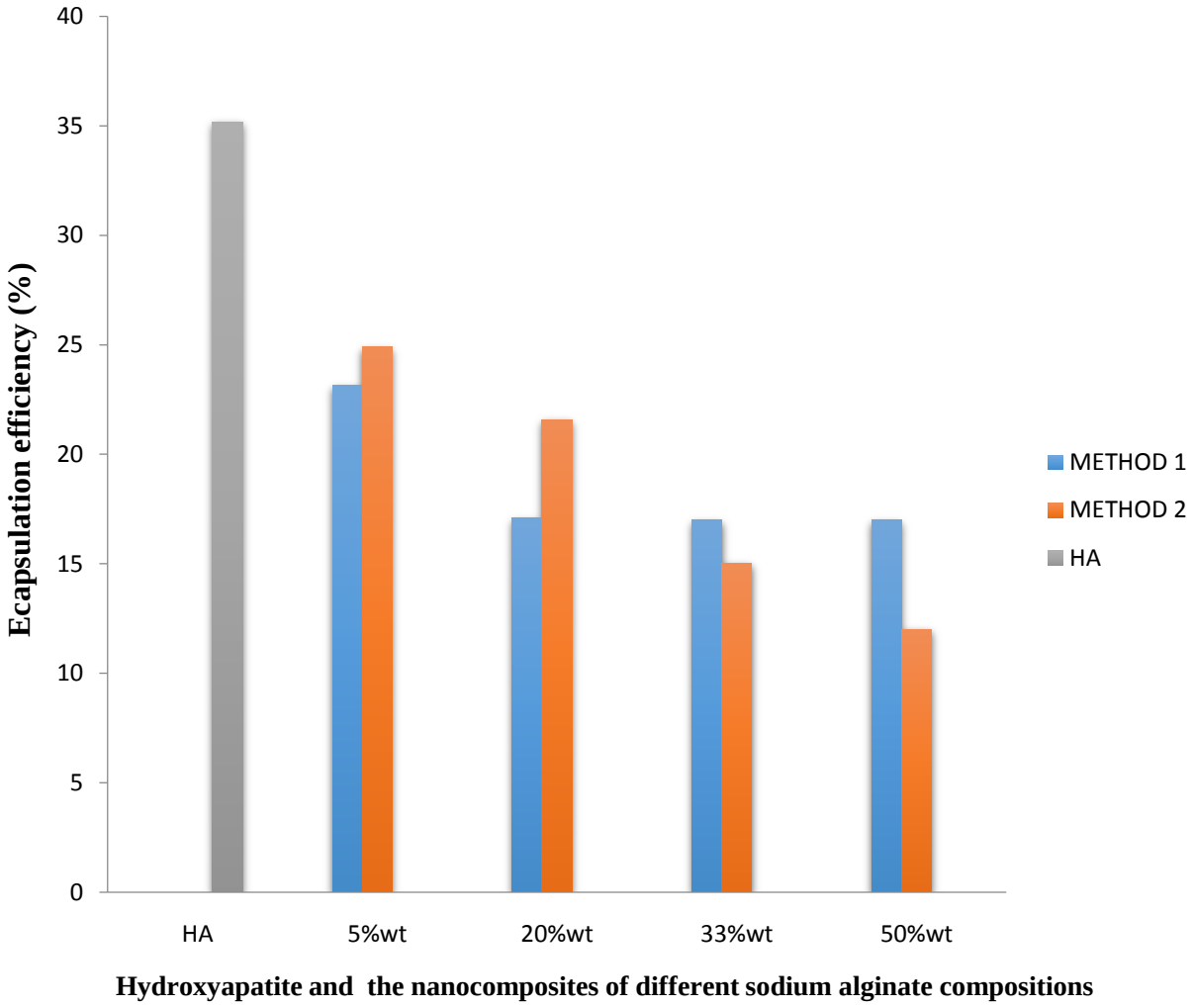


**Figure 4.20**: Comparison of loading efficiency of MTX in HA and the nanocomposites prepared by the two synthetic routes

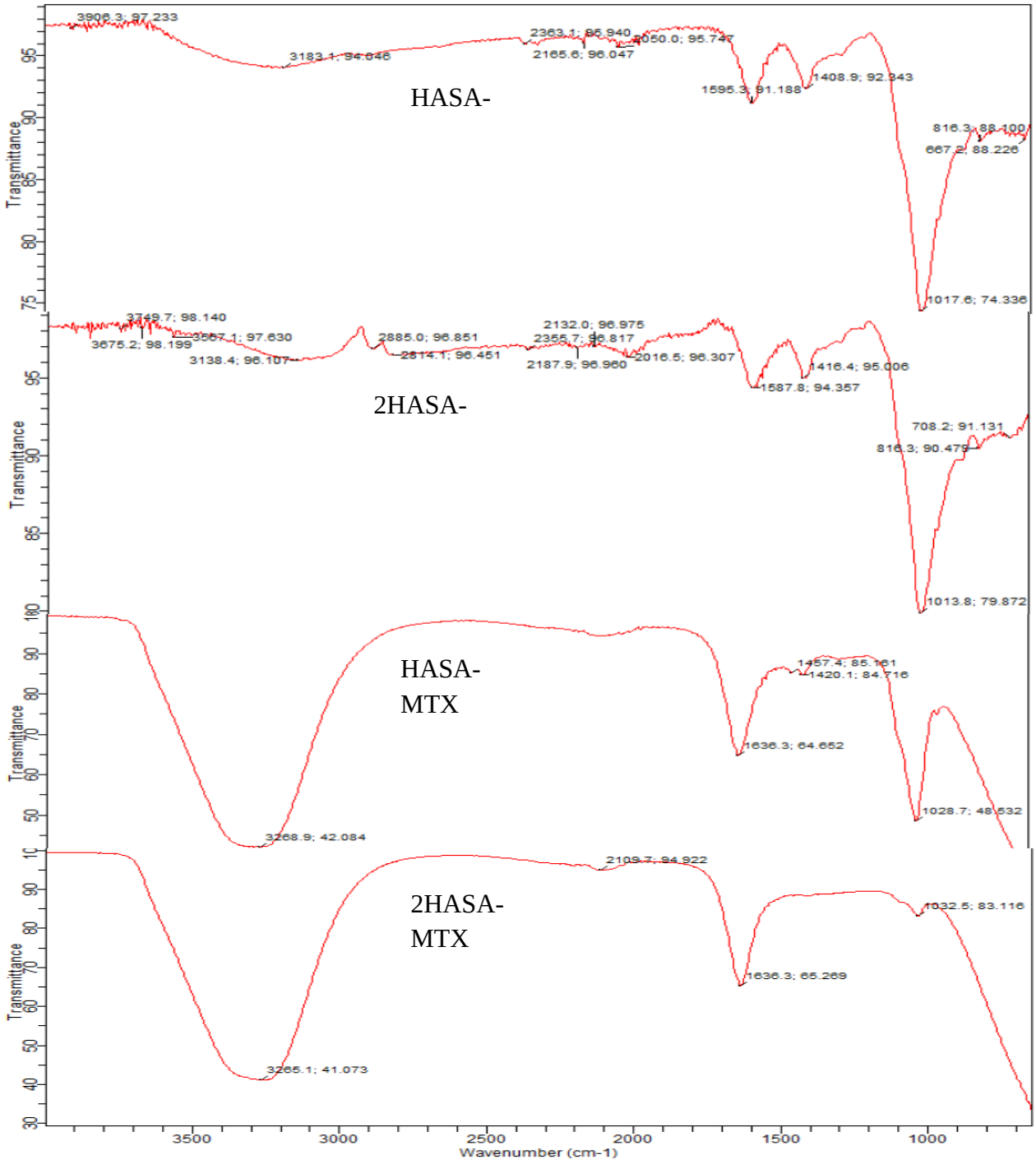


**Figure 4.21**: FTIR Spectra of DOX-loaded nanocomposite by the first synthetic route (HASA-DOX), DOX-Loaded nanocomposite by the second synthetic route (2HASA-DOX), MTX-Loaded nanocomposite by the first synthetic route (HASA-MTX), and MTX-loaded nanocomposite by the second synthetic route (2HASA-MTX)

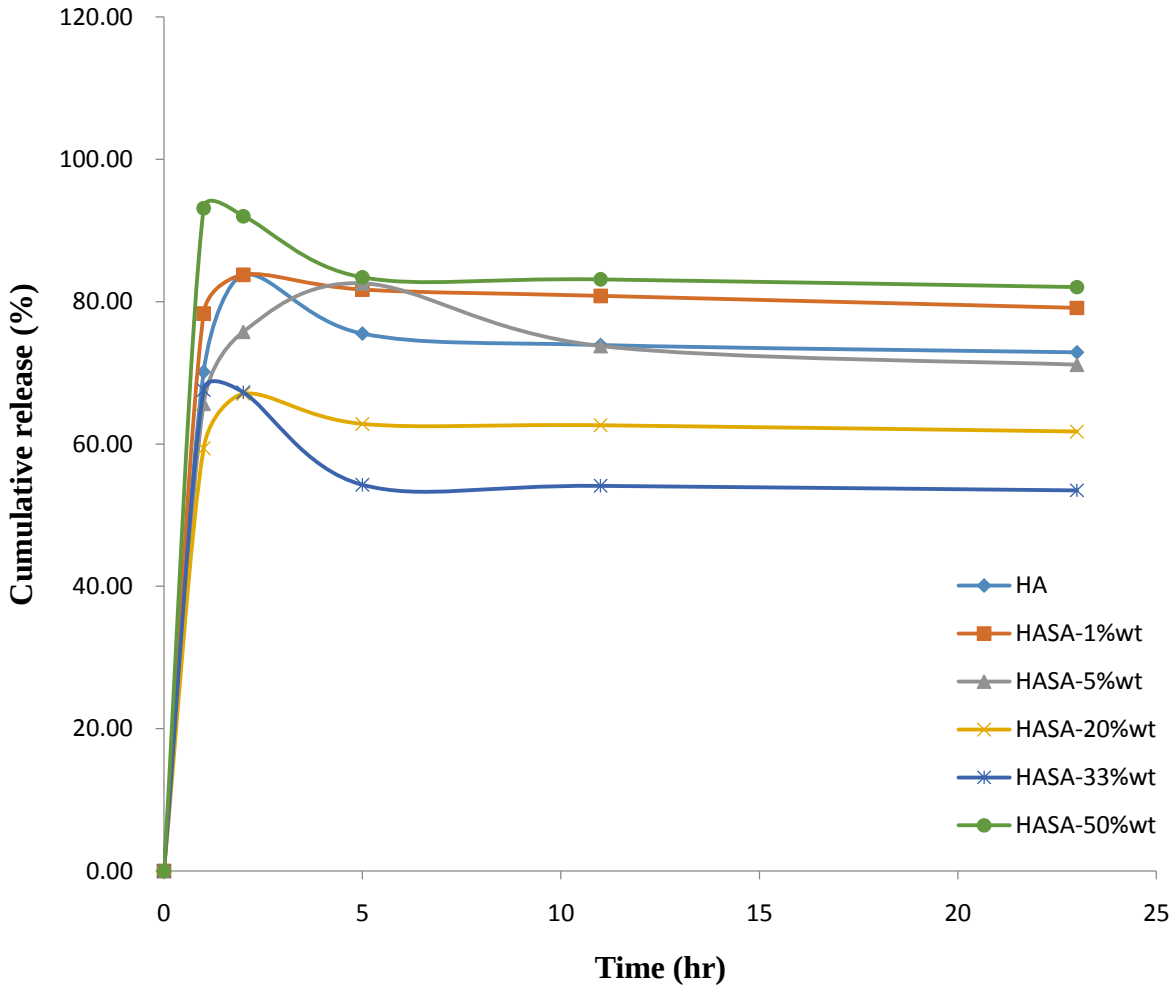


**Figure 4.22**: Drug release profiles of MTX from HA and HASA of different formulations

**Table 4.9** Comparison MTX release profile from HA and HASA nanocomposites using similarity factors

| | HA |
|---|---|
| HASA-1%wt | 55.76 |
| HASA-5%wt | 50.14 |
| HASA-20%wt | 65.02 |
| HASA-33%wt | 36.58 |
| HASA-50%wt | 33.35 |

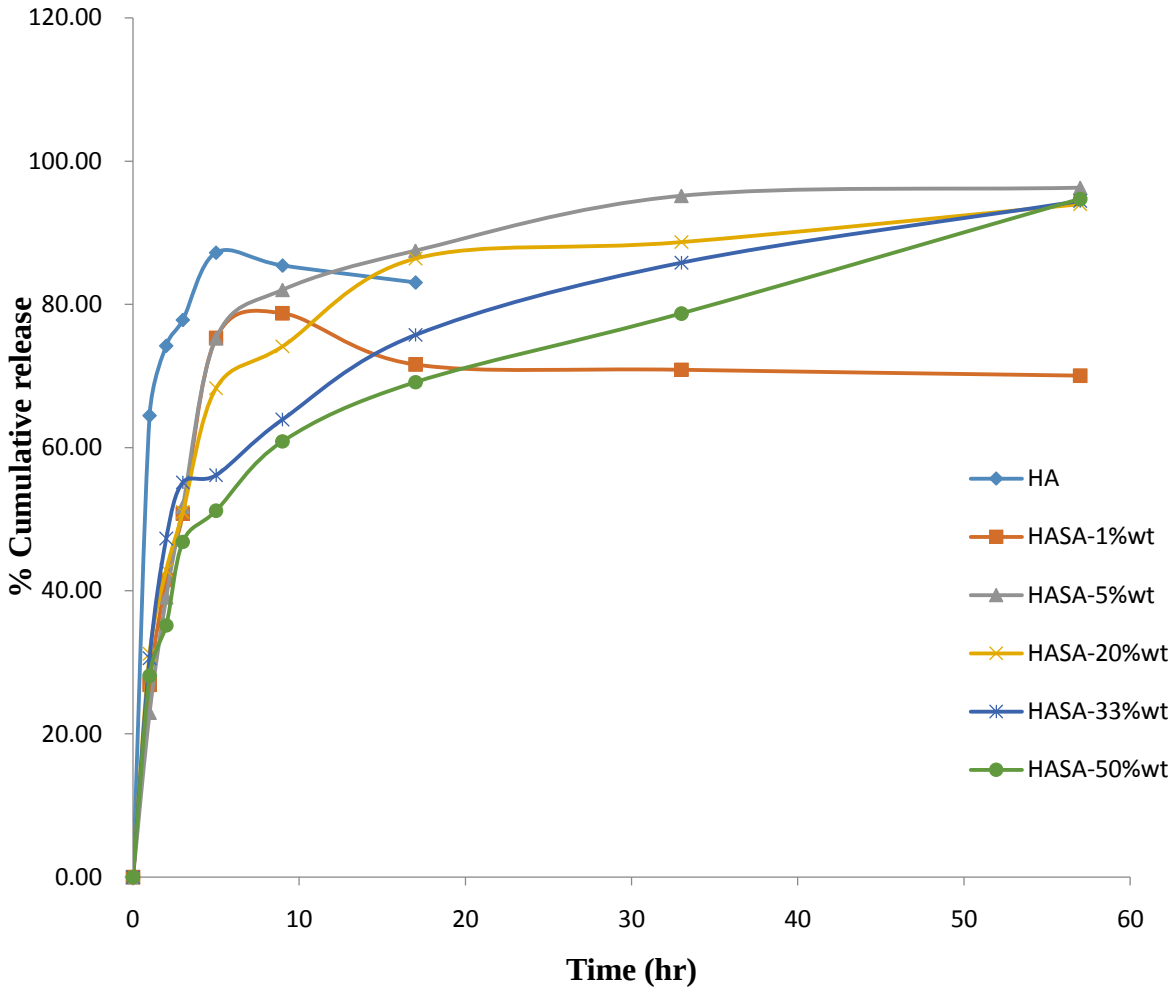


**Figure 4.23**: Drug release profiles of DOX from HA and HASA of different formulations

**Table 4.10:** Comparison of DOX release profiles from nanocomposites of different formulations using similarity factor (f2)

| | HA | HASA - 1%wt | HASA-5%wt | HASA-20%wt | HASA-33%wt | HASA-50%wt |
|---|---|---|---|---|---|---|
| HA | 100 | | | | | |
| HASA-1%wt | 32.39 | 100 | | | | |
| HASA-5%wt | 31.59 | 43.92 | 100 | | | |
| HASA-20%wt | 33.13 | 46.75 | **63.89** | 100 | | |
| HASA-33%wt | 31.42 | 44.46 | 48.15 | **58.26** | 100 | |
| HASA-50%wt | 26.84 | 43.45 | 43.01 | 49.26 | **59.96** | 100 |

**Table 4.11**: Kinetic and mechanistic models of DOX release from HA and HASA

| MODELS | Parameters | HA | HASA-1%wt | HASA-5%wt | HASA-20%wt | HASA-33%wt | HASA-50%wt |
|---|---|---|---|---|---|---|---|
| Zero Order | $R^2$ | 0.5711 | 0.4346 | 0.5201 | 0.7884 | 0.7830 | 0.8360 |
| | $R^2$-adj | 0.4281 | 0.3403 | 0.4402 | 0.6216 | 0.7468 | 0.8087 |
| | MSC | 0.0464 | 0.0702 | 0.2343 | 0.4718 | 1.0278 | 1.3078 |
| | $K_0(mol.L^{-1}s^{-1})$ | 2.791 | 0.726 | 1.024 | 0.928 | 0.967 | 1.055 |
| First Order | $R^2$ | 0.6379 | 0.5555 | 0.9720 | 0.9555 | 0.9334 | 0.9454 |
| | $R^2$-adj | 0.6379 | 0.5555 | 0.9720 | 0.9481 | 0.9223 | 0.9363 |
| | MSC | 0.6159 | 0.5608 | 3.3258 | 2.6161 | 2.2094 | 2.4084 |
| | K1 ($s^{-1}$) | 1.000 | 0.2350 | 0.2640 | 0.138 | 0.0700 | 0.0540 |
| Korsmeyer-Peppas | $R^2$ | 0.9760 | 0.9089 | 0.9185 | 0.9590 | 0.8175 | 0.9599 |
| | $R^2$-adj | 0.9639 | 0.8785 | 0.8913 | 0.9453 | 0.7566 | 0.9465 |
| | MSC | 2.728 | 1.595 | 1.707 | 2.384 | 0.9008 | 2.416 |
| | N | 0.220 | 0.4580 | 0.4970 | 0.3740 | 0.2500 | 0.3350 |
| Higuchi | $R^2$ | 0.6067 | 0.6005 | 0.6004 | 0.6955 | 0.8410 | 0.8955 |
| | $R^2$-adj | 0.4755 | 0.5340 | 0.5338 | 0.6448 | 0.8145 | 0.8781 |
| | MSC | 0.1331 | 0.4176 | 0.4173 | 0.6892 | 1.3388 | 1.7584 |
| | $K_H$ | 23.03 | 7.313 | 13.92 | 12.82 | 12.68 | 12.68 |
| Hixon-Crowel | $R^2$ | 0.9007 | 0.5635 | 0.8203 | 0.8931 | 0.9177 | 0.9248 |
| | $R^2$-adj | 0.8677 | 0.4908 | 0.7904 | 0.8752 | 0.9040 | 0.9122 |
| | MSC | 1.510 | 0.3291 | 1.216 | 1.735 | 1.997 | 2.087 |
| | KHC | 0.092 | 0.0160 | 0.0220 | 0.0200 | 0.0150 | 0.012 |
| Hopfenberg | $R^2$ | 0.9263 | 0.6304 | 0.9720 | 0.9555 | 0.9332 | 0.9454 |
| | $R^2$-adj | 0.8525 | 0.4825 | 0.9673 | 0.9377 | 0.9064 | 0.9235 |
| | MSC | 1.407 | 0.2453 | 3.075 | 2.362 | 1.955 | 2.157 |
| | N | 1.160 | 179.2 | 2816 | 1573 | 146.6 | 932.4 |

### 4.7.3 Comparison of DOX release profiles from HASA and 2HASA

DOX release profiles from nanocomposites synthesized from the first synthetic route (HASA) and second synthetic route (2HASA) are presented in Figures 4.24 – 4.27. The comparison was carried out for nanocomposites when the same quantities of precursors were used following the two different routes. Each pair of these profiles was subjected to similarity test in order to ascertain the statistical equivalence or otherwise of the profiles. The result presented in Figure 4.28 shows that the release profiles for all the compared pairs are above 50, showing that they are all similar.

## 4.8 Evaluation of Different Loading Methods

Result of DOX loading efficiency by the four different methods is presented in Figure 4.29. It shows high encapsulation for all the methods with no significant difference among the methods. The values as follows: method 1 (88.11%), method 2 (87.40%), method 3 (89.64%), and method 4 (88.64%). Release profiles for DOX loaded by the different methods are shown in Figure 4.30. The results show higher initial burst release for method 1 than other methods, with sustained release which lasted for 57 hours.

Figure 4.31 is the result of MTX loading efficiency by the four different loading methods. It shows that method 2 and method 4 loaded MTX better than method 1 and method 3. The release profiles presented in Figure 4.32 shows that method 4 sustained the release of MTX more than other methods.

## 4.9 Effect of medium of synthesis on Drug Loading and Release

The result of DOX loading from nanocomposites synthesized using different solvents is presented in Figure 4.33. The result shows that nanocomposite prepared from water medium has the highest drug encapsulation efficiency. The release profiles shown in Figure 4.34 also indicate that nanocomposites synthesized from water medium has slower release rate than others. Profile comparison using difference factor (f1), showed that there is no significant difference between release profile of DOX from nanocomposite synthesized in acetone and ethylacetate (Table 4.12) Presented in Table 4.13 are the results of kinetic and mechanistic study, using zero order model, first order model, Korsmeyer-Peppas model, Higuchi model, Hixon-Crowel model and Hopfenberg model. All the formulations follow first order release rate, while the n exponent in the Korsmeyer-Peppas equation indicates that the release mechanism is dominated by Fickian diffusion.

In order to examine the effect of these solvents on the functional groups present in the nanocomposites, FTIR analysis was carried out. The result is presented in Figure 4.35. The results show similar functional groups for all the nanocomposites.

## 4.10 Effect of pH Medium on Release of DOX

The release profiles of DOX at different pH media (pH 3, pH 5 and pH 7.4) are presented in Figure 4.36. The results shows higher initial release for acidic pH (pH 3 and pH 5) which slowed down at the latter part of the release study

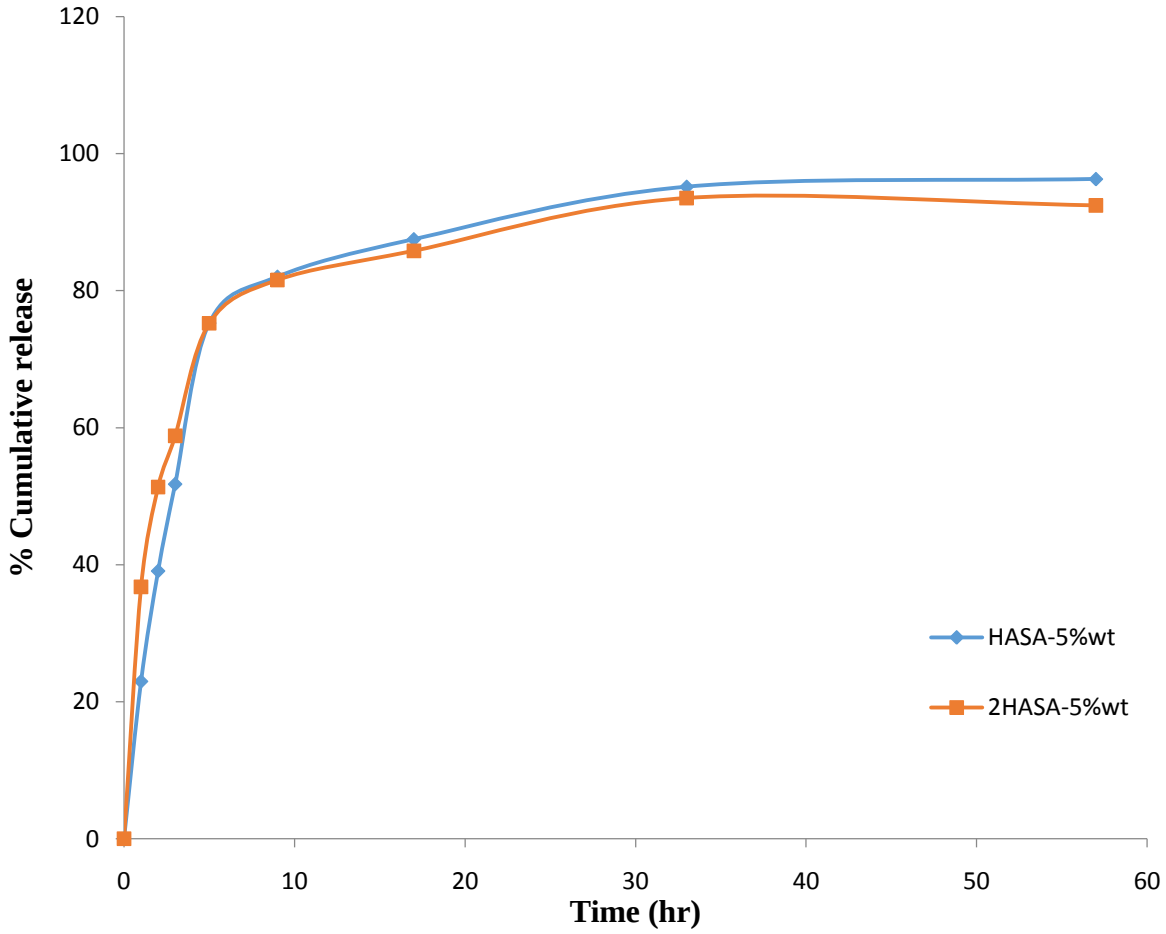


**Figure 4.24**: DOX release profiles from nanocomposites prepared with 5%wt sodium alginate following first route (HASA-5%wt) and route (2HASA-5%wt)

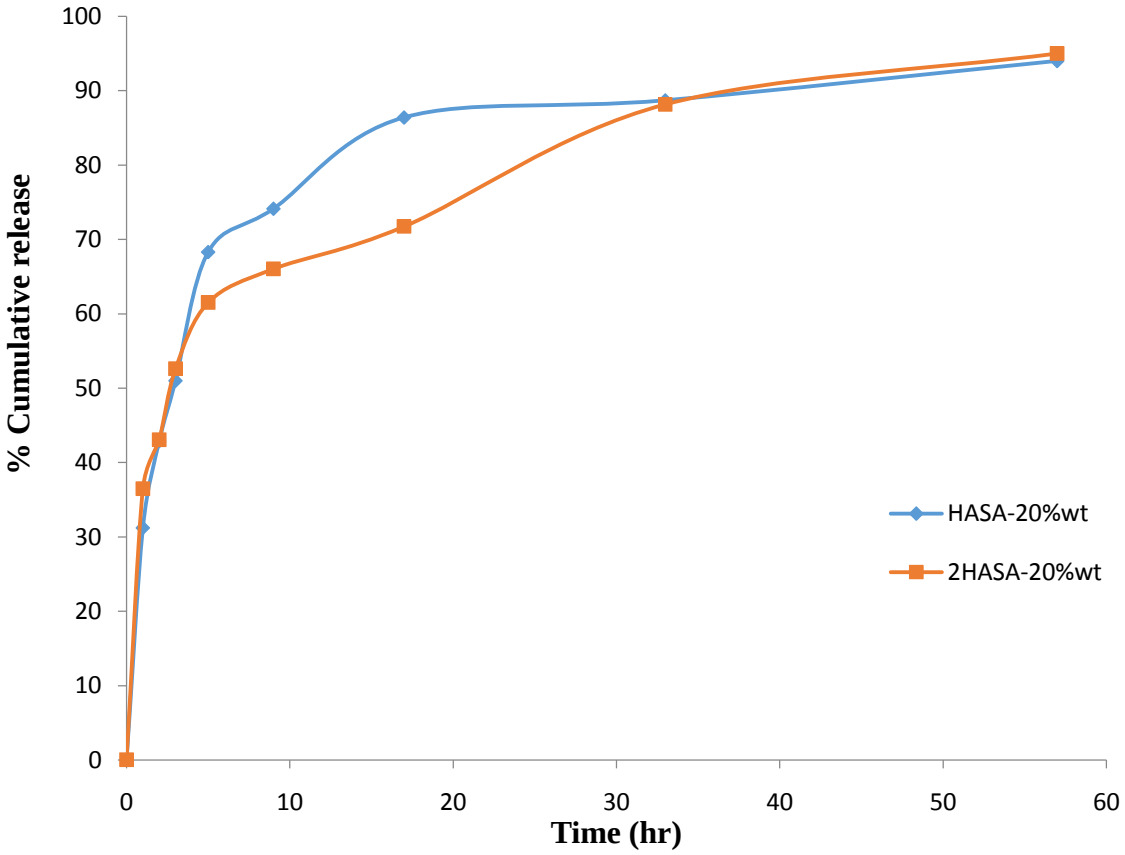


**Figure 4.25**: DOX release profiles from nanocomposites prepared with 20%wt sodium alginate following first route (HASA-20%wt) and second route (2HASA-20%wt)

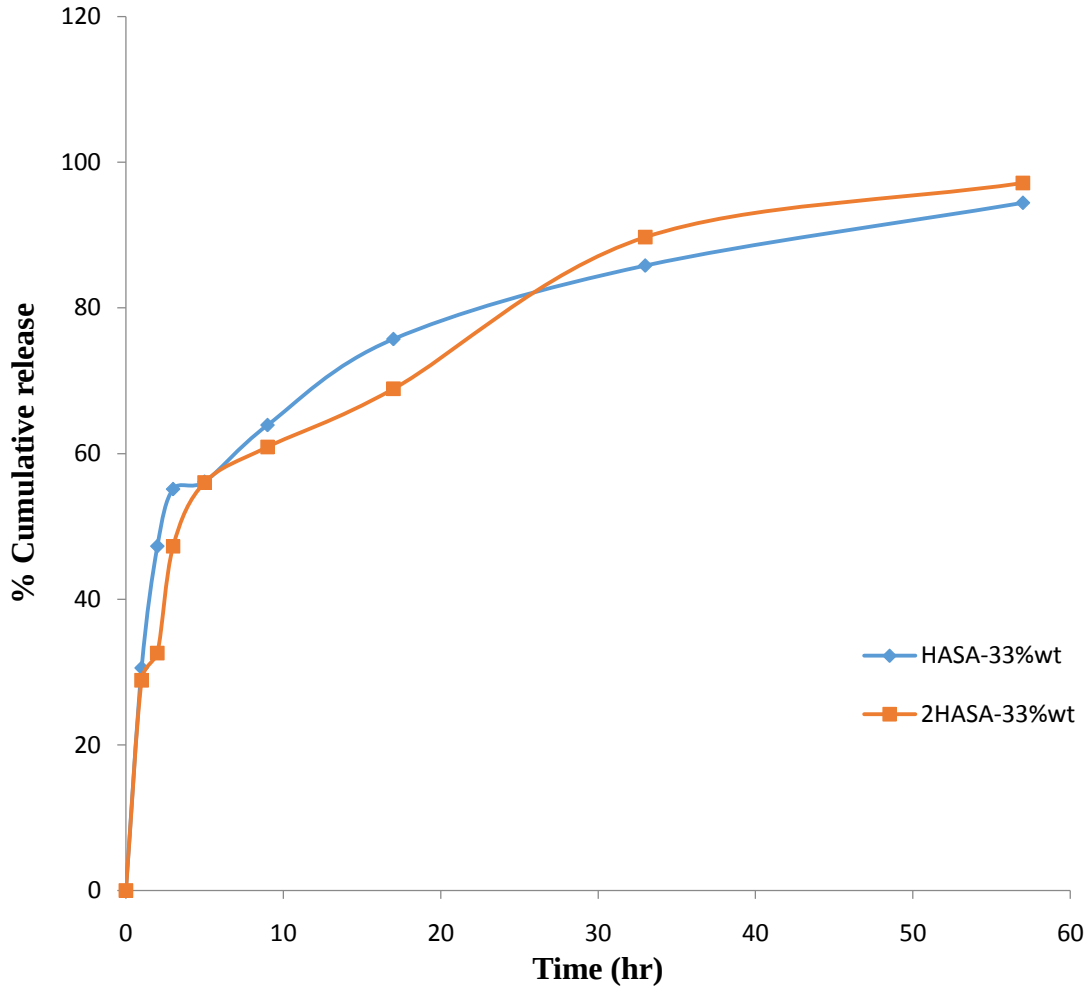


**Figure 4.26**: DOX release profiles from nanocomposites prepared with 33%wt sodium alginate following first route (HASA-33%wt) and second route (2HASA-33%wt)

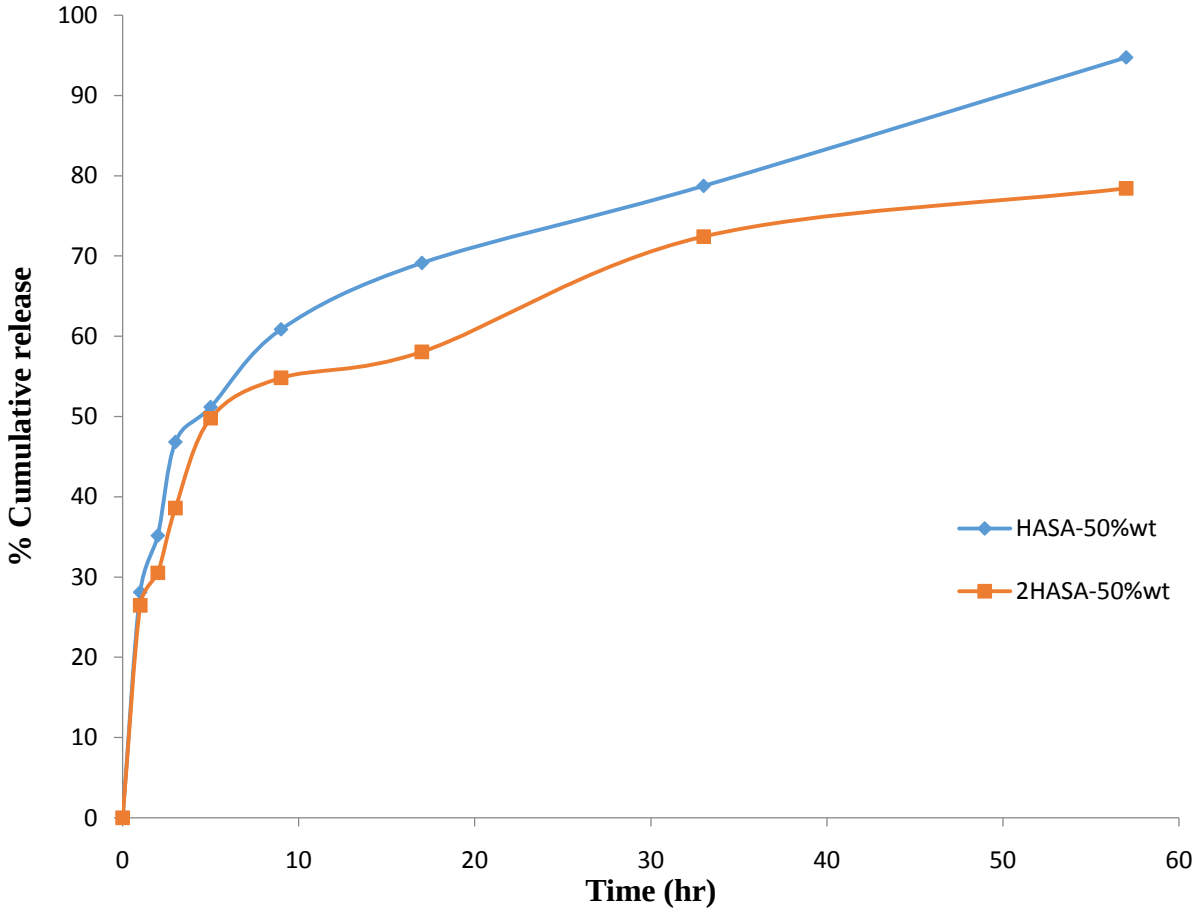


**Figure 4.27:** DOX release profiles from nanocomposites prepared with 50%wt sodium alginate following first route (HASA-50%wt) and second route (2HASA50%wt)

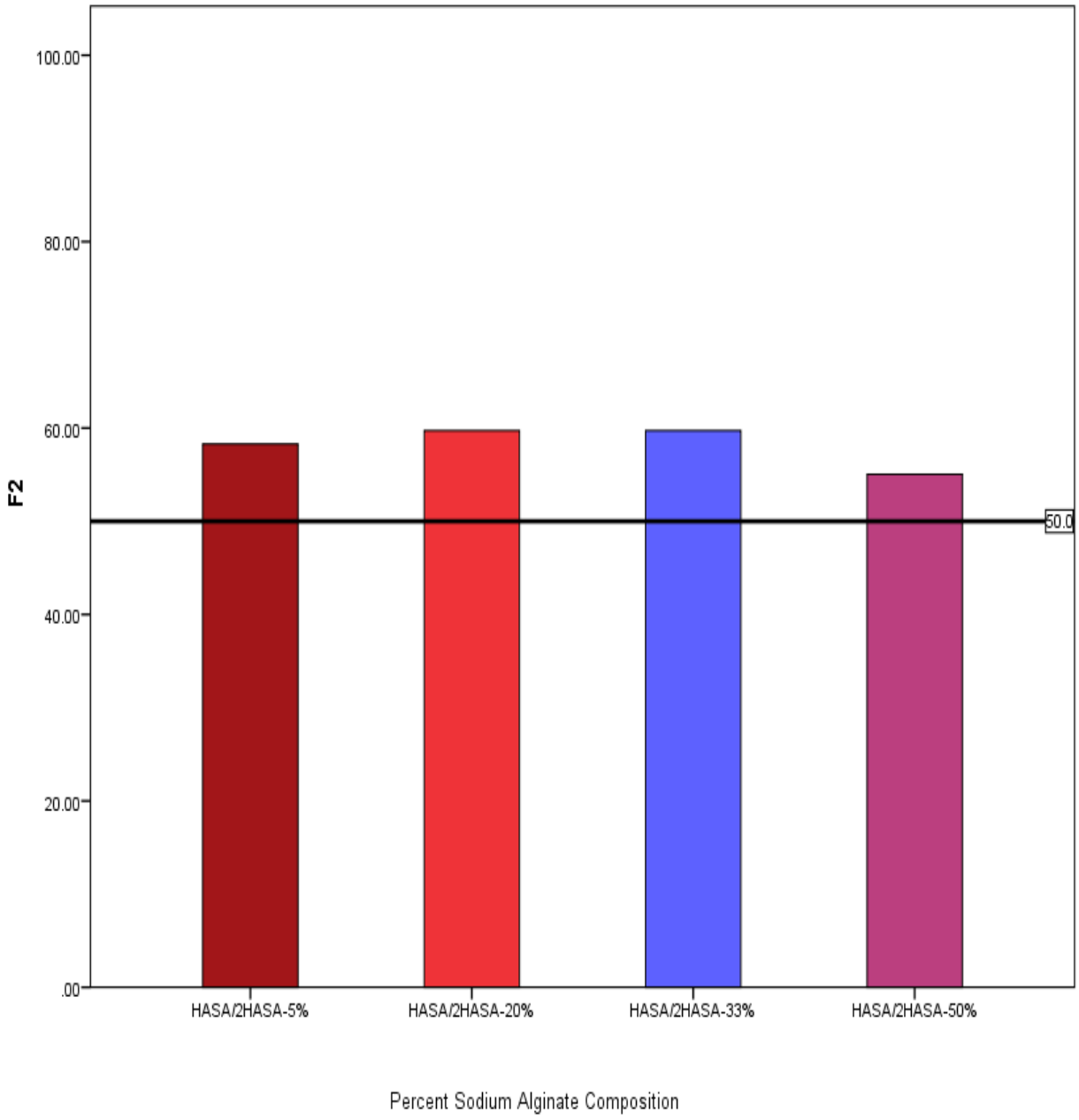


**Figure 4.28**: Comparison of DOX release profiles from nanocomposites prepared from first synthetic route (HASA) and second synthetic route (2HASA)

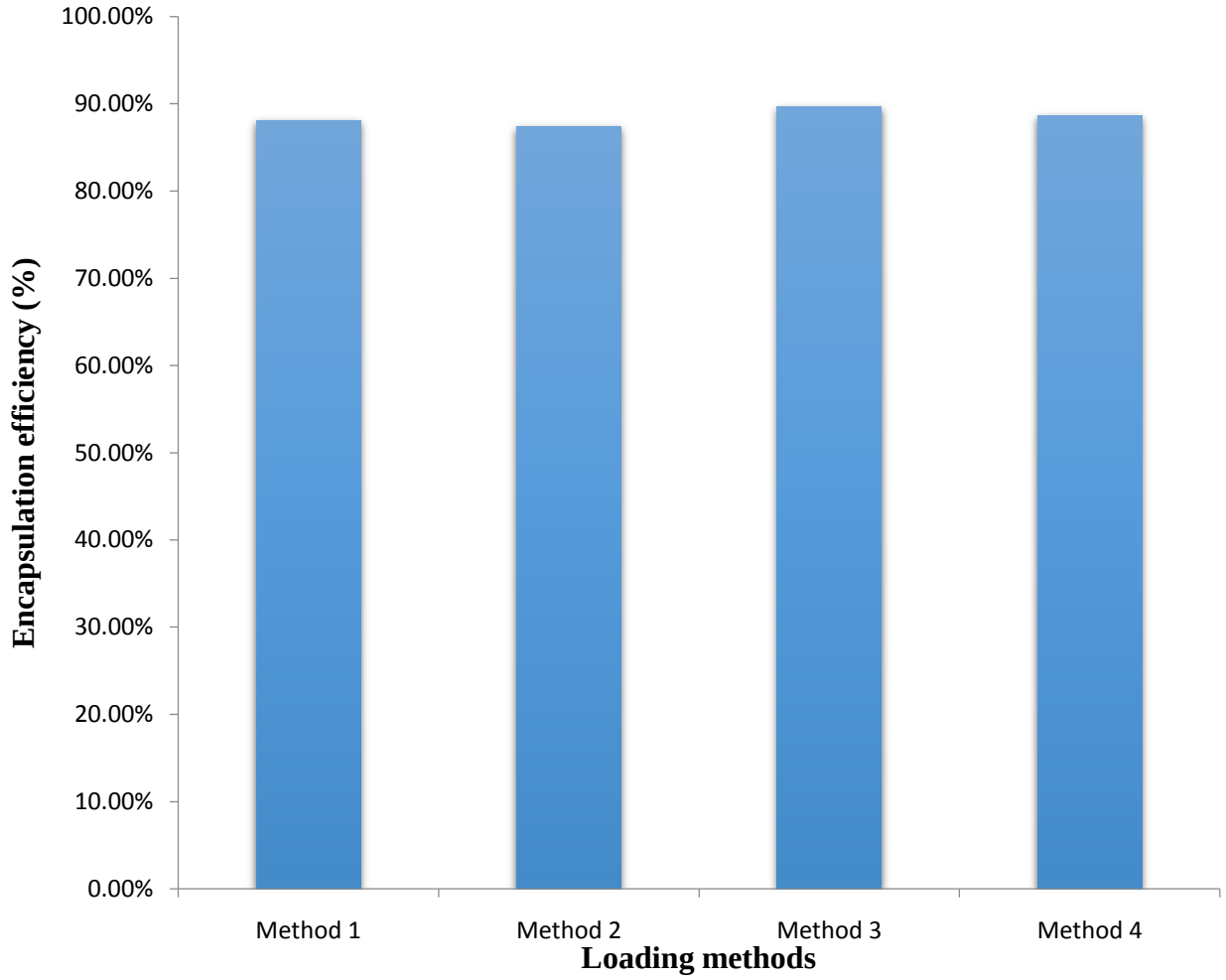


**Figure 4.29**: Loading efficiency of DOX encapsulated using different methods

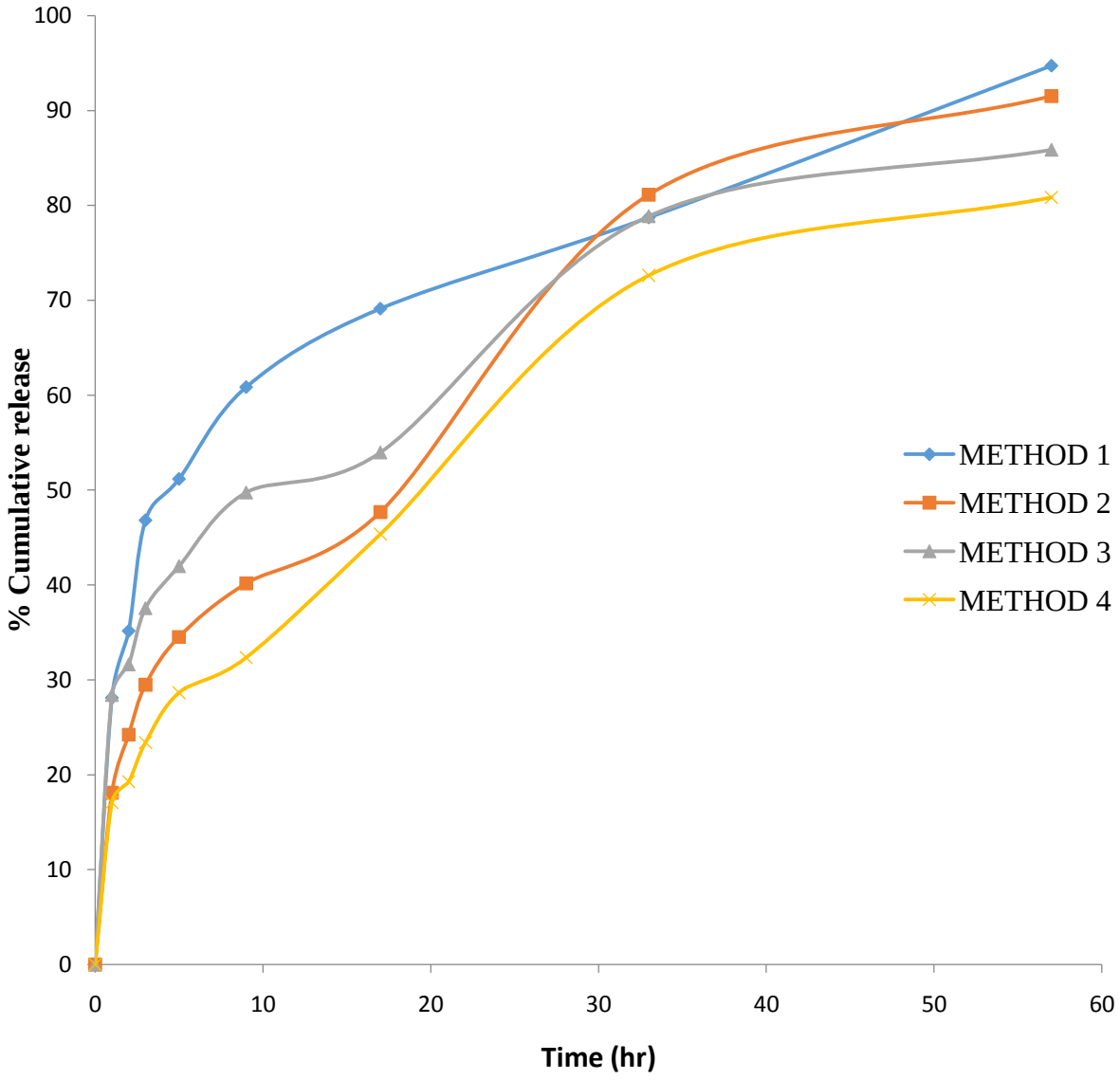


**Figure 4.30**: Release profiles of DOX loaded into HASA by different loading methods

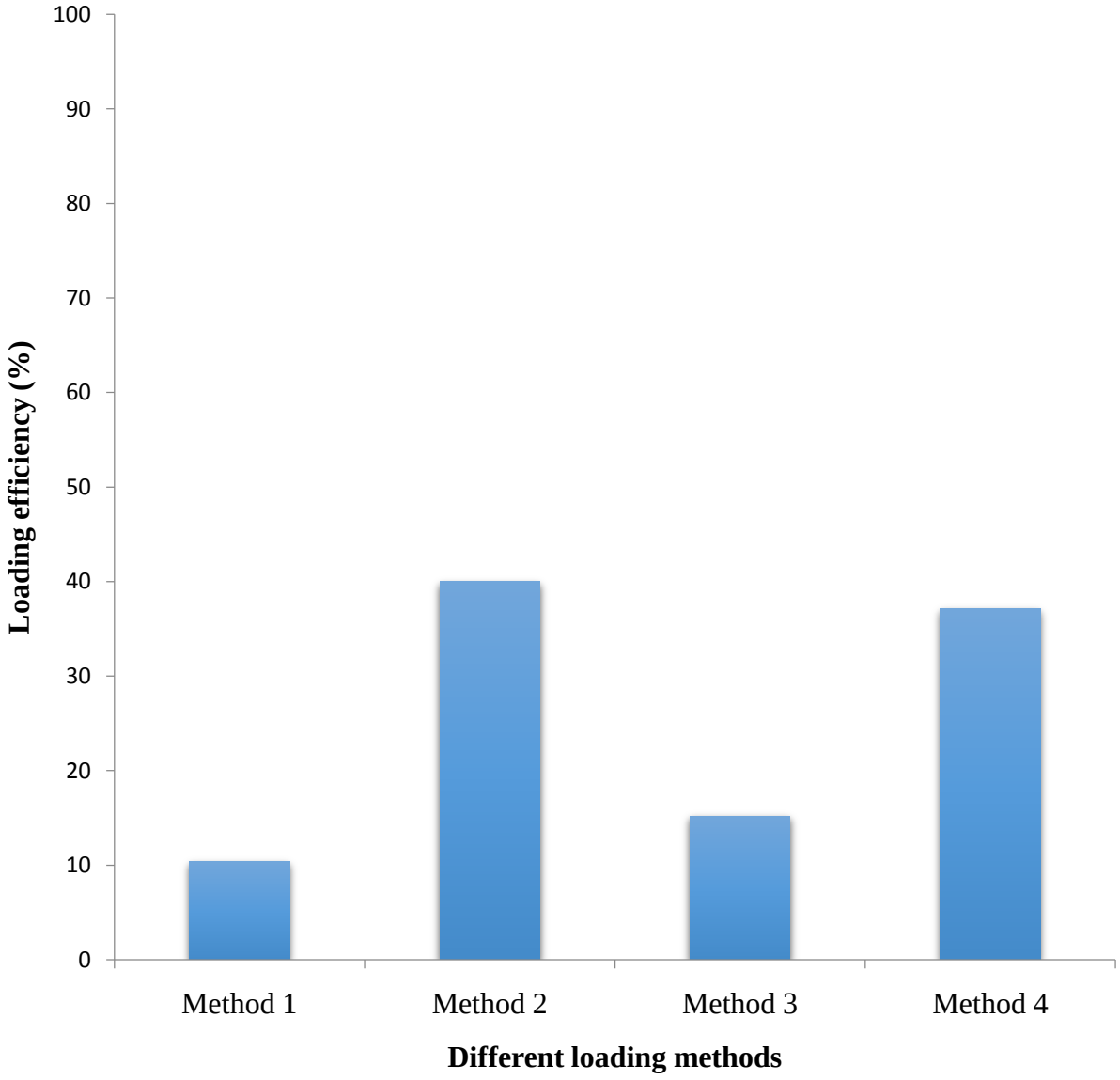


**Figure 4.31**: Loading efficiency of MTX encapsulated using different methods

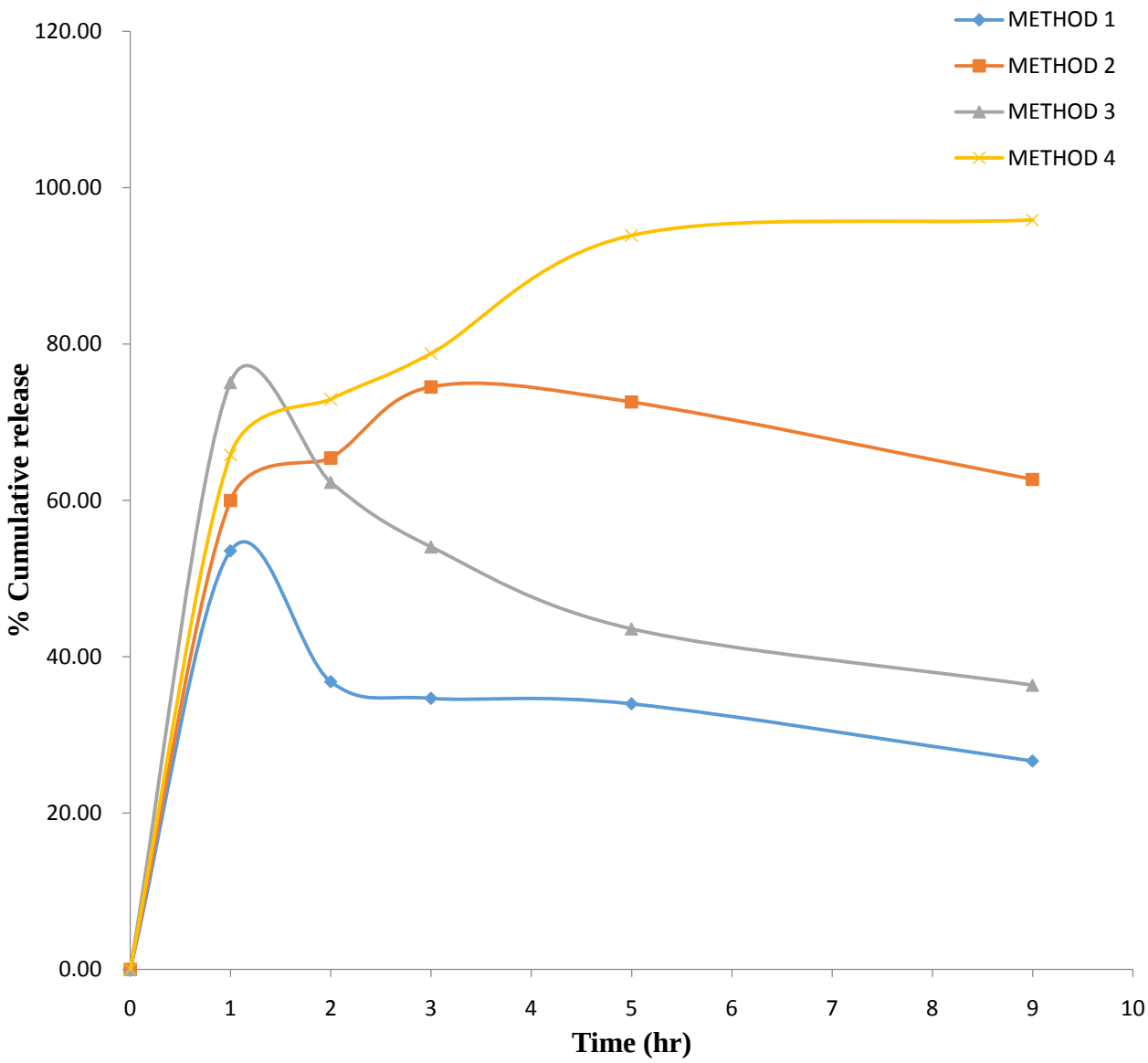


**Figure 4.32**: Release profiles of MTX loaded into HASA nanocomposites by different loading methods

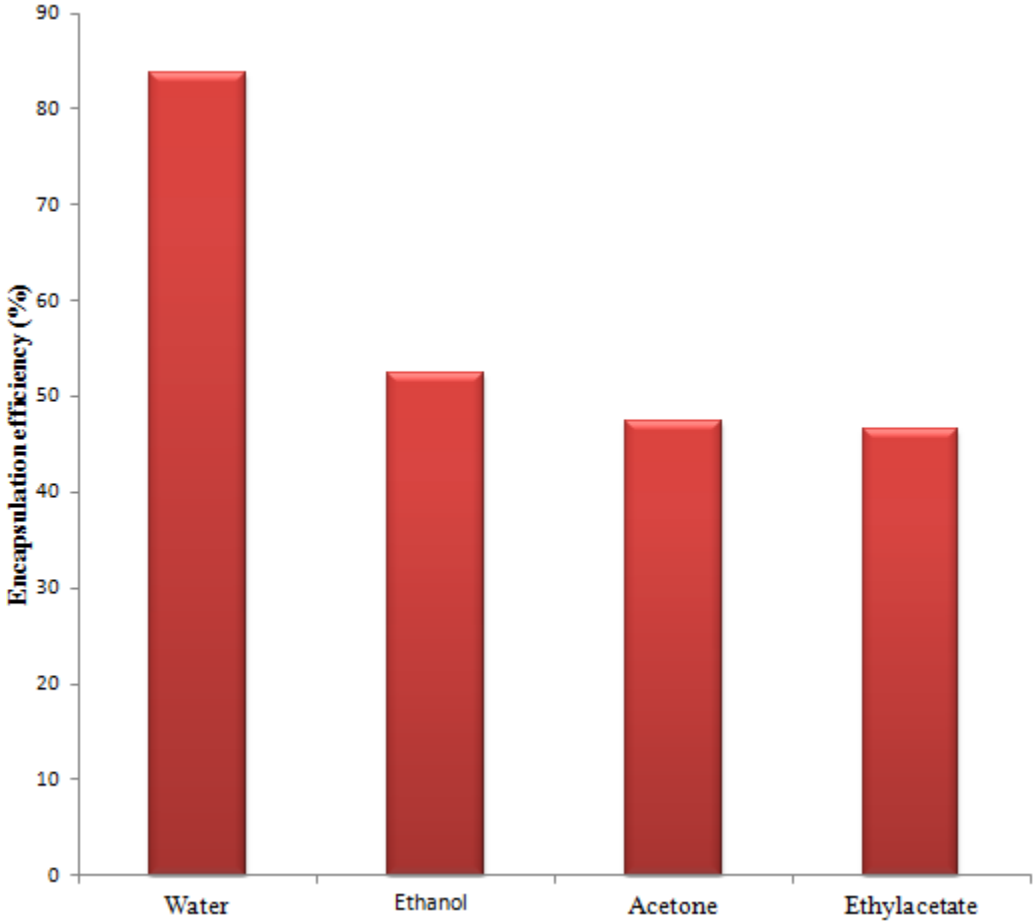


**Figure 4.33**: DOX encapsulation efficiency from nanocomposites prepared in different solvents

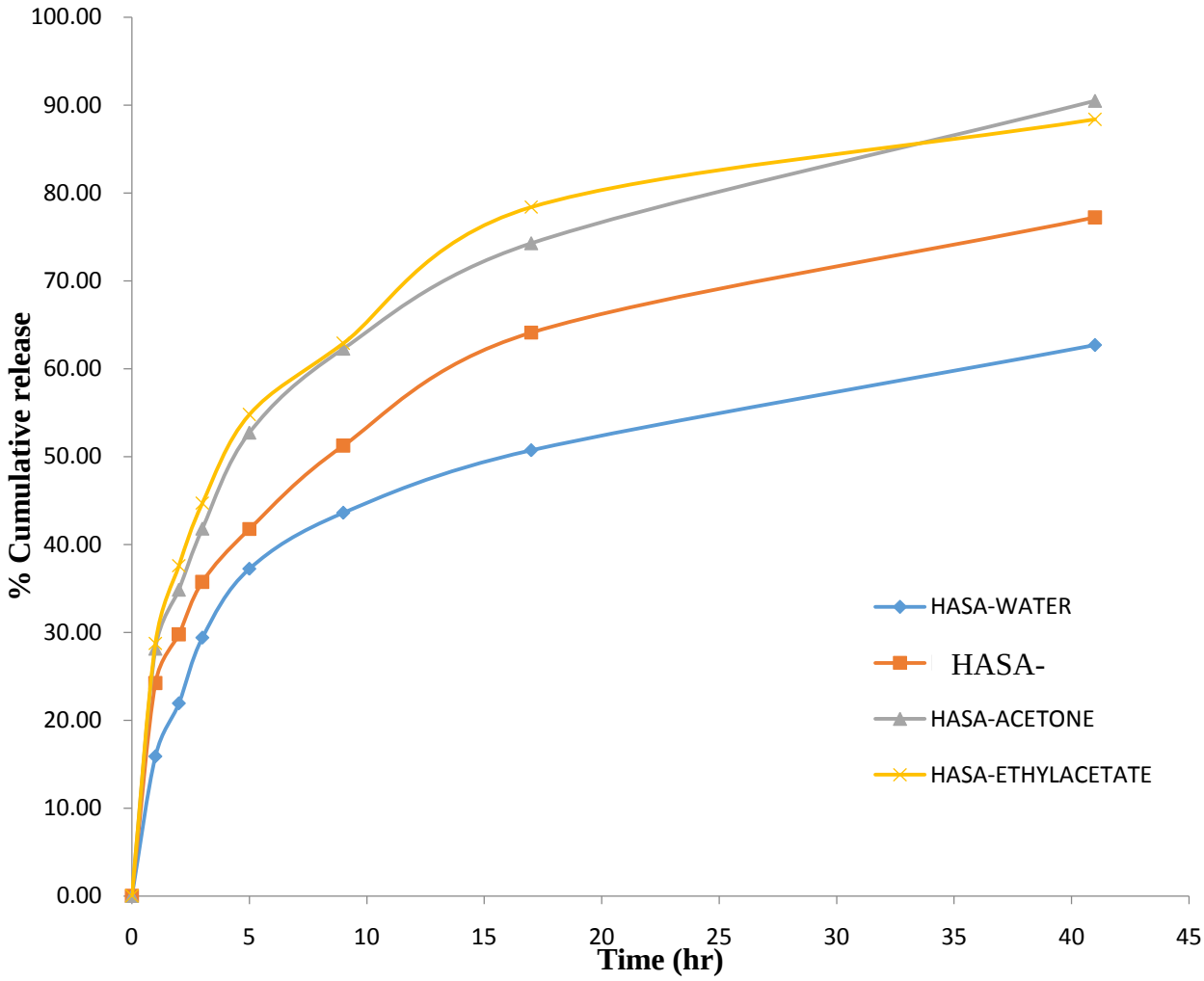


**Figure 4.34**: DOX release profiles from nanocomposites prepared in different media (solvents)

**Table 4.12**: Comparison of DOX release profiles from nanocomposites synthesised in different media (solvents) using difference factors ($f_2$)

| | Water | Ethanol | Acetone | Ethylacetate |
|---|---|---|---|---|
| Water | 0 | | | |
| Ethanol | 23.96 | 0 | | |
| Acetone | 47.1 | 18.67 | 0 | |
| Ethylacetate | 51.26 | 22.02 | **3.92** | 0 |

**Table 4.13**: Kinetic and mechanistic models of DOX release from HASA synthesized in different solvents

| MODEL | PARAMETER | WATER | ACETONE | ETHANOL | ETHYLACETATE |
|---|---|---|---|---|---|
| Zero Order | $R^2$ | 0.7837 | 0.8244 | 0.8479 | 0.7729 |
| | $R^2$-adj | 0.7405 | 0.7892 | 0.8175 | 0.7275 |
| | MSC | 0.9597 | 1.168 | 1.312 | 0.911 |
| | $K_0$ ($mol.L^{-1}s^{-1}$) | 1.021 | 1.421 | 1.233 | 1.33 |
| First Order | $R^2$ | 0.9297 | 0.9749 | 0.9501 | 0.9600 |
| | $R^2$-adj | 0.9157 | 0.9698 | 0.9401 | 0.9520 |
| | MSC | 2.083 | 3.112 | 2.426 | 2.646 |
| | K1 ($s^{-1}$) | 0.224 | 0.0670 | 0.0370 | 0.0710 |
| Korsmeyer-Peppas | $R^2$ | 0.9722 | 0.9916 | 0.9977 | 0.9864 |
| | $R^2$-adj | 0.9629 | 0.9888 | 0.9969 | 0.9818 |
| | MSC | 2.782 | 3.979 | 5.277 | 3.494 |
| | N | 0.4410 | 0.372 | 0.345 | 0.349 |
| Higuchi | $R^2$ | 0.9222 | 0.9503 | 0.9638 | 0.9192 |
| | $R^2$-adj | 0.9066 | 0.9403 | 0.9566 | 0.9030 |
| | MSC | 1.982 | 2.428 | 2.748 | 1.944 |
| | $K_H$ | 8.377 | 11.53 | 9.937 | 10.99 |
| Hixon-Crowel | $R^2$ | 0.8314 | 0.9488 | 0.9196 | 0.9286 |
| | $R^2$-adj | 0.7977 | 0.9385 | 0.9036 | 0.9143 |
| | MSC | 1.208 | 2.399 | 1.949 | 2.067 |
| | KHC | 0.006 | 0.0160 | 0.0090 | 0.0180 |
| Hopfenberg | $R^2$ | 0.8560 | 0.9747 | 0.9500 | 0.9599 |
| | $R^2$-adj | 0.7841 | 0.9621 | 0.9250 | 0.9398 |
| | MSC | 1.081 | 2.820 | 2.138 | 2.359 |
| | N | 648.9 | 399.4 | 928.2 | 1029 |

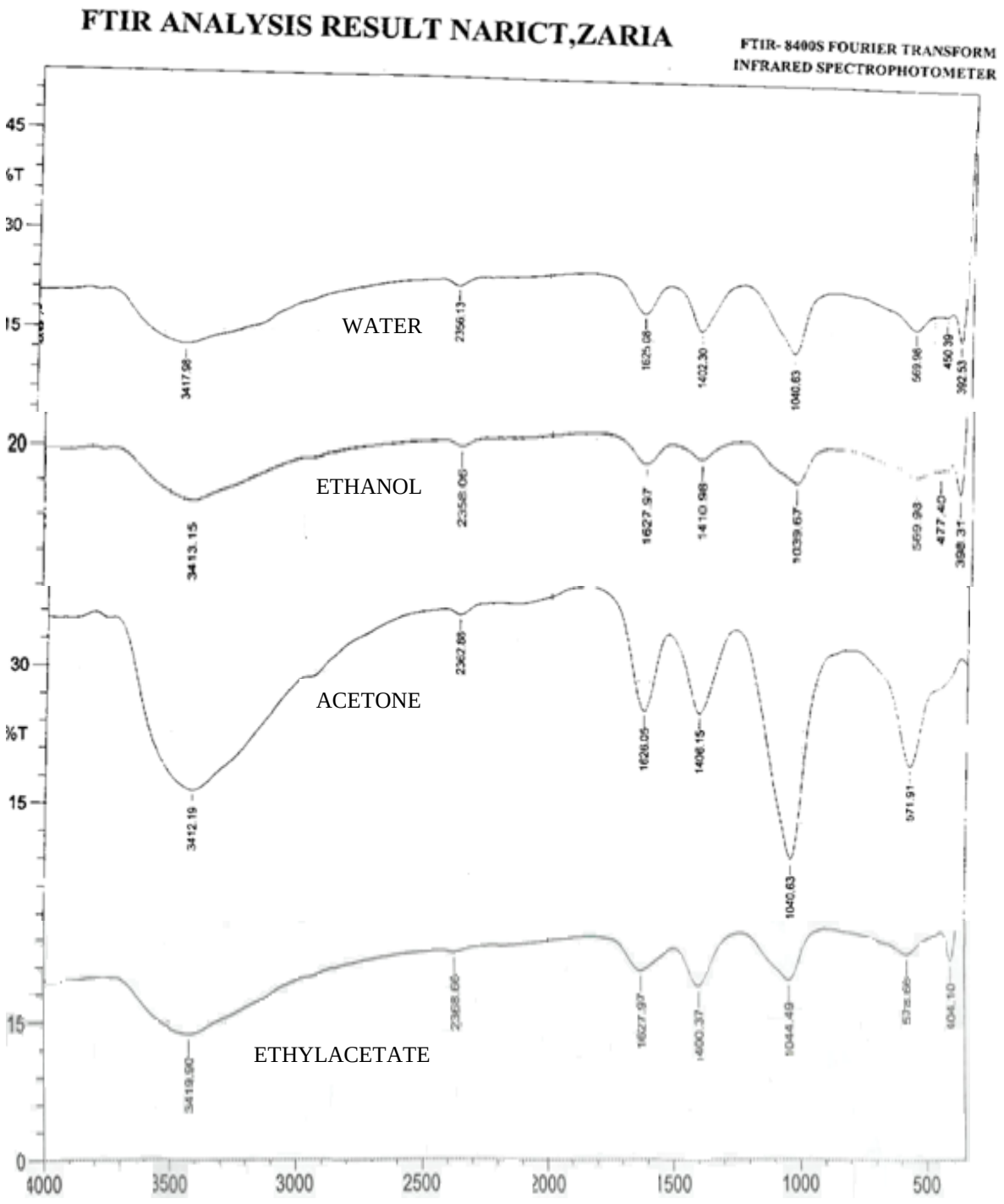


**Figure 4.35**: FTIR spectra of HASA synthesised under water, Ethanol, Acetone, and Ethylacetate media

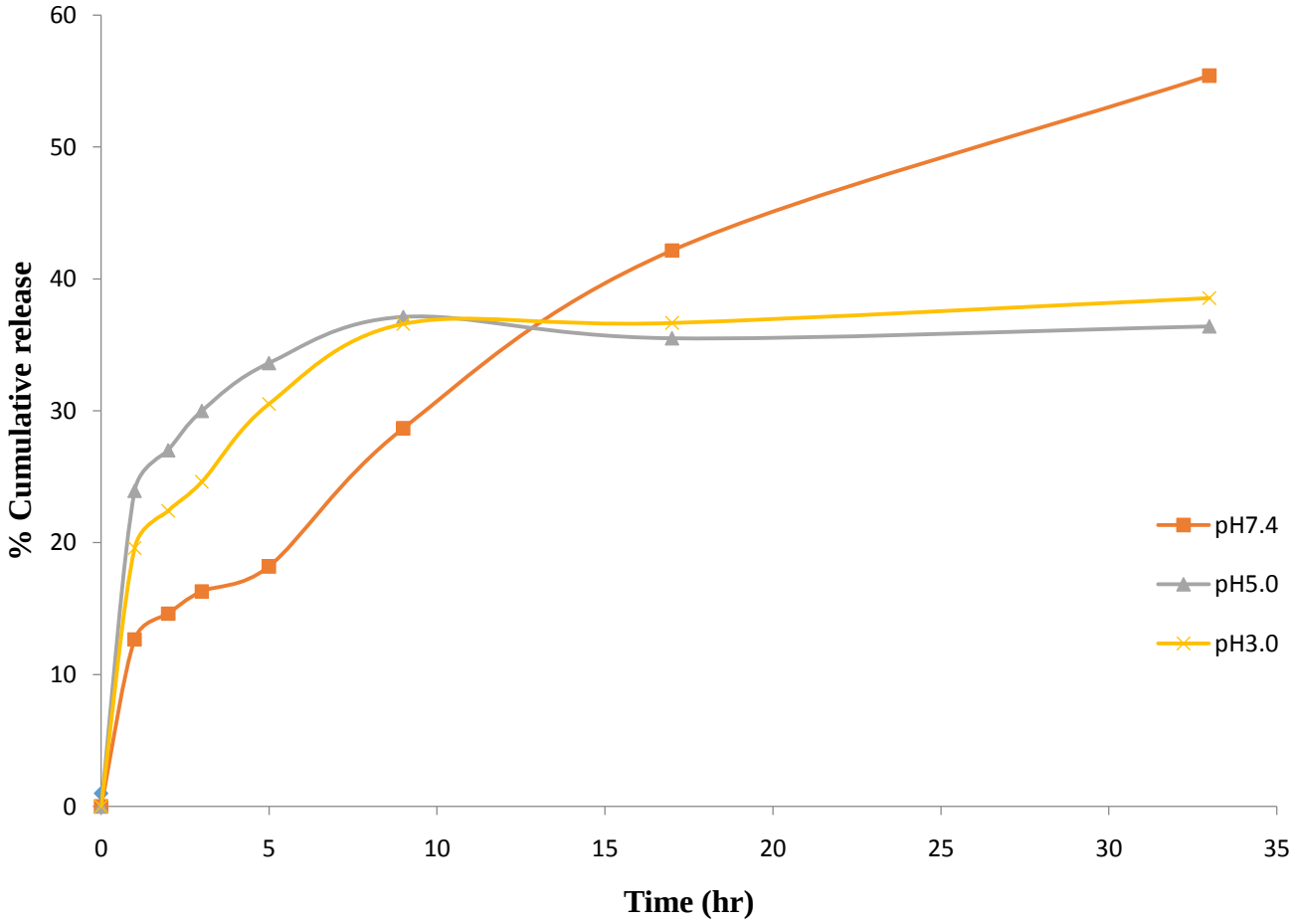


**Figure 4.36**: Release profiles of DOX-loaded HASA nanocomposites at different pH medium

### 4.11 Drug Combination Study

The results of DOX and MTX encapsulation efficiency at different combination ratio are presented in Figure 4.37. The study was conducted at DOX: MTX combination ratio of 16:1, 4:1, 1:1, 1:4, and 1:16 at loading efficiencies of 86.50%, 88.42%, 90.00%, 89.15% and 87.90% respectively. This shows that DOX was loaded high in the nanocomposites irrespective of the combination ratio. The loading efficiency for MTX decreased with increasing concentration of the drug. The release profiles for the different combination ratio are presented in Figures 4.38 – 4.42. The release of DOX was sustained in all the compositions, while MTX had high burst release.

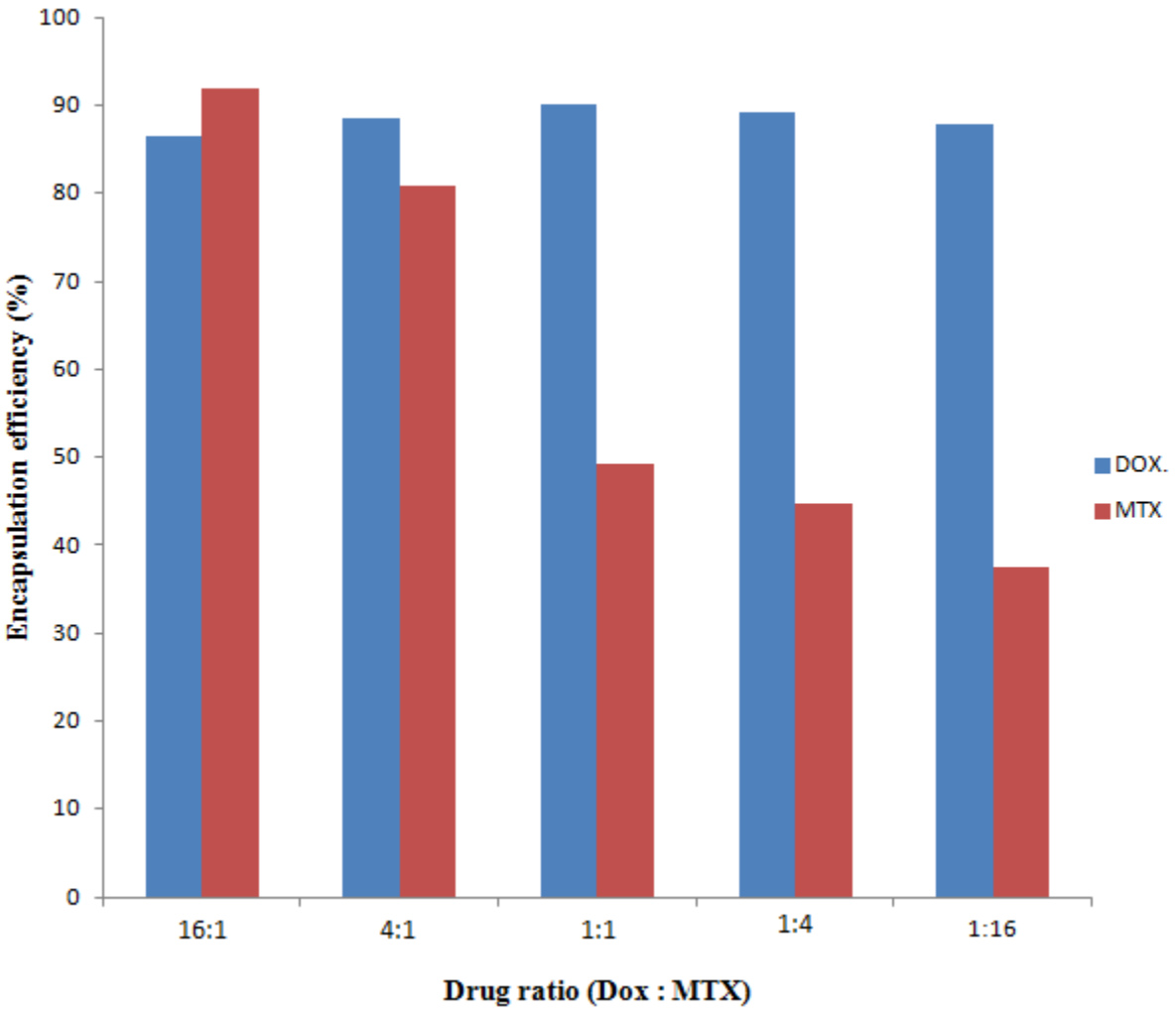


**Figure 4.37**: Loading efficiencies of drugs combined at different ratios (DOX: MTX)

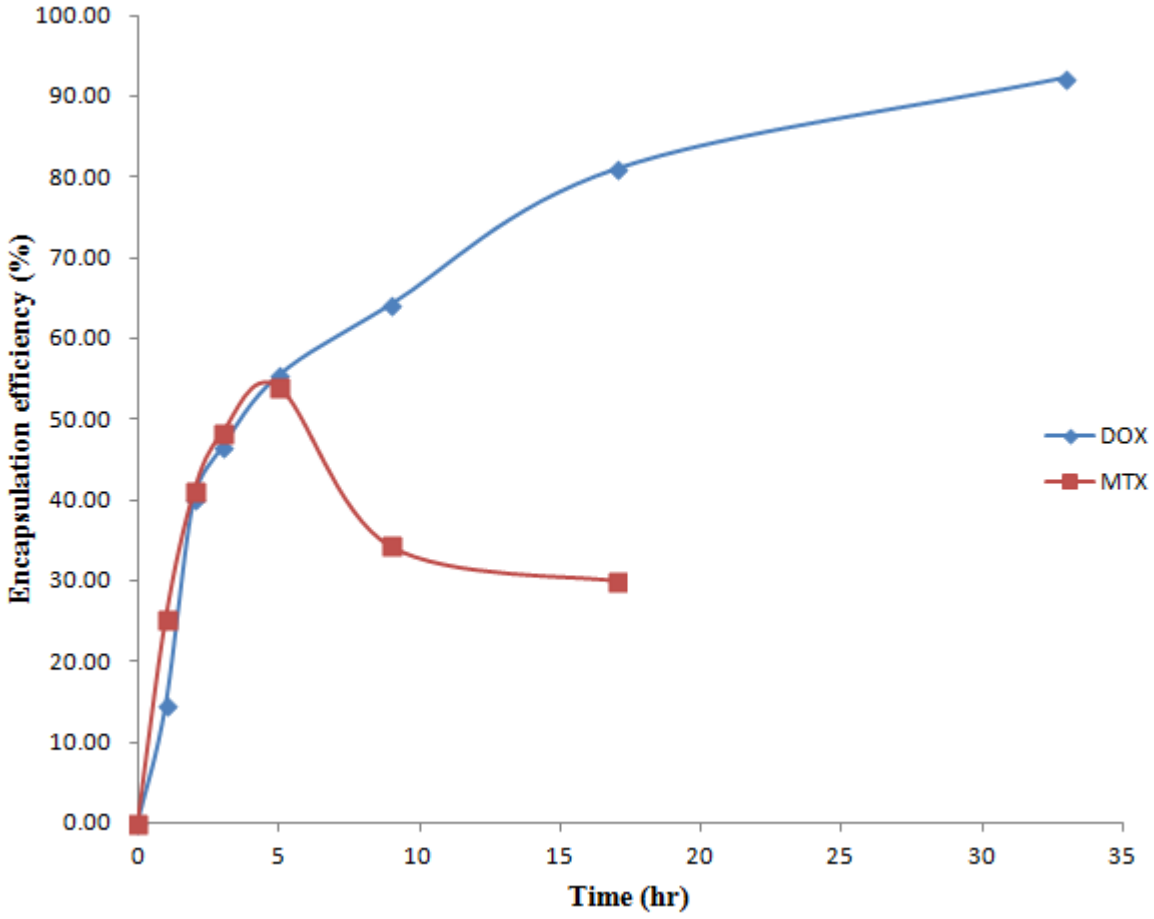


**Figure 4.38**: Release profiles of DOX and MTX at a combination ratio of 16: 1 (DOX:MTX)

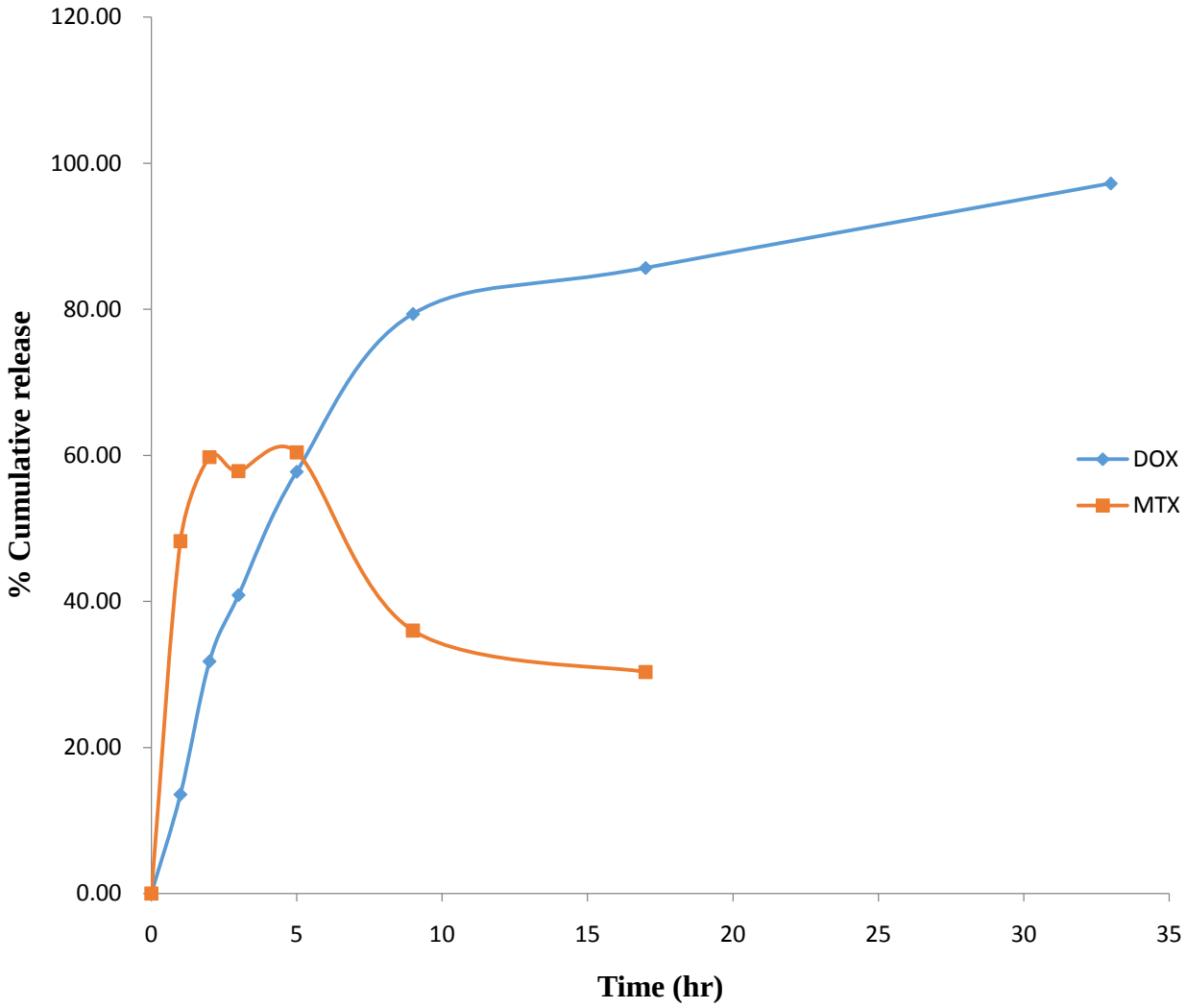


**Figure 4.39**: Release profiles of DOX and MTX at a combination ratio of 4: 1 (DOX: MTX)

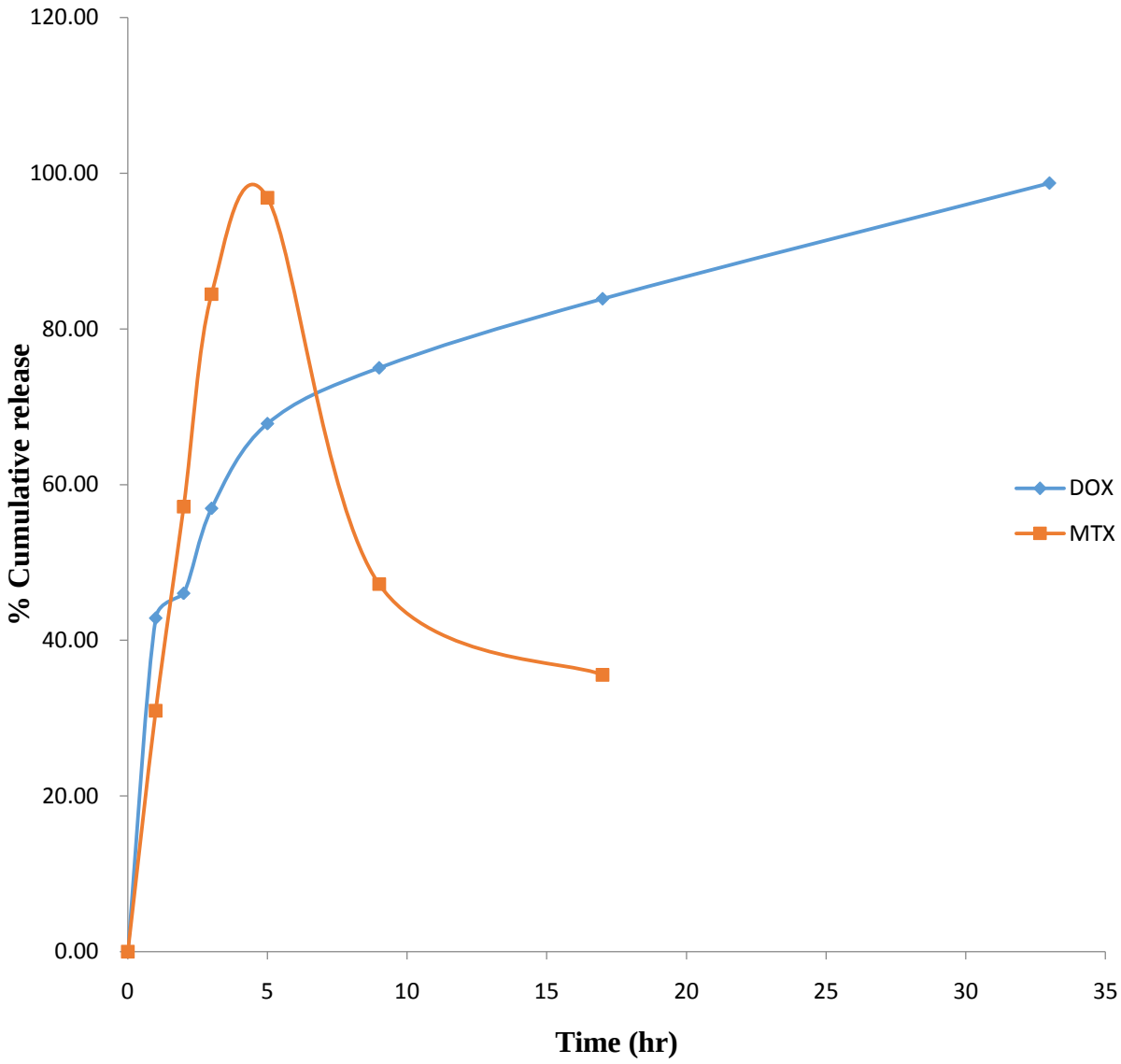


**Figure 4.40**: Release profiles of DOX and MTX at a combination ratio of 1: 1 (DOX: MTX)

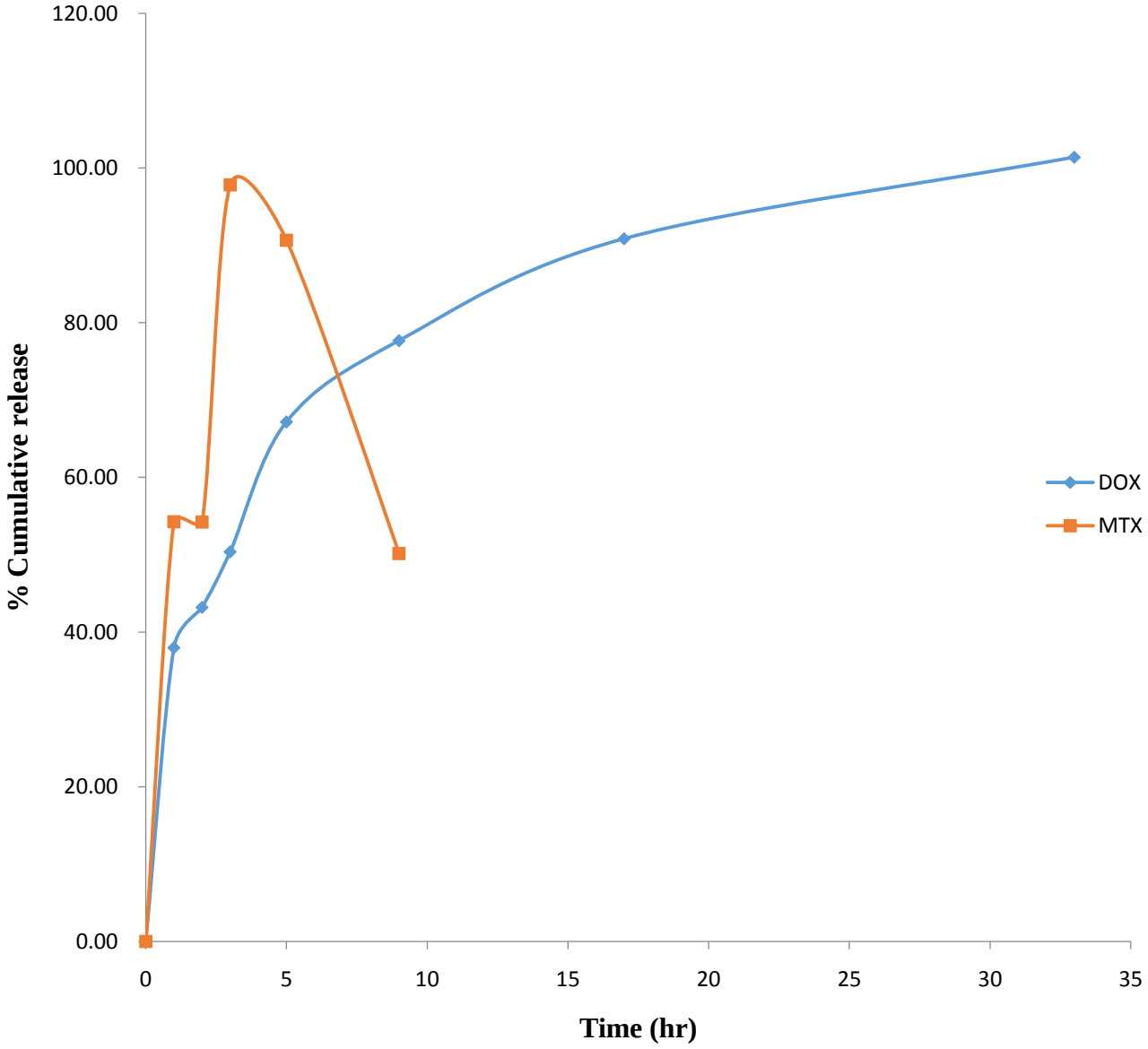


**Figure 4.41**: Release profiles of DOX and MTX at a combination ratio of 1: 4 (DOX: MTX)

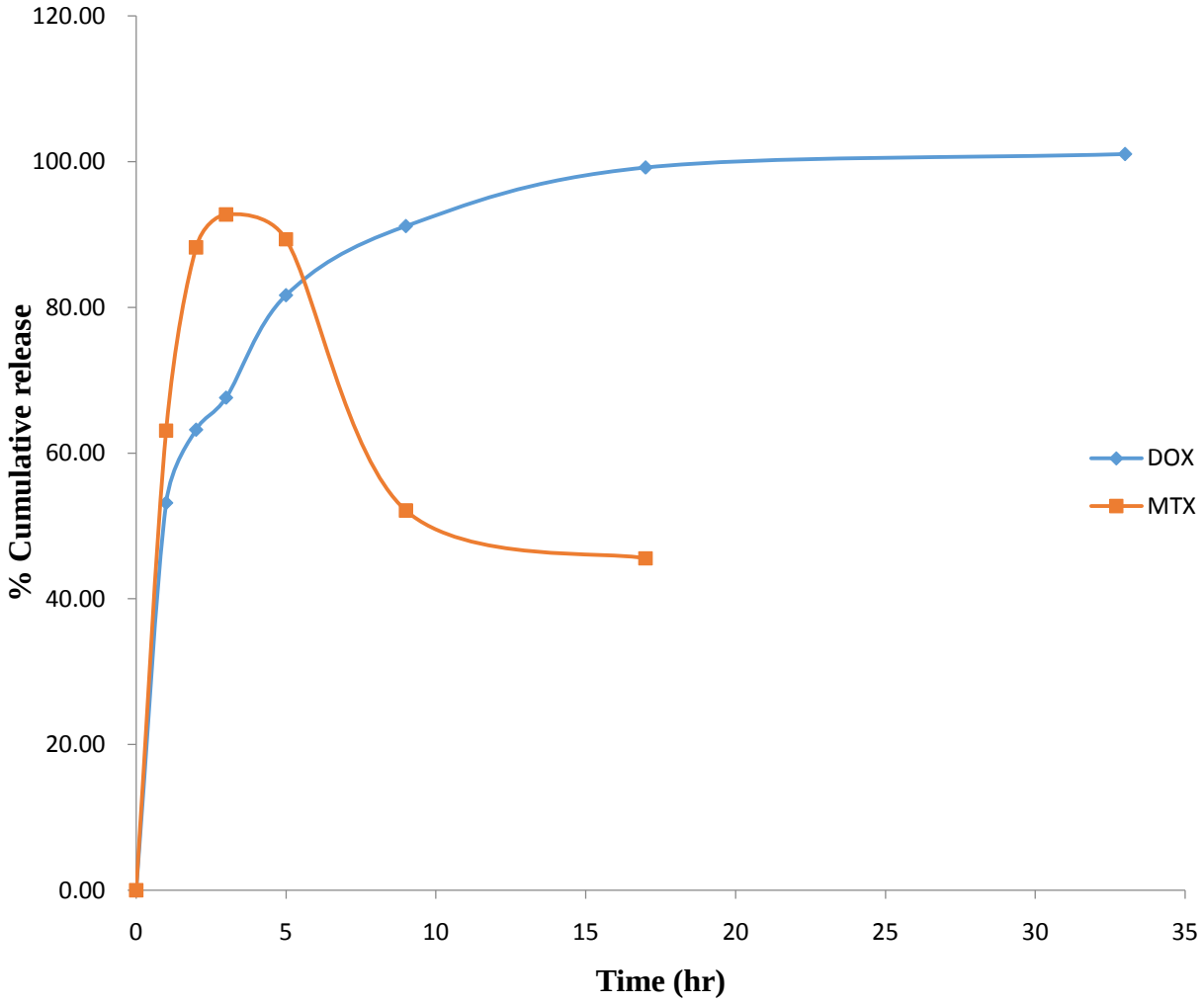


**Figure 4.42**: Release profiles of DOX and MTX at a combination ratio of 1: 16 (DOX:MTX)

# CHAPTER FIVE

## 5.0 DISCUSSION

### 5.1 Results of FTIR Analysis

Spectrum of SA (Figure 4.1) exhibited peaks which are in agreement with those reported in literature. The peak at 3236.3 $cm^{-1}$ attributed to O-H stretching mode was also reported by Kesavan *et al*. (2010), (3448 $cm^{-1}$), Trif *et al*. (2007), (3242 $cm^{-1}$), Jana *et al*. (2015), (3182 $cm^{-1}$), and Kulig *et al*. (2016), (3293 $cm^{-1}$). The peak at 2922.2 $cm^{-1}$ due to C-H asymmetric stretching, was also reported by Jana *et al*. (2015), (2977 $cm^{-1}$), and Kulig *et al*. (2016), (2926 $cm^{-1}$); while the peaks at 1595.3 $cm^{-1}$ and 1405.2 $cm^{-1}$ due to $COO^-$ stretching vibrations were reported by Kesavan *et al*. (2010), (1597 $cm^{-1}$ and 1413 $cm^{-1}$), Trif *et al*. (2007), (1596 $cm^{-1}$ and 1407 $cm^{-1}$), Kulig *et al*. (2016), (1605 $cm^{-1}$ and 1410 $cm^{-1}$). The C-O and C-O-C stretching vibrations peaks at 1103.3 $cm^{-1}$ and 1025 $cm^{-1}$ were also reported by Trif *et al*. (2007), (1081 – 1024 $cm^{-1}$) and Kulig *et al*. (2016), (1124 $cm^{-1}$ and 1031 $cm^{-1}$).

The HA peak values (Figure 4.1) are similar to those reported for HA by Roul *et al*. (2013), (3448 $cm^{-1}$, 1630 $cm^{-1}$, 1456 $cm^{-1}$, 1421 $cm^{-1}$, 1039 $cm^{-1}$, 962 $cm^{-1}$, 876 $cm^{-1}$), Rajkumar *et al*. (2010), (3400 $cm^{-1}$, 2067 $cm^{-1}$, 1416 $cm^{-1}$, 1032 $cm^{-1}$, 962 $cm^{-1}$, 874 $cm^{-1}$), Sanosh *et al*. (2009), (3350 $cm^{-1}$, 1650 $cm^{-1}$, 1465 $cm^{-1}$, 1037 $cm^{-1}$, 967 $cm^{-1}$, 875 $cm^{-1}$) and Nabipour *et al*. (2016), (3571.9 $cm^{-1}$, 1458.08 $cm^{-1}$, 1411.78 $cm^{-1}$, 1049.2 $cm^{-1}$, 964.34 $cm^{-1}$, 879.47 $cm^{-1}$). The weak peak at 2012.8 $cm^{-1}$ which was assigned to overtone and/or combination band is also in agreement with the values reported in literature (Pramanik *et al*., 2006; Rajkumar *et al*., 2010; Rajkumar *et al*., 2011).

The presence of carbonate ions in apatite has been reported and is believed to occur during the preparation of HA when $CO_2$ from the atmosphere reacts with hydroxyl ion and forms carbonate (Azami *et al*., 2010; Cunniffe *et al*., 2010; Rajkumar *et al*., 2010; Anuar *et al*., 2013).

Carbonate formation occurs in HA synthesized at low temperature, and is reduced after sintering at 800$^{o}$C (Alobeedallah, 2011). According to Sanosh *et al*. (2009), the presence of carbonate ions in HA is likely to improve its bioactivity. It increases the solubility of HA, and reduces its crystallite size.

The formation of the nanocomposite was confirmed by the spectrum of HASA in Figure 4.1. It was observed that the peak at 3236.3 $cm^{-1}$ in alginate shifted to 3220.4 $cm^{3}$, while the peaks at 1595.3 $cm^{-1}$ and 1405.2 $cm^{-1}$ shifted to 1599.0 $cm^{-1}$ and 1408.9 $cm^{-1}$ respectively. As divalent metal ions replace sodium ions in the SA, the charge density, the radius and atomic weight of the cation are different, creating a new environment around the carbonyl group, hence the observed peak shift (Azami *et al*., 2010). This also leads to the formation of new peak at 1341.8 $cm^{-1}$. It has been documented that formation of chemical bond between carbonyl group and divalent metal leads to a new peak around 1340 $cm^{-1}$ (Kikuchi *et al*., 2004; Itoh *et al*., 2005; Azami *et al*., 2010;).

MTX, HA-MTX and HASA-MTX (Figure 4.2) exhibited similar bands at 3268.9 $cm^{-1}$ assigned to O-H stretching vibration overlapped with N-H stretching mode; band at 1636.3 $cm^{-1}$ assigned to N-H bending mode; 1036.2 $cm^{-1}$ due to C-O stretch and $PO_4^{3-}$ from HA. The bands around 2101$cm^{-1}$ – 2106 $cm^{-1}$ is probably as a result of overtone or combinational band. There was no evidence of chemical interaction between the MTX and HA or the nanocomposites.

The HA-DOX spectra shown in Figure 4.2, is dominated by peaks from HA, except the weak peaks at 1636 $cm^{-1}$ and 704 $cm^{-1}$ which are due to $NH_2$ bending and out-of-plane wagging respectively. The predomination of HA peaks may be due to low encapsulation efficiency of HA and the presence of very strong phosphate peak in HA which dominate the few DOX vibration peaks.

Prominent peaks in HASA-DOX spectrum (Figure 4.2) shows some differences from the nanocomposites alone or the drug. It is important to note from the spectrum that the O-H stretching peak shifted down to 3183.1 $cm^{-1}$, while the C=O peak (1718.3 $cm^{-1}$) and COO-Ca peak (1341.8 $cm^{-1}$) were not observed. These observations point to the possibility of chemical interaction between DOX and the nanocomposite.

## 5.2 Scanning Electron Microscope (SEM) Analysis

In order to extract valuable information from the electron micrograph of HA and HASA nanocomposite (Figures 4.3 – 4.8), particle size and shape factors were measured using image analysis technique. Shape factors may dictate the behaviour of a product or correlate to a response of interest (Olson, 2011). United State Pharmacopeia (USP) <776> Optical Microscopy (2011) also emphasized the need for shape factor determination, including information on the type of diameter measured for irregularly shaped particles.

Two types of particle size measurements were used, the SED, and the F.D. These were used because the particles are irregularly shaped. The Spherical Equivalent Diameter, also called the area equivalent diameter, or circular equivalent diameter, is defined as the diameter of a circle with the same area as the particle (Olson, 2011). Feret Diameter which is the longest distance

between any two points along the particle boundary, tend to overestimate the particle size; hence spherical equivalent diameter is most widely cited (Dune Sciences, 2011).

According to ISO 13322-2, (2006) it is wrong and misleading to report result of particles measurements using single value such as mean. A better approach is to report both a central point of the distribution along with one or more values (such as D10, D90 and standard deviation) to describe the width of the distribution. The size of the HA particles ranges from 24.68 nm to 724.90 nm (Table 4.3). D10 (10%) of the synthesized HA particles have diameter less than 46.16 nm; (In order words, 90% of the particles have sizes more than 46.16 nm); the sizes of 50% of the particles are below 85.50 nm; and only 10% of the particles have sizes above 280.89 nm. This result indicates that all the particles are within nanometre size range. This is particularly important for powders, suspensions and emulsion as particle size has great influence on their properties and behaviours. For example, the size and shape of powders influence flow and compactness properties. Larger, more spherical particles will typically flow more easily than smaller or low aspect ratio particles. Smaller particles dissolve more quickly and lead to higher suspension viscosities than larger ones (Horiba Scientific, 2014).

The HA particles are of irregular shapes as can be seen from the results of the shape parameters such as aspect ratio and circularity (Table 4.3). Symmetric particles have high aspect ratio ($0 \geq A.R \leq 1$) (ISO 9276-6, 2008). These values range from 0.231 to 1, with median value of 0.578. The result also shows that 10% of the particles (D10) has aspect ratio below 0.380, while 10% have aspect ratio above 0.802 (D90) (This also means that 90% of the particles have aspect ratio below 0.802).

Circularity is a measure of how spherical the particles are. The values range from 0 to 1, the closer it is to unity the more spherical the particles. This means that the further away from a perfectly round and smooth circle that a particle becomes, the lower the circularity value. In this study, the particles have circularity values in the range of 0.248 to 0.988. Also the D10, D50 and D90 values were 0.439, 0.703 and 0.922 respectively. Only 10% of the particles have circularity above 0.922, which means that the particles can be described as predominantly non-spherical.

The results of particle size and morphological characterization of HASA with different alginate compositions (Table 4.4 - 4.8**)** show variation in particle size, the Feret diameter and the spherical equivalent diameter across the different formulations. Addition of 1%wt of SA to the HA led to increase in particle size from 85.50 nm to 309.41 nm (median values), however, on further addition of SA, the particle size decreased (Figure 4.10)**.** Similar observation was made by Cunniffe *et al*., (2010**)** for the synthesis of HA/poly (vinyl alcohol). Cunniffe *et al*., (2010**)** explained that the initial increase in particle size is due to agglomeration/crystallization of HA; however, on further addition of the polymer there was inhibition on HA aggregation which leads to decrease in particles size.

On the other hand, there was no significant change in the morphology of the particles with increase in composition of SA as aspect ratio and circularity remained fairly constant. The wide difference between the SED and the FD is a further evidence of non-spherical morphology of the particles. The more spherical the particles are the closer the values of spherical equivalent diameter and Feret diameter would be.

## 5.3 X-Ray Diffraction (XRD) Analysis

The phases of the HA were identified by matching the patterns obtained with Crystallography Open Database (COD-Inorg REV173445), and using FullProf program for Rietveld refinement. Two apatite phases were identified (Appendix I): HA, (entry number 96-900-2215), and carbonate-HA (entry number 96-900-3553). The HA has hexagonal crystal, with calculated density of 3.145 g/cm$^3$, and lattice parameters, a = 9.4394 Å and c = 6.8861 Å, while the carbonate-HA has hexagonal crystal, with calculated density of 3.141 g/cm$^3$, and lattice parameters, a = 9.4234 Å and c = 6.8801 Å. Both phases were responsible for the major peaks at $2\theta = 25.88^0$ (d-value = 3.4394 Å), $31.77^0$ (d-value = 2.8144 Å), and $32.15^0$ (d-value = 2.7818 Å), which were assigned Miller indices of (002), (121), and (112) planes respectively.

These planes were also present in all the HASA samples (Figure 4.12). There was no notable effect on the peak positions with the addition of SA. However, there was significant broadening which can be due to a combination of size and strain effect. This was further evaluated using the full width at half maximum values (FWHM) (Appendix II) and applying appropriate equations for size and strain (Equation 2.3 and 2.7 respectively). The crystallite sizes of both HA and HASA were calculated using the Scherrer formula for (121) planes, which is the strongest peak. Scherrer formula assumes that the strain contribution to the peak broadening is negligible. The results revealed that the crystallite size decreased with increase in the composition of SA (Figure 4.13). The values ranged from 9.47 nm to 32.36 nm. There was also significant reduction in particle yield as particle size decreased.

Crystallite size for pure HA has been reported to be in range of 8 nm to 17 nm **(**Rajkumar *et al*., 2010**)**; 8 nm to 15 nm **(**Azami *et al.,* 2010**)**, 30 nm to 34 nm (Raj *et al*., 2013) 13 nm to 23 nm

**(**Senthilarasan *et al*., 2014**).** The decrease in the crystallite size of HA with addition of polymer has been reported for HA/PVA **(**Rajkumar *et al*., 2010**)**, HA/PVA **(**Cunniffe *et al*., 2010**).**

The specific surface area of any particle varies inversely as the particles size. This trend was observed for the specific surface area of the different particles size calculated using equation 3.6 (Figure 4.12). The calculated values are as follows: HA (58.99 $m^2/g$), HASA-1%wt (67.24 $m^2/g$), HASA-5%wt (98.50 $m^2/g$), HASA-20%wt (158.29 $m^2/g$), HASA-33%wt (184.62 $m^2/g$), and HASA-50%wt (201.58 $m^2/g$). The specific surface area increased with increasing SA composition. The unique properties of nanoparticles that enable them to be used as biomaterials are due to their higher specific surface area (Chen, 2010). This means that nanocomposites with higher SA have better quality for biomaterial applications.

The variation in crystallinity of HA with the addition of SA (using equation 3.5) shows that the synthesized HA had a high degree of crystallinity of 72.87% (Figure 4.13). Like crystallite size, the crystallinity also decreased with increase in composition of SA. Both crystallite size and crystallinity varies inversely as the full width at half maximum value (FWHM) (Equations 2.3 and 2.7). As the crystals become smaller, the contribution to the peak broadening increases (i.e. increase in the value of FWHM), and consequently crystallinity increases. According to Kucherov *et al*. (2003), materials with low crystallinity are preferred for biomaterial purposes due to their high in-vivo resorbability. This suggests that according to the results obtained in this research, HASA is preferred to pure HA for biomedical purposes such as in drug delivery applications and material implants.

Microstrain was observed to increase with increasing addition of SA (Figure 4.14). It is due to imperfections within the crystalline lattice. The introduction of SA to HA distorts the crystalline

lattice of HA which leads to the observed increase in strain. Although microstrain is sometimes neglected in biomaterial characterization, Baig *et al*. (1999), has reported that microstrain was the dominant factor governing the solubility of carbonated apatites.

### 5.4 X-Ray Fluorescence (XRF)

The result of X-Ray fluorescence (Figure 4.15) confirms the elemental composition of the HA to be calcium, phosphorus, and oxygen with Ca/P ratio of 1.72. This value is close to the stoichiometric amount in HA which is 1.67. Ansari *et al*., (2011) reported that the Ca/P of apatite is influenced by the precipitation pH. From his work, the Ca/P ratio varied from 1.8 – 1.9 as pH was changed from 7.5 – 11.5. These values are different from what was obtained by Alobeedallah *et al*., (2011) and V´azquez *et al*., (2005) which were less than 1.67 respectively, while Costescu *et al*., (2010) reported Ca/P ratio of exactly 1.67. According to Dorozhkin (2012), apatites are classified based on their Ca/P ratio as follows: Ca/P of 1.5 can either be α or β -tricalcium phosphate (α-TCP or β-TCP), between 1.5 to less than 1.67 is calcium deficient HA (CDHA), while 1.67 to less than 2 is HA, fluorapatite (FA), or oxyapatite (OA), and CaP ratio of 2 is tetracalcium phosphate (TTCP). Based on this classification, the apatite synthesised in this research work can be identified as a HA. Also present are Iron (Fe) (0.008%), samarium (Sm) (0.006%), and titanium (Ti) (0.007%), which are trace impurities (Appendix 11I).

### 5.5 Comparison of the two Synthetic Routes of HASA Nanocomposites

The two synthetic routes involved changing the order of addition of SA as described in chapter three. The first synthetic route was designated HASA, while the second synthetic route was designated 2HASA. From the FTIR spectra shown in Figure 4.16, it was observed that the major peaks, which includes the O-H stretching peak (3220.4 $cm^{-3}$), the $COO^-$ stretching peaks (1602.8

$cm^{-1}$ and 1401.5 $cm^{-1}$), the COO-Ca absorption peak (1341.8 $cm^{-1}$), and the peak due to $PO_4^{3-}$ stretching (1025.0 $cm^{-1}$) were present in both formulations. This shows that the two synthetic routes yielded two nanocomposites with similar functional groups. In other words, the nanocomposites synthesised from both routes can be said to be chemically the same.

Both crystallite size and particle size of 2HASA were consistently higher than those of HASA (Figure 4.17). As was observed in HASA, morphological characterizations for all the formulations in 2HASA are similar. In addition, the variation in crystallinity and microstrain for both methods are similar. It can be concluded that both methods yielded nanocomposites with similar chemical and physical characteristics except for slight variation in sizes.

## 5.6 Drug Loading and Release Results

### 5.6.1 DOX loading

DOX loading into HA and HA- SA nanocomposite as a function of the amount of SA showed that loading efficiency increased with increasing amount of SA (Figure 4.18). Pure HA recorded the lowest loading efficiency of 21.93%, which increased with increasing alginate content. This trend can be attributed to the observed chemical interaction between DOX and HA-SA nanocomposite. The interaction was probably from the SA part of the nanocomposite as this interaction was not observed for pure HA, hence the higher the amount of SA, the higher the interaction and consequently the higher DOX loading efficiency.

### 5.6.2 MTX loading

The amount of MTX loading depends on the quantity of HA relative to the SA. MTX loading was highest in HA alone (35.24%), and decreased with increasing addition of SA (Figure 4.18).

It was observed from the FTIR spectra that there was no chemical interaction between HA and MTX, which suggests that the higher loading efficiency is not due to chemical interaction between HA and MTX. A possible reason for the higher drug loading in HA may be due to higher porosity of pure HA compared to the nanocomposites.

MTX loading was generally low compared to DOX loading. As DOX loading increased with increase in relative amount of SA, MTX loading decreased with increase in relative amount of alginate.

### 5.6.3 Comparison of the loading efficiencies of the two synthetic methods

Comparison of the loading efficiencies of the two synthetic methods is presented in Figure 4.19 for DOX and Figure 4.20 for MTX. The second synthetic route (2HASA) presented higher DOX loading efficiency than the first synthetic route (HASA) (Figure 4.19). However, for MTX (Figure 4.20) 2HASA recorded higher loading efficiencies at lower amount of SA (HASA-5%wt and HASA-20%wt), but as the quantity of SA was increased to HASA-33%wt and HASA-50%wt, HASA was found to load MTX more than 2HASA. DOX and MTX-loaded nanocomposites from both routes also displayed similar functional groups (Figure 4.21).

### 5.6.4 Methotrexate release study

The release profile of a drug from in vitro study gives valuable insight into its in vivo behaviour. The release profiles of the MTX-loaded HA and the MTX-loaded HA-alginate nanocomposites using simulated body fluid as the release medium (SBF), at pH 7.4 and 37 $^{o}$C was conducted for 23 hours (Figure 4.22). HA and HASA-1%wt released 83.82% and 83.17% of the loaded drug in 2 hours respectively, while HASA-5%wt and HASA-20%wt released 82.27% and 66.12% of the

drug in 5 and 2 hours respectively. For HASA-33%wt and HASA-50%wt formulations, there was no further release of the drug after the first sampling period as the percent cumulative decreased continuously. It can then be inferred that addition of small amount of alginate up to 5%wt to HA extended the release of the MTX for additional three hours, after which further addition reduced drug loading and increased burst release effect.

In order to further characterize the release profiles, profile comparison of the different formulations was carried out using DDSolver, an excel add-In. Pair-wise model independent procedure was followed and similarity factor ($F_2$) was chosen for the comparison. The results showed that HA had similar release profiles with HASA-1%wt and HASA-5%wt with similarity factors ($F_2$) of 62.03 and 65.58 respectively (i.e. HA vs. HASA-1%wt and HA vs. HASA-5%wt). On the other hand, HA did not exhibit similar release profile with HASA-20%wt, HASA-33%wt and HASA-50%wt, as the similarity factors ($F_2$) are 46.75, 40.04 and 46.43 respectively (Table 4.9). (note: two release profiles are similar if $50 \leq F_2 \leq 100$ (Zuo *et al*., 2014)).

5.6.5 Doxorubicin release study

The *in-vitro* release study for HA and the nanocomposites was conducted for 57 hours (Figure 4.23). HA and HASA-1%wt however released DOX for 5 hours and 9 hours respectively, while for other formulations (HASA-5%wt, HASA-20%wt, HASA-33%wt, and HASA-50%wt), DOX release was observed throughout the study period. The results indicate that after 33 hours, the percent cumulative release for these formulations – HASA-5%wt, HASA-20%wt, HASA-33%wt and HASA-50%wt are 95.15%, 88.70%, 85.82%, and 78.72% respectively (Appendix VI). The decreasing percent cumulative release is an indication of increase in more sustained release and decreasing burst release effect. That is to say that increase in the relative amount of SA increased

the sustained release of DOX. Higher polymer concentration in a nanocomposite material has been reported to give rise to more effective diffusion barrier leading to decrease in release rate **(**Liew *et al*., 2006**)**

The results of profile comparison (Table 4.10) indicate that the following release profiles are similar: HASA-5%wt and HASA-20%wt, HASA-20%wt and HASA-33%wt, HASA-33%wt and HASA-50%wt. The similarity factors (f2) for the similar profiles (indicated in bold in Table 4.10) are above 50. The results show that release profiles which have close composition of alginate are similar. This means that the similarity of different profiles depends on the closeness of their SA compositions.

### 5.6.6 DOX release mechanisms and kinetics

DOX release profiles (Figure 4.23) show that formulations containing highest relative amount of HA displayed fast and higher release rate than those formulations containing relatively lower amount of HA. The release half time $t_{50}$ (time required for releasing 50% wt of the loaded drug) increased with increase in SA content, which indicates that a sustained release can be obtained by incorporating SA into HA.

In order to understand the underlying kinetics and mechanism of DOX release from the different formulations, the release profiles were fitted to different kinetic and mechanistic models such as zero order model, first order model, Korsmeyer-Peppas model, Higuchi model, Hixon-Crowel model, and Hopfenberg model (Table 4.11). Kinetic study was not possible for MTX because of the short release time points.

A number of statistical criteria exist for selection of a suitable model for fitting dissolution data. The most popular ones in the field of dissolution model identification are the adjusted coefficient of determination ($R^2_{adj}$), the Akaike Information Criteria (AIC), and the Model Selection Criteria (MSC) (Adams *et al*., 2001). MSC was selected for evaluation of the goodness of fit in this study because of its simplicity and ease of interpretation. An MSC value of more than two indicates a good fit (Zhang *et al*., 2010). It was observed that none of the formulations followed zero order kinetics. The ideal release profile for most drugs is the one that follows zero order kinetics, which means that the release rate is constant independent of the concentration in the release material (Cojocariu *et al*., 2012).

Except for HA and HASA-1%wt, the release of DOX from other formulations can best be explained by first order kinetics. This means that the release rate is directly proportional to the concentrations of the drug in the nanocomposites. The observation here indicates that DOX release kinetics is governed by the amount of SA. This is in line with the report by Jesus *et al.*, (2016) that two main factors that influence drug release kinetics are material pore size and functional groups present in both the material and the drug.

In order to elucidate the potential transport mechanism, Korsmeyer-Peppas model was used (Equation 2.20). Release mechanisms refer to the ways through which drug molecules are transported or released from the carrier system to the surrounding medium. The value of the exponent n is used to indicate the type of release mechanism, where K is a constant which depends on diffusion coefficient and thickness of the film (Siepmann and Peppas, 2001).

When mechanistic models are evaluated, model selection is based on the mechanistic plausibility of the model in addition to its goodness of fit (Zhang *et al*., 2010). The value of n in Table 4.11

ranged from 0.220 to 0.497. These values indicate that DOX release for all the formulations followed Fickian diffusion mechanism. Drug release from systems with n < 0.45 is due to diffusion through matrix and water filled pores (Shende and Marathe, 2015). These values are similar to observation by Cojocariu *et al*., (2012) where n = 0.39, 0.46, and 0.44 for Chitosan-Dellite, Chitosan and Chitosan-Dellite2 release respectively; and report by Shende and Marathe, (2015) where n ranged from 0.221 to 0.345. These were explained to be due to Fickian diffusion mechanism, where molecular diffusion of the drug due to chemical potential gradient is the rate limiting step.

### 5.6.7 Comparison of the release profiles from the two synthetic methods

Comparison of DOX release profiles from nanocomposites prepared using the same percent composition of SA following the two different synthetic routes was carried out using similarity factor (f2) in order to statistically establish the similarities or otherwise of these profiles (Figures 4.25 - 4.28). It was observed that the similarity factor for all the compared groups are above 50, indicating that DOX release from nanocomposites prepared following the two synthetic methods have similar release profiles (Figure 4.28).

## 5.7 Evaluation of Different Loading Methods

### 5.7.1 Doxorubicin

The effects of different loading methods on DOX loading and release were evaluated. Method 1 is the adsorption method as previously described in chapter three section 3.6.1, while method 2, method 3 and method 4 involved different variations of incorporation method (as explained in section 3.6.2, 3.6.3, and 3.6.4 respectively). The result of drug loading by the four different loading methods (Figure 4.29) showed that the loading efficiencies for method 1, method 2,

method 3 and method 4 were 88.11%, 87.47%, 89.64%, and 88.64% respectively. This result implied that there was high DOX loading efficiency for all the four different methods, and there was no significant difference in loading efficiency of DOX by the four methods compared.

The release profiles for the four different loading methods (Figure 4.30) show that after fifty seven hours (57 hours), the percent cumulative releases for different methods were as follows: Method 1 - 94.72%, Method 2 - 91.54%, Method 3 - 85.87% and Method 4 - 80.84%. That is to say that all the four different loading methods prolonged the release of DOX for fifty seven hours. To compare the release rate, the release half time ($t_{50}$) was used. It was observed that the $t_{50}$ values for method 1, method 2, method 3 and method 4 are 4 hours, 18 hours, 10 hours and 20 hours respectively (Figure 4.30). This result indicated that method 1 released DOX at a faster rate than any other method. The higher release rate observed in adsorption is because in adsorption, some drug molecules get trapped on the surface of the delivery system and are released immediately upon contact with the release medium (Huang and Brazel, 2001).

The release profiles for the incorporation methods (method 2, method 3, and method 4) display sigmoid biphasic phases. The first phase of these profiles indicates drug release due to diffusion. However, after about seventeen hours, there was rapid increase in drug release. This point indicates degradation of SA matrix leading to rapid release of the entrapped drug. This observation is corroborated by the high fit of these methods with Hopfenberg model, which further shows that drug release was due to polymer degradation (Costa, and Sousa Lobo, 2001).

### 5.7.2 Methotrexate

The MTX loading efficiency by the four different loading methods (Figure 4.31) shows that method 2 and method 4 recorded higher loading efficiency of 39.98% and 37.10% respectively,

than method 1 (10.39%) and method 3 (15.21%). The two methods that loaded higher amount of MTX are incorporation methods. Adsorption method did not load appreciable amount of MTX in the nanocomposite.

The release profiles of MTX-loaded nanocomposites prepared by the four different methods (Figure 4.32) showed that as previously observed in this research work, adsorption method (method 1) did not sustain the release of MTX. The release profile of method 3 is similar to method 1 as the two did not sustain the release of MTX even for 1 hour. However, with method 2 (incorporation method), MTX release was sustained for three hours, while method 4 which has the best release profile, sustained the release of MTX for nine hours.

This study has shown that the efficiency of a material to load and release a drug depends, to a very large extent, on the loading method applied.

### 5.8 Effect of Medium of Synthesis on Drug Loading and Release

Nanocomposites prepared in different solvents were loaded with DOX to investigate the effect of these solvents on the loading and release of DOX. The result of the drug loading (Figure 4.33) showed that nanocomposites prepared using distilled water had highest DOX loading efficiency of 83.67%. This was followed by nanocomposites prepared in ethanol medium with loading efficiency of 52.46%, while nanocomposites prepared in acetone medium and ethyl acetate medium had approximately equal loading efficiency of 47.35% and 46.50%, respectively.

From the drug release profile (Figure 4.34), it is interesting to note that nanocomposite prepared in aqueous medium which exhibited highest loading efficiency had slower release rate, hence more sustained release than other formulations. The release half time ($t_{50}$) (time required for

releasing 50% of the loaded drug) for water formulation, ethanol formulation, acetone formulation and ethyl acetate formulation were 16 hours, 8 hours, 4 hours and 4 hours respectively (Figure 4.34).

Profile comparison showed that water formulation and other organic solvent formulations are significantly different. The difference factor ($f_1$) for water versus ethanol, water versus acetone, and water versus ethyl acetate are 23.96, 47.10, and 51.26 respectively. Among all the release profiles, only the profiles of acetone formulation and ethyl acetate formulation did not show significant difference ($f_1 = 3.92$) (Table 4.12)

All the formulations followed first order release rate, while the n exponent in the Korsmeyer-Peppas equation indicates that the release mechanism was dominated by Fickian diffusion. In addition, the formulations with organic solvents showed good fit with Higuchi model, Hixon-Crowel model, and Hopfenberg model, with Model Selective Criteria (MSC) above 2. (Table 4.13)

The FTIR study (Figure 4.35) indicated that replacement of water with organic solvent did not introduce additional functional group to the material as they had similar absorption peaks. That is to say that the difference in loading and release observed was not due to presence/absence of chemical interaction but probably due to physical difference in microstructure of the nanocomposites.

Based on the toxicity profiles of the solvents used and the loading and release study, it can be concluded that it is not necessary to use these organic solvents for the synthesis of the nanocomposites. Nanocomposite prepared in aqueous medium had better loading and release profile, and water is non-toxic to the body system as compared to organic solvents.

## 5.9 Effect of the pH of the Release Medium on DOX Release Profile

Solution pH and ionic strength have great influence on the stability of drug/polymer ionic complex, and consequently the drug release (Manocha, and Margaritis, 2010). Cancer is one of the diseases where pH-sensitive delivery system is highly desirable because of the more acidic environment of tumour cells compared to normal cells. Therefore, preferential release at acidic pH will provide targeted release to cancer cells, which in turn reduces toxicity to normal cells.

The effect of the pH of the release medium on the release profile of DOX from HASA was studied (Figure 4.36). The study was conducted at pH 7.4 (the physiological pH), pH 5.0 (the extracellular environment of solid tumour, and pH 3.0 (the lysosomal pH). It was observed that at the initial time period (up to nine hours), DOX release rate was faster at acidic conditions than at physiologic conditions. Higher release of DOX at lower pH has been previously observed (Manocha and Margaritis, 2010; Kamba *et al*., 2013; Madhusudhan *et al*., 2014). DOX is a weak base with a pKa of 8.30 and can adsorb by electrostatic interaction (Seib *et al*., 2013). In DOX-loaded HASA studied in this research work, the carboxylic group in SA might have interacted with the amino group of DOX. However, at acidic pH the carboxylic group ionizes thereby releasing the drug, hence the observed higher initial release at acidic pH. Another possible reason might be due to increased solubility DOX at acidic pH. According to Wang *et al*., (2010), the increase in solubility of DOX at mildly acidic pH, could lead to higher release rate.

It was also observed that after nine hours, the release rate of DOX at acidic medium decreased sharply while the drug continued to be released at physiologic medium. From the research by Davidovich-Pinhas and Bianco-Peled (2010), alginate shrinks at low pH, which makes the encapsulated drugs more difficult to be released under acidic conditions. Assuming that the

observed decrease in release rate in this study was due to the shrinkage, we can infer that the shrinkage did not occur until after about nine hours, hence the observed initial fast release.

### 5.10 Drug Combination Study

The quest for nanoparticles-assisted combination therapy is driven by its ability to unify the pharmacokinetics of different drugs by simultaneously delivering multiple drugs; this in turn offers synergistic therapeutic effect between the drugs and suppresses drug resistance.

The encapsulation efficiency of DOX at DOX: MTX ratio of 16:1, 4:1, 1:1, 1:4 and 1:16 are 86.50%, 88.42%, 90.00%, 89.15% and 87.90% respectively (Figure 4.37). This indicates that the encapsulation efficiency of DOX was high irrespective of the relative concentration of DOX in the mixture. In other words, DOX encapsulation efficiency did no depend on loading concentration within the concentration range studied (2 $mg/cm^3$ – 0.125 $mg/cm^3$). However, for MTX the encapsulation efficiency decreased as the concentration of MTX increased. There was high encapsulation efficiency (91.80%) at low concentration of MTX (0.125 $mg/cm^3$), which decreased to 37.54% at high concentration (2 $mg/cm^3$).

The release profiles for all the combination ratios showed high burst release for MTX with total release time not exceeding five hours (Figure 4.38 - 4.42). However, for DOX the drug release had initial burst release and then sustained for the thirty three hours of the study. Combination therapy enhances transport and penetration of drugs to deep tissue of solid tumours (Hu *et al*., 2010). To achieve this enhanced transport and penetration, the high burst release of MTX can be beneficial. The first released drugs can induce partial cancer apoptosis and expands the interstitial space of the solid tumour, thus the nanoparticles can diffuse into the deep tumour tissue and continue to release the second drug.

# CHAPTER SIX

## 6.0 SUMMARY, CONCLUSION AND RECOMMENDATIONS

### 6.1 Summary

HA nanoparticles and HASA nanocomposites were successfully synthesized. This was confirmed by the FTIR study which showed spectra characteristic of HA. The FTIR study also confirmed the formation of the nanocomposite. From the Scanning Electron Microscope (SEM) and image analysis, the particles were shown to be of nanometre size with irregular morphology. The size however decreased with increase in SA composition, while the morphology was fairly constant.

From the X-Ray Diffraction (XRD) analysis, the HA phase was identified as having carbonate-HA and pure HA. The average crystallite size for HA was 32.32 nm, while the degree of crystallinity was (72.87%) both of which decreased with increase in SA composition. On the other hand, microstrain and specific surface increased with increase in SA composition.

Comparison of nanocomposites synthesised from both synthetic routes using FTIR shows that they are chemically the same, while image analysis indicated that method 1 had particles with larger sizes. The drug loading efficiency also showed that the second synthetic route (2HASA) loaded higher that the first synthetic route (HASA), while the release profiles for the two synthetic routes are similar.

Drug loading study showed that the nanocomposites had high loading efficiency for DOX, which increased with increase in SA composition, while for MTX the loading efficiency was relatively low and decreased with increase in SA composition. The release study on the other hand showed

that the release of DOX by the nanocomposites was sustained, while MTX exhibited high burst effect, with total release time being less than five hours. The DOX release followed first order release kinetics, with Fickian diffusion mechanism as the predominant release mechanism.

Investigation into the effect of medium of synthesis on loading and release profiles showed that nanocomposites prepared in aqueous medium has better loading and release profile. The release kinetic and mechanism however, did not depend on the medium of synthesis.

Effect of loading methods showed that, for DOX the four studied methods loaded DOX to approximately the same level, while for MTX methods 2 and 4 loaded MTX better than methods 1 and 3. For DOX, the release study indicated that adsorption method (method 1) had higher release rate than other methods; for MTX, only method 4 sustained the release of the drug, while other methods had high burst release effects.

From the study of the effect of the release medium pH, DOX release rate was initially significantly faster at acidic conditions than at physiologic conditions, but became slower at later release time. The drug combination study showed that the release profiles for all the combination ratios showed high burst release for MTX with total release time not exceeding five hours. However, for DOX the drug release was sustained throughout the thirty three hours of the study.

## 6.2 Conclusion

The synthesised HA is a mixture of HA and carbonate-HA phases, which were nanometre sized with irregular morphology. The incorporation of SA to the nano-HA improved its ability to load and release DOX, while it decreased the loading of MTX. This shows that the ability of a material to effectively encapsulate and release a drug depend on the nature of the material as well

as that of the drug. The release profile of the drugs can be improved by optimizing the quantity of the polymer added.

HASA nanocomposite prepared in aqueous medium had better loading and release profile than those prepared in organic solvents, and water is non-toxic to the body system. Drug loading and release depends to a large extent on the loading method employed. Drug loading by incorporation method had slower release rate and better release profiles than loading by adsorption method, both for DOX and MTX.

The prepared HASA exhibited pH dependent release of DOX, which was favourable for release at the acidic pH of solid tumour.

HA-SA nanocomposite is a potential carrier for effective delivery of DOX.

### 6.3 Recommendations

Based on the findings of this research, the following are recommended:

- **i.** *In vivo* study should be carried out on the release of the nanocomposites for DOX.
- **ii.** Further study should be carried out on other loading methods for MTX, to obtain a method with more sustained release profile.
- **iii.** There should be further investigation into the drug combination study using other methods of drug loading, and other different drug combination ratios, in order to establish the effect and dose level for synergism.

## REFERENCES


Abidi, S.S.A., and Murtaza, Q. (2013). Synthesis and characterization of nanoHA powder using wet chemical precipitation reaction. *U.P.B Science Bulletin, Series B*, 75(3), 3 – 12.

Adams, E., Coomans, D., Smeyers-Verbeke, J and Massart, D.L. (2001). Application of linear mixed effects models to the evaluation of dissolution profiles. *International Journal of Pharmarcy*, 226:107–25.

Aggarwal, S., Goel, A and Singla, S. (2012). Drug delivery: special emphasis given on biodegradable polymers. *Advances in Polymer Science and Technology: An International Journal*, 2 (1), 1-15.

Agrawal, P. (2014). Significance of polymers in drug delivery system. *Journal of Pharmcovilagence*, 3(1), 1 – 2. http://dx.doi.org/10.4172/2329-6887.1000e127

Ahirrao, S.P., Gide, P.S., Shrivastav, B and Sharma, P. (2015). Ionotropic Gelation: A Promising Cross Linking Technique for Hydrogels. *Achieves of Scientific Research,* 1(1), 4 – 10.

Akbari, B., Tavandashti, M.P and Zandrahimi, M. (2011). Particle Size Characterization of Nanoparticles – A Practical approach. *Iranian Journal of Materials Science & Engineering, 8(2): 48 – 56.*

Alimardan, Z., Darabi, M and Natori, R. (2014). Drug delivery of indomethacin in use nature starch based nanocomposite hydrogel in vitro. *International Journal of Bioscience*, 5(11), 51-56. http://dx.doi.org/10.12692/ijb/5.11.51-56

Allermann, E., Gury, R and Doelker, E. (1993). Drug-loaded nanoparticles-preparation methods and drugs targeting issues. *Europian Journal of Pharmacy and Biopharmacy*, 39, 173-191.

Alobeedallah, H., Ellis, J.L., Rohanizadeh, M., Coster, H and Dehghani, F. (2011). Preparation of Nanostructured HA in Organic Solvents for Clinical Applications. *Trends Biomater. Artif. Organs, 25(1), 12-19.*

Ansari, M., Naghib, S.M., Moztarzadeh, F and Salati, A. (2011). Synthesis and Characterization of HA-calcium Hydroxide for Dental Nanocomposites. *Ceramics*, 55 (2) 123-126.

Antosiak-Iwariska, M., Sitarek, E., Sabat, M., Godlewska, E., Kinasiewicz, J and Weynski, A. (2009). Isolation, banking, encapsulation and transportation of different types of Langerhans islets. Polskie *Archiwum Medycyny Wewnetrznej*, 119, 311 – 317.

Anuar, A., Salimi, M. N., Daud, M. Z and Yee, F.Y. (2013). Characterizations of HA (HAp) nanoparticles produced by sol-gel method. *Advances in Environmental Biology*, x(x), 3587-3590.

Asadishad, B., Vassoughi, M and Alamzadeh, I. (2010). *In vitro* release behavior and cytotoxicity of DOX loaded gold nanoparticles in cancerous cells. *Biotechnology Letters*, 32(5), 649 – 654.

Azami, M., Samadikuchaksaraei, A and Poursamar, S.A. (2010). Synthesis and characterization of a laminated HA/gelatin nanocomposite scaffold with controlled pore structure for bone tissue engineering. *International Journal of Artificial Organ*, 33 (2): 86-95.

Bach, L. G., Islam, M. R., Mai, T. B., Nga, T. T., Niranjanmurthi, L and Lim, K. T. (2012, June). *Synthesis, characterization, and protein immobilization study of phema grafted HA nanocrystals via surface initiated radical polymerization*. Paper Presented at the 15th European Conference on Nanocomposite Materials, Venice, Italy, 24-28 June 2012.

Badri, W., Eddabra, R., Fessi, H and Elaissari, A. (2014). Biodegradable Polymer Based Nanoparticles: Dermal and Transdermal Drug Delivery. *Journal of Colloid Science and Biotechnology*, 3, 141 – 149.

Baig, A.A., Fox, J.L., Young, R.A., Wang, Z., Hsu, J., Higuchi, W.I, Chnetty, A., Zhang, H and Otsuka, M. (1999). Relationship among carbonated apatite solubility, crystallite size, and microstain parameters. *Calif Tissue Internationals*, 64(5), 437 – 490.

Balakrishnan, B., Mohanty, M., Fernandez, A.C., Mohanan, P.V and Jayakrishnan, A. (2006). Evaluation of the effect of incorporation of dibutyryl cyclic adenosine monophosphate in an in situ forming hydrogel wound dressing based on oxidized alginate and gelatin. *Biomaterials*, 27, 1355–1361.

Balavandy, S.K., Shameli, K and Abidin, Z.Z. (2015). Rapid and green synthesis of silver nanoparticles via SA media. *International Journal of Electrochemical Science*, 10, 486 – 497.

Bennet, D and Kim, S. (2014). Polymer nanoparticles for smart drug delivery. InTech, 257 - 310 *http://dx.doi.org/10.5772/58422*

Bertrand, N., Wu, J., Xu, X., Kamaly, N and Farokhzad, K.C. (2013). Cancer nanotechnology: The impact of passive and active targeting in the era of modern cancer biology. *Advanced Drug Delivery Reviews.* http://dx.doi.org/10.1016/j.addr.2013.11.009

Bidarra, S.J., Barrias, C.C., Barbosa, M.A., Soares, R and Granja, P.L. (2010). Immobilization of human mesenchymal stem cells within RGD-grafted alginate microspheres and assessment of their angiogenic potential. *Biomacromolecules*, 11, 1956–1964.

Biondi, M., Ungaro, F., Quaglia, F and Netti, P.A. (2008). Controlled drug delivery in tissue engineering. *Advances in Drug Delivery Review*, 60:229–227.

Bonacucina, G., Cespi, M and Palmieri, G.F. (2009). Evaluation of dissolution kinetics of hydrophilic polymers by use of acoustic spectroscopy. *International Journal of Pharmacy*, 377: 153–158.

Bouhadir, K.H., Alsberg, E and Mooney, D.J. (2001). Hydrogels for combination delivery of antineoplastic agents. *Biomaterials*, 22, 2625–2633.

Boyle, P and Levin, B. (Eds). (2008). World Cancer Report 2008, *IARC Press*, Lyon, France.

Bragg, W.L. (1913). The diffraction of short electromagnetic waves by a crystal. *Proceedings of the Cambridge Philosophical Society*, 17, 43 – 57.

Brouwer, P. (2010). Theory of XRF (3rd Edition). *PANalytical* B.V, Almelo, The Netherlands, pp 4 – 25.

Brown, W. E and Chow, L. C. (1983). A new phosphate petting cement. *Journal of Dental Research*, 5, 672.

Byrappa, K and Yoshimura, M. (2001). Handbook of Hydrothermal Technology - A Technology for Crystal Growth and Materials Processing. William Andrew Publishing, LLC Norwich, New York, U.S.A.

Carstensen, H., Maller, R.H and Muller, B. (1992). Particle size, surface hydrophobicity and interaction with serum of parenteral fat emulsions and model drug carriers as parameters related to RES uptake. *Clinical Nutrition*, 11(5), 289 – 297.

Chahatray, R., Sahoo, D., Mohanty, D.P and Nayak, P.L. (2013). Guargum-SA Blended with Cloisite 30B for Controlled Release of Anticancer Drug Curcumin. *World Journal of Nano Science & Technology*, 2(1), 26-32. DOI: 10.5829/idosi.wjnst.2013.2.1.21136

Chalmers, J. M., Hannah, R. W and Mayo, D. W. (2002). Spectra–Structure Correlations: Polymer Spectra, in *Handbook of Vibrational Spectroscopy*, Vol. 3, Chalmers, J. M. and Griffiths, P. R. (Eds), Wiley, Chichester, pp. 1893–1918.

Chan, A.W and Neufeld, R.J. (2010). Tuneable semi-synthetic network alginate for absorptive encapsulation and controlled release of protein therapeutics. *Biomaterials*, 31, 9040–9047.

Chandrasekar, A., Sagadevan, S and Dakshnamoorthy, A. (2013). Synthesis and characterization of nano-HA (n-HAP) using the wet chemical technique. *Journal of Physical Science*, 8(32), 1639 – 1645. DOI:10.5897/IJPS2013.3990

Chasin, M and Langer, R. (1990). Biodegradable Polymers as Drug Delivery Systems (ed) Marcel Dekker Inc, New York.

Chen, Z. (2010). Small molecule delivery by nanoparticles for anticancer therapy. *Trends in Molecular Medicine*, 16(12), 594 – 602.

Chime, S.A., Onunkwo, G.C and Onyishi, I. (2013). Kinetics and Mechanisms of Drug Release from Swellable and Non Swellable Matrices: A Review. *Research Journal of Pharmaceutical, Biological and Chemical Sciences*, 4(2), 97 – 103.

Cho, K., Wang, X., Nie, S., Chen, Z and Shin D.M. (2008). Therapeutic nanoparticles for drug delivery in cancer. *Clinical Cancer Research*, 14, 1310 – 1316.

Chowdhury, J.A., Jahan, S.T., Morshed, M.M., Mallick, J., Nath, A.K., Uddin, M.Z., Dutta, M., Kaisarul, I. M and Kawsar, M.H. (2011). Development and evaluation of Dixlofenac sodium loaded alginate cross-linked beads. *Bangladesh Pharmaceutical Journal*, 14(1), 41 – 48.

Coates, J. (2000). Interpretation of infrared spectra: A practical approach. In Encyclopaedia of Analytical Chemistry, Meyers R.A (Ed.), John Wiley and Sons Ltd, Chichester, pp 10815 – 10837.

Cojocariu, A., Porfire, L., Cheaburu, C and Vasile, C. (2012). Chitosan/montmorillonite nanocomposites as matrices for prolonged delivery of some novel nitric oxide donor compounds based on theophylline and paracetamol. *Cellulose Chem*istry *Technology*, 46 (1-2), 35-43.

Colthrup, N.B., Daly, L.H and Wiberley, S.E. (1990). Introduction to Infrared and Raman Spectroscopy, Academic Press, San Diego, CA, 1–73.

Comyn, J. (1985). Introduction to Polymer Permeability and the Mathematics of Diffusion, In: *Polymer Permeability*, pp 1-10, Elsevier Applied Science, ISBN 0-85334-322-5, Northern Ireland.

Cong, H., Radosz, M., Towler, B.F and Shen, Y. (2007). Polymer–inorganic nanocomposite membranes for gas separation. *Separation and Purification Technology*, 55, 281–291.

Costa, P., and Sousa-Lobo, J.M. (2001). Modeling and comparison of dissolution profiles. *European Journal of Pharmaceutical Sciences*, 13, 123–133.

Costescu, A., Pasuk, I.,Ungureanu, F., Dinischiotua, A., Costachea, M., Huneaub, F., Galaupc, S., Le Coustumerb, P and Predoi, D. (2010). Physico-chemical properties of nano-sized hexagonal HA powder synthesized by sol-gel. *Digest Journal of Nanomaterials and Biostructures*, 5(4), 989-1000.

Couvreur, P and Vauthier, C. (2006). Intelligent design to treat complex disease. *Pharmaceutical Research*, 24, 1417 – 1450.

Cunniffe, G.M., O'Brien, F.J., Partap, S., Levingstone, T.J., Stanton, K.T and Dickson, G.R. (2010). The synthesis and characterisation of nanophase HA using a novel disperant-aided precipitation method. *Journal of Biomedical Materials Research. Part A*, 95(4):1142-9.

Cypes, S.H., Saltzman, W.M and Giannelis, E.P. (2003). Organosilicate-polymer drug delivery systems: controlled release and enhanced mechanical properties. *Journal of Controlled Release, 90*, 163-169.

D'Ayala, G.G., Malinconico, M and Laurienzo, P. (2008). Marine derived polysaccharide for biomedical applications: Chemical modification approaches. *Molecules*, 13, 2069 – 2106.

Das, P.R., Nanda, R.M., Behara, A and Nayak, P.L. (2011). Gelatin blended with nanoparticles cloisite30B (MMT) for control drug delivery of anticancer drug paclitaxel. *International Research Journal of Biochemistry and Bioinformatics*, 1(2), 035-042.

Dash, S., Murthy, P.N., Nath, L and Chowdhury, P. (2010). Kinetic modeling on drug release from controlled drug delivery systems. *Acta Poloniae Pharmaceutica – Drug Research*, 67(3), 217 – 223.

Davidovich-Pinhas, M and Bianco-Peled, H. (2010). A quantitative analysis of alginate swelling. *Carbohydrate Polymer*, 79, 1020–1027.

De Vols, P., Faas, M.M., Strand, B and Calafiore, R. (2006). Alginate based microcapsules for immunoisolation of pancreatic islets. *Biomaterials*, 27, 5603 – 5617.

Devanand, V.G., Ramasamy, S., Ramakrishnan, V and Kumar, J. (2011). Hydroxyapatite – Alginate nanocomposite as drug delivery matrix for sustained release of ciprofloxacin. *Journal of Biomedical Nanotechnology*, 7, 1- 9.

Dixit, N., Maaurya, S. D and Sagar, P.S. (2013). Sustained release drug delivery system. Indian *Journal of Research in Pharmacy and Biotechnology*, 1(3), 305 – 310.

Dorozhkin S.V. (2012). Nanodimensional and Nanocrystalline Calcium Orthophosphates. *American Journal of Biomedical Engineering*, 2(3): 48-97. DOI:10.5923/j.ajbe.20120203.01

Drummond, D.C., Meyer, O., Hary, K., Kirpotin, D.B and Papahadjopoulos, D. (1999). Optimizing liposomes for delivery of chemotherapeutic agents to solid tumours. Pharmacological Reviews, 51, 691 – 743.

Duncan, R., Sat-Klopsch, Y.N., Burger, A.M., Bibby, M.C., Fiebig, H.H and Sausville, E.A. (2013). Validation of tumour models for use in anticancer nanomedicine evaluation: The EPR effect and cathepsin B-mediated drug release rate. *Cancer Chemotherapy and Pharmacology*, *72*, 417–427.

Dune Sciences, Inc. (2011). Particle Size Analysis – Standard Operating Protocol. www.dunesciences.com

Encyclopedia of Nanoscience & Nanotechnology. (2005). Vol. 9. Edited by: H.S. Nalwa, American Scientific Publishers.

Fattah, E.A.E., Grant, D.J.W., Gabr, K.E and Meshali, M.M. (1998). Physical characteristics and release behaviour of salbutamol sulphate beads prepared with different ionic polysaccharides. *Drug Development in Industrial Pharmacy, 24* (6), 541–547.

Ferlay, J; Soerjomataram I; Ervik M; Dikshit R; Eser S; Mathers C; Rebelo M; Parkin D.M; Forman D and Bray F. (2013). GLOBOCAN 2012 v1.0, Cancer Incidence and Mortality Worldwide: IARC Cancer Base No. 11. Available from http://globocan.iarc.iarc.fr

Ferraz, M.P., Monteiro, F.J and Manuel, M. (2004). HA nanoparticles: A review of preparation methodologies. *Journal of Applied Biomaterials & Biomechanics*, 2, 74-80.

Fischer, F.G and Dörfel, H. D. (1955). Polyuronsauren der braunalgen-(kohlenhydrate der algen-I). *Z Physiol Chem.*, 302, 186–203.

Ford, J.L, Rubinstein, M.H and Hogan, J.E (1985). Propranolol hydrochloride and aminophylline release from matrix tablets containing hydroxypropyl methylcellulose. *International Journal of Pharmacy*, 24:339-350.

Fukui, Y and Fujimoto, K. (2012). Bio-inspired nanoreactor based on a miniemulsion system to create organic-inorganic hybrid nanoparticles and nanofilms. *Journal Material Chemistry, 22*, 3493–3499.

Fultz, B and Howe, J.M. (2013). Transmission electron microscopy and Diffractometry of materials. Graduate Texts in Physics, Springer-Verlag Berlin Heidelberg.

George, M and Abraham, T.E. (2006). Polyionic hydrocolloids for the intestinal delivery of protein drugs. *Journal of Controlled Release*, 114, 1–14.

Goenka, S., Sant, V and Sant, S. (2014). Graphene-based nanomaterials for drug delivery and tissue engineering. *Journal of Control Release*, 173(1), 75–88.

Goldstein, J., Newbury, D., Joy, D., Lyman, C., Echlin, P., Lifshin, E., Sawyer, L and Michael, J. (2003). Scanning electron microscopy and X-ray microanalysis. *Plenum Press, New York*, 3rd edition, pp. 1-9.

Gottesman, M. M. (2002). Mechanisms of cancer drug resistance. *Annual Review of Medicine, 53*, 615-627.

Gottesman, M.M. (1993). How cancer cells evade chemotherapy: Sixteenth Richard and Hinda Rosenthal Foundation Award Lecture. *Cancer Research*, 53, 747-54.

Hamberger, A., Ziener, U and Landfester, K. (2013). Encapsulation of *in situ* nanoprecipitated inorganic materials in confined geometries into a polymer shell using inverse miniemulsion. *Macromol. Chem. Phys. 214*, 691–699.

Harish, S.G., Medapati, R., Gantasala P, Raju, B and Damodharan, N. (2010). Oral sustained delivery of Salbutamol using *in situ* gelation of SA. *International Journal of Current Pharmaceutical Research,* 2(3), 61 – 64.

Hasan, A.S., Socha, M, Lamprecht, L, Ghazouani, F.E and Sapin, A. (2007). Effect of the Microencapsulation of Nano- particles on the Reduction of Burst Release. *International Journal of Pharmaceutics*, 344, 1-2, 53-61.

Higuchi, T. (1961). Rate of release of medicaments from ointment bases containing drugs in suspension. *Journal of Pharmaceutical Science*, 50: 847-875.

Hood, M.A., Mari, M and Munoz-Esp, R. (2014). Synthetic strategies in the preparation of polymer/inorganic hybrid nanoparticles. *Materials*, 7, 4057 – 4087.

Hood, M.A., Wang, B., Sands, J.M., La Scala, J.J., Beyer, F.L and Li, C.Y. (2010). Morphology control of segmented polyurethanes by crystallization of hard and soft segments. *Polymer, 51*, 2191–2198.

Horiba Scientific. (2014). A guide book to particle size analysis. Horiba Instruments, Inc. Irvine, CA 92618 USA. www.horiba.com/us/particle

Hu, C.J and Zhang, L. (2009). Therapeutic Nanoparticles to Combat Cancer Drug Resistance. *Current Drug Metabolism, 10*, 836-841.

Hu, C.J and Zhang, L. (2009). Therapeutic nanoparticles to combat cancer drug resistance. *Current Drug Metabolism*, 10, 836 – 841.

Hu, C.J., Aryal, S and Zhang, L. (2010). Nanoparticles-assisted combination therapies for effective cancer treatment. *Therapeutic Delivery*, 1(2), 323–334.

Hua, S., Yang, H and Wang, A. (2010). A pH-sensitive nanocomposite microsphere based on chitosan and montmorillonite with in vitro reduction of the burst release effect. *Drug Development and Industrial Pharmacy*, 36(9), 1106–1114. DOI: 10.3109/03639041003677798

Huang, X and Brazel, C.S. (2001). On the importance and mechanisms of burst release in matrix-controlled drug delivery systems. *Journal of Controlled Release,* 73, 121–136.

Iliescu, R.I., Andronescu, E., Ghiţulică, D.C., Berger, D and Ficai, A. (2011). Montmorillonite-alginate nanocomposite beads as drug carrier for oral administration of carboplatin – preparation and characterization. *U.P.B Science Bulletin Series B,* 73(3), 3 – 16.

Iliescu, R.I., Andronescua, E., Ghitulicaa, C.D., Voicua, G, Ficai, A and Hoteteu, M. (2014). Montmorillonite–alginate nanocomposite as a drug delivery system – incorporation and in vitro release of irinotecan. *International Journal of Pharmaceutics*, 463, 184– 192. http://dx.doi.org/10.1016/j.ijpharm.2013.08.043

ISO 13322-2. (2006). Particle size analysis-Image analysis method-Part 2: Dynamic image analysis methods.

ISO *9276-6: (2008*). Representation of results of particle size analysis–Part 6: Descriptive and quantitative representation of particle shape and morphology.

Itoh, S., Kikuchi, M and Koyama, Y. (2005). Development of a novel biomaterial, HA/collagen (HAp/Col) nanocomposite for medical use. *Biomedical and Material Engineering*, 15, 29-41.

IUPAC. (1997). Compendium of Chemical Terminology, 2nd ed. (the "Gold Book"). Compiled by A. D. McNaught and A. Wilkinson. Blackwell Scientific Publications, Oxford.

Jana, D., Jana, C., Vojtech, A., Marketa, R., Tomas, E., Jaromir, H. and Rene, K. (2013). Nanocarriers for Anticancer Drugs - New Trends in Nanomedicine. *Current Drug Metabolism, 14*, 547-564.

Jana S, Trivedi, M.K., Tallapragada, R.M., Branton, A., Trivedi, D., Nayak, G and Mishra, R.K. (2015). Characterization of Physicochemical and Thermal Properties of Chitosan and SA after Biofield Treatment. *Pharmaceutica Analytica Acta*, 6(10), 1 - 9. http://dx.doi.org/10.4172/2153-2435.1000430

Janssens, K.H., Adams, F.C and Rindby, A. (2000). Microscopic X-ray Fluorescence Analysis, John Wiley, Chichester.

Javid, A., Ahmadian, S., Saboury, A.A., Kalantarc, S.M and Rezaei-Zarchid, S. (2014). Novel biodegradable heparin-coated nanocomposite system for targeted drug delivery. *Royal Society of Chemistry Advances*, 4, 13719 – 13728.

Jenkins, R. (2000). Wavelength-dispersive X-ray Fluorescence Analysis, in: Encyclopedia of Analytical Chemistry, R. A. Meyers (Ed.), pp. 13422-13444, John Wiley & Sons Ltd., Chichester.

Jesus, R.A., Rabelo, A.S., Figueiredo, R.T., Cides da Silva L.C., Codentino, I.C., Fantini, M.C.A., G.L.B. Araújo, G.L.B., Araújo, A.A.S and Mesquita, M.E. (2016). Synthesis and application of the MCM-41 and SBA-15 as matrices for in vitro efavirenz release study. *Journal of Drug Delivery Science and Technology*, 31, 153 – 159. http://dx.doi.org/10.1016/j.jddst.2015.11.008

Joshi, J. R. and Patel, R.P. (2012). Role of biodegradable polymers in drug delivery. *International Journal of Current Pharmaceutical Research*, 4(4), 74 – 81.

Jung, T., Kamm, W., Breitenbach, A., Kaiserling, E., Xiao, J.X and Kissel, T. (2000). Biodegradable nanoparticles for oral delivery of peptides: is there a role for polymers to affect mucosal uptake?. *Europian Journal of Pharmacy and Biopharmacy*, 50, 147-160.

Kailasapathy, K. (2002). Microencapsulation of probiotic bacteria: Technology and potential applications.*Current Issues in Intestinal Microbiology*, 3, 39 – 48.

Kakde, D., Jain, D., Shrivastava, V., Kakde, R and Patil, A.T. (2011). Cancer Therapeutics-Opportunities, Challenges and Advances in Drug Delivery. *Journal of Applied Pharmaceutical Science,* 01(09), 01-10.

Kamba, S.A., Ismail, M., Hussein-Al-Ali, S.H., Ibrahim, T.A.T and Zakaria Z.A.B. (2013). *In Vitro* Delivery and Controlled Release of DOX for Targeting Osteosarcoma Bone Cancer. *Molecules*, *18*, 10580-10598. doi:10.3390/molecules180910580

Kanjickal, D.G., and Lopina, S.T (2004). Modeling of drug release from polymeric delivery systems-A review. *Critical Review Therapeutic Drug Carrier System*, 21: 345-386.

Karakoti, R., Bhatt, V., Singh, A.K and Sharma, D.K. (2014). Development and evaluation of floating Diclofenac sodium-alginate bead using biopolymer obtained from Vigna Radita. *World Journal of Pharmaceutical Research*, 3(9), 1146 – 1153.

Karimi, M. (2011). Diffusion in Polymer Solids and Solutions, Mass Transfer in Chemical Engineering Processes, Dr. Jozef Marko Å (Ed.), ISBN: 978-953-307-619-5, *InTech*.

Kato, Y., Onishi, H and Machida, Y. (2003). Application of chitin and chitosan derivatives in the pharmaceutical field. *Current Pharmaceutical Biotechnology*, 4, 303–309.

Kellen, J.A. (2003).The reversal of multidrug resistance: an update. *Journal of Experimental and Therapeutic Oncolology*, 3, 5-13.

Kesavan, K., Nath, G and Pandit, J.K. (2010). SA Based Mucoadhesive System for Gatifloxacin and its In Vitro Antibacterial Activity, *Scientia Pharmaceutica*, 78, 941–957.

Khaled, R. M., Hanan, H. B and Zenab, M. E. (2014). In-vitro study of nano-hyroxyapatite/gelatine-chitosan nanocomposites for bio-application. *Journal of Advanced Research*, 5, 201 – 208.

Khan, M. S., Priyadarshini, M., Sumbul, S and Bano, B. (2010). MTX binding causes structural and functional changes in lung cystatin. *Acta Biochimica Polonica*, 57 (4), 499-503.

Khanedan, N., Motalebi, A. A., Khanipour, A. A., Koochekian, Sabour, A., Seifzadeh, M and Hasanzati, R A. (2011). Effects of different concentrations of SA as an edible film on chemical changes of dressed Kilka during frozen storage. *Iranian Journal of Fisheries Sciences*, 10(4), 654 – 662.

Khotimchenko, Y.S., Kovalev, V.V., Savchenko, O.V and Ziganshina, O.A. (2001). Physical – chemical properties, physiological activity and usage of alginates, the polysaccharides of Brown algae. *Russian Journal of Marine Biology*, 27, 53 – 64.

Kikuchi, A., Kawabuchi, M., Watanabe, A., Sugihara, M., Sakurai, Y and Okano, T. (1999). Effect of $Ca^{2+}$ alginate gel dissolution on release of dextran with different molecular weights. *Journal of Control Release, 58* (1), 21–28.

Kikuchi, M., Matsumoto, H.N., Yamada, T., Koyama, Y., Takakuda, K and Tanaka, J. (2004). Glutaraldehyde cross-linked HA/collagen self-organized nanocomposites. *Biomaterials*, 25, 63-9.

Kogashiwa, Y and Kohno, N. (2013). Combination chemotherapy for solid tumors in head and neck. *Drug Metabolism and Toxicology*, 4(1), 1 – 7.

Kokubo, T., Kushitani, H., Sakka, S., Kitsugi, T and Yamamuro, T. (1990). Solutions able to reproduce in vivo surface-structure changes in bioactive glass-ceramic A-W. *Journal of Biomedical Materials Research,* 24:721–734.

Konda, N., Arvind, G., Shah, S., Prashanth, P. (2013). Formulation and Evaluation of Non-Pegylated Doxorubicin Liposomal Drug Delivery System. *International Journal of Pharmacy and Pharmaceutical Sciences*, 5(2), 541-547.

Krisanapiboon, A., Buranapanitkit, B and Oungbho, K. (2006).Biocompatibility of HA nanocomposite as a local drug delivery system. *Journal of Orthopaedic Surgery*, 14(3), 315 – 318.

Krishna, R and Mayer, L.D. (2000). Multidrug resistance (MDR) in cancer: Mechanisms, reversal using modulators of MDR and the role of MDR modulators in influencing the pharmacokinetics of anticancer drugs. *Europian Journal Pharmaceutical Sciences*, 11, 265–283.

Kucherov, A.V., Kramareva, N.V., Finashina, E.D., AKoklin, A.E and Kustov, L.M. (2003). Heterogenized redox catalysts on the basis of the chitosan matrix. Copper complexes *Journal of Molecular Catalalysis A*, 198, 377–89.

Kulig, D., Zimoch-Korzycka, A., Jarmoluk, A and Marycz, K. (2016). Study on Alginate Chitosan Complex Formed with Different Polymers Ratio. *Polymers*, 8, 167; doi:103390/polym8050167

Landfester, K. (2009). Miniemulsion polymerization and the structure of polymer and hybrid nanoparticles. *Angew. Chem. Int. Edit. Engl*, 48, 4488–4507.

Landgraf, W., Li, N.H and Benson, J.R. (2005). New polymer enables near zero order release of drugs. *Drug Delivery Technology*, 5, 48-55.

Lee, J and Lee K Y. (2009). Injectable microsphere/hydrogel combination systems for localized protein delivery. *Macromolecules and Bioscience*, 9, 671–676.

Lee, K.Y and Mooney, D.J. (2012). Alginate: properties and biomedical applications. *Progress in Polymer Science*, 37(1), 106 – 126.

LeGeros, R. Z., Chohayeb, A., Shulman, A. (1982). Apatitic calcium phosphates: possible dental restorative. *Journal of Dental Res*earch, 61, 343.

Liew, C.V., Chan, L.W., Ching, A.L and Heng, P.W. (2006). Evaluation of SA as drug release modifier in matrix tablets. *International Journal of Pharm*acy, 309, 25-37.

Liu, T., Chen, S., Li, J and Liu, D. (2006). Study on drug release behaviour of CDHA/chitosan nanocomposites—Effect of CDHA nanoparticles. *Journal of Controlled Release*, 112, 88–95.

Madan, T., Munshi, N., De, T.K., Maitra, A., Sarma, P.U and Aggarwal, S.S. (1997). Biodegradable nanoparticles as a sustained release system for the antigens/allergens of Aspergillus fumigatus: Preparation and characterisation. *International Journal of Pharmacy*, 159, 135.

Madhusudhan, A., Reddy, G.B., Venkatesham, M., Veerabhadram, G., Kumar, D.A., Natarajan, S., Yang, M., Anren Hu, A and Singh, S.S. (2014). Efficient pH Dependent Drug Delivery to Target Cancer Cells by Gold Nanoparticles Capped with Carboxymethyl Chitosan. *International Journal of Molecular Sciences, 15*, 8216-8234; doi:10.3390/ijms15058216

Maeda, H., Bharate, G.Y and Daruwalla, J. (2009). Polymeric drugs for efficient tumour-targeted drug delivery based on EPR-effect. *Europian Journal of Pharmacy and Biopharmaceutics*, *71*, 409–419.

Maeda, H., Nakamura, H., and Fang, J. (2012). The EPR effect for macromolecular drug delivery to solid tumours: Improvement of tumour uptake, lowering of systemic toxicity, and distinct tumour imaging in vivo. *Advanced Drug Delivery Reviews*. *http://dx.doi.org/10.1016/j.addr.2012.10.002*.

Maeda, H and Matsumura, Y. (2011). EPR effect based drug design and clinical outlook for enhanced cancer chemotherapy. *Advanced Drug Delivery Review*, *63*, 129–130.

Magadala, P., van Vlerken, L.E., Shahiwala, A and Amiji, M.M. (2008). Multifunctional Polymeric Nanosystems for Tumour-Targeted Delivery, In Multifunctional Pharmaceutical Nanocarriers, V. Tochilin (Ed.), Springer Science, pp 33 – 66.

Makishima, A. (2004). Possibility of Hybrids Materials. *Ceramic Japan*, 39, 90-91.

Malesu, V.K., Sahoo, D and Nayak, P.L. (2011). Chitosan–SA nanocomposites blended with cloisite 30b as a novel drug delivery system for anticancer drug curcumin. *International Journal of Applied Biology and Pharmaceutical Technology, 2(3), 402 – 411.*

Mallick, J., Sahoo, D., Kar, M.D and Makwana J. (2013). Alginate beads of Ibuprofen for oral sustained drug delivery: An in vitro evaluation. *International Journal Pharmaceutical, Chemical and Biological Sciences*, 3(3), 595 – 602.

Man, Y., Wang, P., Guo, Y., Xiang, L., Yang, Y., Qu, Y., Gong, P and Deng, L. (2012). Angiogenic and osteogenic potential of platelet-rich plasma and adipose-derived stem cell laden alginate microspheres. *Biomaterials*, 33, 8802–8811.

Manocha, B and Margaritis, A. (2010). Controlled Release of DOX from DOX/$\gamma$-Polyglutamic Acid Ionic Complex. *Journal of Nanomaterials*, 2010, 1 – 9. doi:10.1155/2010/780171

Marques, C., Ferreira, J. M., Andhenronescu, E., Ficai, D., Sonmez, M and Ficai, A. (2014). Multifunctional Material for bone cancer treatment. *International Journal of Nanomedicine*, 9, 2713 – 2725.

Martinho, N., Damge, C and Reis, C.P. (2011). Recent advances in drug delivery systems. *Journal of Biomaterials and Nanotechnology*, 2, 510 – 526.

Marwa, M., EL-Tayieb, M.M., El-Shafei, S and Mahmoud, M.S. (2013). The role of alginate as polymeric material in treatment of tannery wastewater. *International Journal of Science and Technology*, 2(2), 218 – 224.

Masayuki, Y. (2005). Drug targeting with nano-sized carrier systems. *Journal of Artificial Organs*, 8, 77–84.

Mateus, A.Y., Barrias, C C., Ribeiro, C., Ferraz, M.P and Monteiro, F. J. (2008). Comparative study of nanoHA microspheres for medical applications. *Journal of Biomed Material Resource A*, 86, 483 – 93.

Matsumure Y, and Maeda H. (1986). A new concept for macromolecular therapeutics in cancer chemotherapy: mechanism of tumouritropic accumulation of proteins and the anti tumour agent smancs. *Cancer Research*, 46, 6487 – 6392.

Mayer, L.D., Harasym, T.O., Tardi, P.G., Harasym, N.L., Shew, C.R., Johnstone, S.A., Ramsay, E.C., Bally, M.B and Janoff, A.S. (2006). Ratiometric dosing of anticancer drug combinations: Controlling drug ratios after systemic administration regulates therapeutic activity in tumor-bearing mice. *Molecular Cancer Therapeutics*, 5(7), 1854–1863.

Meier, M. (2005). Measuring crystallite size using X-ray diffraction, the Williamson-Hall Technique (DRAFT). Department of Chemical Engineering and Materials Science, University of California, Davis.

Menson, T.V and Sajeeth, C.I. (2013). Formulation and Evaluation of Sustained release SA microbeads of Carvedilol. *International Journal of PharmTech Research*, 5(2), 746 – 753.

Moffitt, M and Eisenberg, A. (1995). Size Control of Nanoparticles in Semiconductor-Polymer nanocomposites control via Multiplet Aggregation Numbers in Styrene-Based Random Ionomers. *Chemistry of Materials*, 7(6): 1178.

Moghimi, S.M., Hunter, A.C and Murray, J.C. (2001). Long circulating and target specific nanoparticles: theory to practice. *Pharmacological Reviews*, 53(2), 283 – 318.

Mohanty D.P, Biswal S.K and Nayak L. (2015). Preparation of Starch-Chitosan Nanocomposites for Control Drug Release of Curcumin. *International Journal of Current Engineering and Technology*, 5(1), 336 – 343.

Moore, J. W and Flanner, H. H. (1996). Mathematical comparison of dissolution profiles. *Pharmaceutical Technology*, 20(6), 64–74.

Mora-Huertasa, C.E, Fessi H and Elaissari A. (2010). Polymer-based nanocapsules for drug delivery. *International Journal of Pharmaceutics*, 385, 113 – 142.

Müller P, Herbst-Irmer R, Spek A.L, Schneider T.R and Sawaya M. (2005). *Crystal Structure Refinement*, Oxford University Press.

Muñoz-Espí, R.., Burger, C., Krishnan, C.V and Chu, B. (2008). Polymer-controlled crystallization of molybdenum oxides from peroxomolybdates: Structural diversity and application to catalytic epoxidation. *Chem. Mater. 20*, 7301–7311.

Murakami, K., Aoki, H., Nakamura, S., Nakamura, S., Takikawa, M., Hanzawa, M., Kishimoto, S, Hattori H, Tanaka Y, Kiyosawa T, Sato Yand Ishihara M. (2010). Hydrogel blends of chitin/chitosan, fucoidan and alginate as healing-impaired wound dressings. *Biomaterials*, 31, 83–90.

*Nabipour, Z., Nourbakhsh, M.S and Baniasadi, M. (2016).* Synthesis, characterization and biocompatibility evaluation of HA- gelatin polyLactic acid ternary nanocomposite. *Nanomedicine Journal*, 3(2): 127-134. DOI:10.7508/nmj.2016.02.006

Nakamoto, K. (2002). Infrared and Raman Spectra of Inorganic and Coordination Compounds, in *Handbook of Vibrational Spectroscopy*, Vol. 3, Chalmers, J. M. and Griffiths, P. R. (Eds), Wiley, Chichester, UK, pp. 1872–1892.

National Cancer Institute (NCI). (2015). What is cancer? U.S Department of Health and Human Services. www.cancer.gov

Neves, C., Jorge, R and Barcelos, A. (2009). The network of MTX toxicity. *Acta Reumatol Port*, 34, 11–34.

Nixon, W.C. (1971). The general principle of scanning electron microscopy. *Philosophical Transactions of the Royal Society of London. Series B, Biological Sciences*, 261 (837): 45 – 50.

Noyes, A.A and Whitney, W.R. (1987). The rate of solution of solid substances in their own solutions. *Journal American Chemical Society*, 19, 930–934.

Olson, E. (2011). Particle shape factors and their use in image analysis – part 1: Theory. *Journal of GXP Compliance*, 15 (3), 85 – 96.

Otterlei, M., Ostgaard, K, Skjakbraek G, Smidsrod O, Soonshiong P and Espevik T. (1991). Induction of cytokine production from human monocytes stimulated with alginate. *Journal of Immunotherapy*, 10, 286–291.

Papadimitriou, S., Bikiaris, D., Avgoustakis, K., Karavas, E and Georgarakis, M. (2008). Chitosan nanoparticles loaded with dorzolamide and pramipexole. *Carbohydrate Polymers*, 73, 44–54.

Parida, U.K, Nayak, A.K., Binhani, B.K and Nayak P.L. (2011). Synthesis and Characterization of Chitosan-Polyvinyl Alcohol Blended with Cloisite 30B for Controlled Release of the Anticancer Drug Curcumin. *Journal of Biomaterials and Nanobiotechnology*, 2, 414-425.

Park, J.H., Ye, M and Park, K. (2005). Biodegradable Polymers for Microencapsulation of Drugs. ***Molecules***, 10, 146 – 161.

Patel, H.V, Vaza, S.S., Mishra, A., Raj, M.M and Patel, N.K. (2014). Evaluation of oral sustained delivery of ciprofloxacin hydrochlorid loaded SA microsphere prepared by ionotropic gelation technique. *World Journal of Pharmacy and Pharmaceutical Sciences*, 3(3), 916 – 925.

Patnaik, N.A., Nagarjuma, T and Thulasiramraju, T.V. (2013). Sustained release drug system: A modern formulation approach. *International Journal of Research in Pharmaceutical and Nano Sciences*, 2(5), 586 – 601.

PDF-2; PDF-4 *Powder Diffraction File* 2010, International Centre for Diffraction Data (ICDD) 20, 12 Campus Boulevard, Newton Square, Pennsylvania 19073-3273, USA. http://www.icdd.com

Peer, D., Karp, J.M., Hong, S., Farokhzad, O.C., Margalit, R and Langer, R. (2007). Nanocarriers as an emerging platform for cancer therapy. *Nature Nanotechnology*, 2, 751 – 760.

Peppas, N.A and Korsmeyer, R.W. (1986). Dynamically swelling hydro gels in controlled release applications, in: N.A. Peppas (Ed.), Hydrogels in Medicine and Pharmacy, Vol. 3, CRC Press, Boca Raton, pp. 109–136.

Peppas, N.A. (1985). Analysis of Fickian and non-Fickian drug release from polymers, *Pharmaceutical Acta Helv*. 60, 110–111.

Pongjanyakul, T and Rongthong, T. (2010). Enhanced entrapment efficiency and modulated drug release of alginate beads loaded with drug-clay intercalated complexes as microreservoirs. *Carbohydrate Polymer*, 81, 409-419.

Prabhu, Y.T., Rao, K.V., Kumar, V.S and Kumari, B.S. (2014). X-Ray Analysis by Williamson-Hall and Size-Strain Plot Methods of ZnO Nanoparticles with Fuel Variation. *World Journal of Nano Science and Engineering*, 4: 21-28.

Pramanik, N., Bhargava, P., Alam, S and Pramanik, P. (2006). Processing and properties of nano-and macro-HA/poly (ethyleneco-acrylic acid) nanocomposites. *Polymer Nanocomposites*, 27, 633-641.

Prasath, P.V., Senthil, K and Ravichandran, K. (2011). Preparation and Cytotoxicity Study of Polycaprolactone/Polyethyleneglycol-HA Nanocomposite for Biomedical Application. *International Journal of Innovative Research in Science & Engineering*

Priya, C., Rajkumari, and Ankita, K. (2013). Polymer: Boon to controlled drug delivery system. *International Research Journal of Pharmacy*, 4(4), 28 – 34.

Raj, M.S., Arkin, V.H., Adalarasu H and Jagannath, M. (2013). Nanocomposites Based on Polymer and HA for Drug Delivery Application. *Indian Journal of Science and Technology*, 6(5S), 4653 – 4658.

Rajan, M and Raj, V. (2013). Formation and characterization of chitosan-polylacticacid-polyethylene glycol-gelatin nanoparticles:A novel biosystem for controlled drug delivery. *Carbohydrate Polymers*, 98, 951– 958.

Rajesh, K.S., Khanrah, A and Biswanath, S. (2003). Release of Ketoprofen from alginate microparticles containing film forming polymers. *Journal of Scientific & Industrial Research*, 62, 985 – 989.

Rajkumar, M., Sundaram, N.M and Rajendran, V. (2010). In-situ preparation of HA nanorod embedded poly (vinyl alcohol) nanocomposite and its characterization. *International Journal of Engineering Science and Technology*, 2(6), 2437 – 2444.

Rajora, A.K., Ravishankar, D., Osborn, H.M.I and Greco, F. (2014). Impact of the Enhanced Permeability and Retention (EPR) Effect and Cathepsins Levels on the Activity of Polymer-Drug Conjugates. *Polymers*, 6, 2186 – 2220.

Rehani, B.R., Joshi, P.B., Lad, K.N and Pratap, A. (2006). Crystallite size estimation of elemental nanocomposite silver nano-powders using XRD principles. *Indian Journal of Pure and Applied Physics*, 44: 157 – 161.

Ritger, P.L and Peppas, N.A. (1987). A simple equation for description of solute release 11. Fickian and anomalous release from swellable devices. *Journal of controlled Release*, 5, 37 – 42.

Roser, M., Fischer, D and Kissel, T. (1998). Surface modified biodegradable albuminandnano- and microphores: effect of surface charge on *in vitro* phagocytosis and biodistribution in rats. *Europian Journal of Pharmaceutics and Biopharmaceutics*, 46(3), 255 – 263.

Roul, J., Mohaptra, R and Sahoo, S.K. (2013).Preparation, characterization and drug delivery behavior of novel biopolymer/HA nanocomposite beads. *Asian Journal of Biomedical and Pharmaceutical Science,* 3(24), 33 – 38.

Ruvinov, E., Leor, J and Cohen, S. (2010).The effects of controlled HGF delivery from an affinity-binding alginate biomaterial on angiogenesis and blood perfusion in a hind limb ischemia model. *Biomaterials*, *31*, 4573–4582.

Sachan,N.K., Pushkar, S., Jha, A and Bhattcharya, A. (2009). SA: the wonder polymer for controlled drug delivery. *Journal of Pharmacy Research*, 2(8), 1191 – 1199.

Sahoo, S., & Nayak, P.L. (2013). Synthesis and Characterization of Gelatin-Chitosan Blended with Cloisite 30B Nanocomposite for Controlled Release of the Ophthalmic Drug Ketorolac. *Journal of pharmaceutical and biomedical sciences*, 30(30), 892-901.

Sahoo, S., Behera, A., Nanda, R.M., Sahoo, R and Nayak, P.L. (2011). Gelatin blended with Cloisite 30B (MMT) for control release of Ofloxacin. *American Journal of Scientific and Industrial Research,* 2(3), 363-368.

Salmaso, S and Caliceti, P. (2013). Stealth properties to improve therapeutic efficacy drug nanocarriers. *Journal of Drug Delivery*, 2013, 1–19. *http://dx.doi.org/10.1155/2013/374252*

Sangeetha, S., Deepika, K., Thrishala, B., Chaitanya, C., Harish, G and Damodharan, N. (2010). Formulation and in vitro evaluation of SA nanospheres containing Ofloxacin. *International Journal of Applied Pharmaceutics*, 2(4), 1 – 3.

Sanosh, K.P., Chu, M., Balakrishnan, A., Kim, T.M and Cho, S. (2009). Preparation and characterization of nano-HA powder using sol–gel technique. *Bulletin of Material Science,* 32(5), 465–470.

Saraei, 1.F., Dounighi, M.N., Zolfagharian, H., Bidhendi, M.S., Khaki, P and Inanlou, F. (2013). Design and evaluation of nanoparticles as protein delivery system. *Archives of Razi Institute*, 68(2), 139 – 146.

Schrade, A., Landfester, K and Ziener, U. (2013). Pickering-type stabilized nanoparticles by heterophase polymerization. *Chemical Society Review, 42*, 6823–6839.

Schweizer, S and Taubert, A. (2007). Polymer-controlled, bio-inspired calcium phosphate mineralization from aqueous solution. *Macromolecules Bioscience,* 7, 1085–1099.

Seema, R and Datta, M. (2013). MMT-PLGA Nanocomposites as an oral and controlled release carrier for 5-Fluorouracil: A novel approach. *International Journal of Pharmacy and Pharmaceutical Sciences*, 5(2), 332 – 341.

Seib, F.P., Jones, G.J., Rnjak-Kovacina, J., Lin, Y and Kaplan, D.L. (2013). pH-Dependent Anticancer Drug Release from Silk Nanoparticles. *Advanced Healthcare Materials*, doi: 10.1002/adhm.201300034

Senthilarasan, K., Ragu, A and Sakthivel, P. (2014). Synthesis and Characterization of Nano HA with Agar-Agar Bio-Polymer. *International Journal of Engineering Research and Applications*, 4(7), 55-59.

Shaikh, K.H., Kshirsagar, R.V and Patil, S.G. (2015). Mathematical models for drug release characterization: A review. *World Journal of Pharmacy and Pharmaceutical Sciences*, 4(4): 324 – 338.

Shargel, L., Wu-Pong, S and Andrew, B. C. (2012). Applied Biopharmaceutics and Pharmacokinetics (Sixth Edition). Mc Graw Hill, USA.

Shende, M.A and Marathe, R.P. (2015). Formulation and development of baclofen gastro retentive mucoadhesive tablets using hibiscus esculentus and xanthan gum. *Indo American Journal of Pharmaceutical Research*, 5(9), 2925 – 2938.

Siegel, R.A and Rathbone, M.J. (2012). Overview of controlled release mechanism, in Fundamentals and Applications of Controlled Release Drug Delivery, Advances in Delivery Science and Technology, J. Siepmann et al. (eds.), *Controlled Release Society*. *DOI 10.1007/978-1-4614-0881-9_2,*

Siepmann, J., Podual, K., Sriwongjanya, M., Peppas, N.A and Bodmeier, R. (1999). A new model describing the swelling and drug release kinetics from hydroxypropyl methylcellulose tablets. *Journal of Pharmaceutical Sciences*, 88, 65 – 72.

Siepmanna, J and Peppas, N.A. (2001). Modelling of drug release from delivery systems based hydroxypropyl methylcellulose (HPMC). *Advanced Drug Delivery Reviews*, 48, 139-157.

Silva, E.A., Kim, E.S., Kong, H.J and Mooney, D.J. (2008). Material-based deployment enhances efficacy of endothelial progenitor cells. Proc Natl Acad Sci USA, 105, 14347–14352.

Singhvi, G and Singh, M. (2011). Review: *in-vitro* drug release characterization models. *International Journal of Pharmaceutical Studies and Research*, 2(1), 77 – 84.

Sivakumar, M and Rao, K.P. (2002). Preparation, characterization and in vitro release of gentamicin from coralline HA–gelatin nanocomposite microspheres. *Biomaterials*, 23, 3175 – 3181.

Skaugrud, O., Hagen, A., Borgersen, B and Dornish, M. (1999). Biomedical and

Pharmaceutical application of alginate and chitosan. *Biotechnology and Genetic Engineering Review*, 16, 23 – 40.

Soppimatha, K.S., Aminabhavia, T.M., Kulkarnia, A.R and Rudzinski, W.E. (2001). Biodegradable polymeric nanoparticles as drug delivery devices. *Journal of Controlled Release*, 70, 1–20.

Stanislavov, A., Sukhodub, L.B., Yanovska, A.A., Kuznetzov, V.N and Sukhodub, L.F. (2014). Alginate-HA beads for medical application. *Proceedings of the International Conference Nanomaterials: Applications and Properties*, 3(2), 02NNSA15 (2pp).

Stuart, B. (2004). Infrared Spectroscopy: Fundamentals and Applications, John Wiley and Sons Ltd.

Sugiura, S., Oda, T., Izumida, Y., Aoyagi, Y., Satake, M., Ochoiai, A., Ohkohchi, N and Nakajima, M. (2005). Size control of calcium alginate beads containing living cells using micro – nozzle array. *Biomaterial*, 3, 34 – 50.

Sukhorukov, G.B., Donath, E., Lichtenfeld, H., Knippel, E., Knippel, M., Budde, A and Möhwald, H. (1998). Layer-by-layer self-assembly of polyelectrolytes on colloidal particles. *Colloid Surface A*, *137*, 253–266.

Sun, J and Tan, H. (2013). Alginate based biomaterials for regenerative medicine applications. *Materials*, 6, 1285 – 1309.

Suryanarayana, C and Norton, M.G. (1998). X-ray diffraction: A practical approach. Plenum Press, New York, pp 207 – 222.

Takka, S., Ocak, O.H and Acarturk, F. (1998). Formulation and investigation of nicardipine HCl-alginate gel beads with factorial design based studies. *European Journal of Pharmaceutical Sciences, 6*(3), 241–246.

Taubert, A., Palms, D., Weiss, O., Piccini, M.T and Batchelder, D.N. (2002). Polymer-assisted control of particle morphology and particle size of zinc oxide precipitated from aqueous solution. *Chem. Mater. 14*, 2594–2601.

Thornton, A.J., Alsberg, E., Albertelli, M and Mooney, D.J. (2004). Shape-defining scaffolds for minimally invasive tissue engineering. *Transplantation*, 77, 1798–1803.

Trif, M., Ansorge-Schumacher, M and Socaciu, C. (2007). Application of FTIR Spectroscopy for determination of oxidation of encapsulated sea buckthorn oil. *XVth International Workshop on Bioencapsulation, Vienna, Au*. Sept 6-8, 2007.

Ueda, M., Iwara, A and Kreuter, J. (1998). Influence of the preparation methods on the drying release behavior of loperamide-loaded nanoparticles. *Journal of Microencapsulation*, 15, 361–372.

United States Pharmacopeia (USP), <776> Optical Microscopy, USP34-NF29, 2011

V´azquez, C.G., Barba, C.P and Mungu´ıa, N. (2005). Stoichiometric HA obtained by precipitation and sol gel processes. *Revista Mexicana De Fi´Sica* ,51 (3) 284–293.

van Vlerken, L.E and Amiji, M.M. (2006). Multi-functional polymeric nanoparticles for tumour-targeted drug delivery. *Expert Opinion for drug delivery*, 3(2), 205 – 216.

Venkatasubbu, G.D., Ramasamy, S., Ramakrishnan, V and Kumar, J. (2011). HA-Alginate nanocomposite as drug delivery matrix for sustained release of ciprofloxacin. *Journal of Biomedical Nanotechnology*, 7, 1 – 9.

Venkatesan, P., Puvvada, N., Dash, R., Kumar, B.N., Devanand, S., Azab, B., Pathak, A., Kundu, S.C., Fisher, P.B and Mandal M. (2011). The potential of celecoxib-loaded HA-chitosan nanocomposite for the treatment of colon cancer. *Biomaterial*, 32, 3794 – 3806. doi:10.1016/j.biomaterials.2011.01.027

Vilar, G., Tulla-Puche, J., and Albericio, F. (2012). Polymers and drug delivery systems. *Current Drug Delivery*, 9(4), 1 – 28.

Viswanathan, S and Nallamuthu, T. (2014). Extraction of SA from Selected Seaweeds and Their Physiochemical and Biochemical Properties. *International Journal of Innovative Research in science, Engineering and Techology*, 3(4), 10998 – 11003.

Wang, L., Shelton, R.M., Cooper, P.R., Lawson, M., Triffitt, J.T and Barralet, J.E. (2003). Evaluation of SA for bone marrow cell tissue engineering. *Biomaterials*, 24, 3475–3481.

Wang, L.S and Hong, R.Y. (2011). Synthesis, Surface Modification and Characterisation of Nanoparticles, Advances in Nanocomposites - Synthesis, Characterization and Industrial Applications, Dr. Boreddy Reddy (Ed.), ISBN: 978-953-307-165-7, InTech, China.

Wang, Z.L. (2004). Scanning Electron Microscope. *Annual Review of Physical Chemistry*, 55, 159 – 196.

Wang, J., Chen, S., Zong, J. Y., Zhao, D., Li, F., Zhuo, R. X and Cheng, S. X. (2010). Calcium carbonate/carboxymethyl chitosan hybrid microspheres and nanospheres for drug delivery. *Journal of Physics and Chemistry C, 114*, 18940–18945.

Wells, L.A and Sheardown, H. (2009). Extended release of high pI proteins from alginate microspheres via a novel encapsulation technique. *Europian Journal of Pharmacy and Biopharmacy.*, 65, 329–335.

Wu, H., Chang, D and Huang, C. (2006). Targeted therapy for cancer. *Journal of Cancer Molecules*, 2(2), 57 – 66.

Yadav, G., Bansal, M., Thakur, N., Sargam and Khare, P. (2013). Multilayer Tablets and Their Drug Release Kinetic Models for Oral Controlled Drug Delivery System. *Middle-East Journal of Scientific Research,* 16(6): 782-795.

Yan, X., Scherphat, G.L and Kamps, J.A. (2005). Liposome opsonisation. *Journal of Liposome Research*, 15(1-2), 109 – 139.

Yao B.L; Ni C.H; Xiong C, Zhu C.P and Hueng B. (2010). Hydrophobic modification of SA and its application in controlled drug release. *Bioprocess Biosystem Engineering*, 33, 457 – 463.

Yousefi G, Foroutan S.M, Zarghi A and Shafaati A. (2010). Synthesis and Characterization of MTX Polyethylene Glycol Esters as a Drug Delivery System. *Chemical and Pharmaceutical Bulletin.* 58(2), 147-53.

Yu, S., Khotimchenko, Yu, S., Kovalev, V.V., Savchenko, O.V and Ziganshina, O. A. (2001). Physical- chemical properties, physiological activity, and usage of alginates, the polysachharides of Brown algae. *Russian Journal of Marine Biology*, 27(1), S53–S64.

Yuan, F. (1995).Vascular permeability in a human xenogreaft – molecular size dependent and cutoff size. *Cancer Research*, 55, 3752 – 3756.

Zhang, Y., Huo, M., Zhou, J., Zou, A., Li, W., Yao, J and Xie, X. (2010). DDSolver: An Add-In Program for Modeling and Comparison of Drug Dissolution Profiles. *American Association of Pharmaceutical Scientists Journal*, 12(3), 263 – 271. DOI: 10.1208/s12248-010-9185-1

Zhao, Q., Han, B., Wang, Z., Gao, C., Peng, C and Shen, J. (2007). Hollow chitosan-alginate multilayer microcapsules as drug delivery vehicle: DOX loading and in vitro and in vivo studies. *Nanomedicine: Nanotechnology, Biology, and Medicine,* 3, 63– 74. doi:10.1016/j.nano.2006.11.007

Zhou, W., Apkarian, R.P., Wang, Z.L and Joy, D. (2005). Fundamentals of scanning electron microscopy.

Zuo, J., Gao, Y., Bou-Chacra, N and Löbenberg, R. (2014). Evaluation of DDsolver software application. *BioMed Research Internationl*, http://dx.doi.org/10.1155/2014/204925

# APPENDIX

## **Appendix I:** Phase analysis report for HA

### Match! Phase Analysis Report

***Sample Data***

| | |
|---|---|
| File name | HA. |
| Data collected | May 16, 2016 13:50:24 |
| Data range | 2.006º - 70.012º |
| Step size | 0.020 |
| Rietveld refinement converged | Yes |
| Alpha2 subtracted | Yes |
| Background subtr. | No |
| Data smoothed | No |
| 2theta correction | 0.00597º |
| Radiation | X-rays |
| Wavelength | 1.540598 Å |

### Matched Phases

| *Index* | *Amount (%)* | *Name* | *Formula sum* |
|---|---|---|---|
| A | 54.5 | Carbonate-hydroxylapatite | Ca5 H1.44 O13.012 P2.928 |
| B | 45.5 | Hydroxylapatite | Ca5 H2 O13 P3 |
| | *14.6* | *Unidentified peak area* | |

***A: Carbonate-hydroxylapatite (54.5%)***

| | |
|---|---|
| Formula sum | Ca5 H1.44 O13.012 P2.928 |
| Entry number | 96-900-3553 |
| Figure-of-Merit (FoM) | 0.729755 |
| Total number of peaks | 134 |
| Peaks in range | 56 |
| Peaks matched | 37 |
| Intensity scale factor | 0.46 |
| Space group | P 63/m |
| Crystal system | hexagonal |
| Unit cell | a= 9.4234 Å c= 6.8801 Å |
| I/Icor | 1.59 |
| Calc. density | 3.141 g/cm³ |

Reference Fleet M. E., Liu X., King P. L., "Accommodation of the carbonate ion in apatite: An FTIR and X-ray structure study of crystals synthesized at
2-4 GPa Sample: xt372", American Mineralogist **89**, 1422-1432 (2004)

***B: Hydroxylapatite (45.5 %)***

| | |
|---|---|
| Formula sum | Ca5 H2 O13 P3 |
| Entry number | 96-900-2215 |
| Figure-of-Merit (FoM) | 0.742129 |
| Total number of peaks | 134 |
| Peaks in range | 57 |
| Peaks matched | 38 |
| Intensity scale factor | 0.39 |
| Space group | P 63/m |
| Crystal system | hexagonal |
| Unit cell | a= 9.4394 Å c= 6.8861 Å |
| I/Icor | 1.63 |
| Calc. density | 3.145 g/cm³ |

**Appendix I1**: Crystallite size, Degree of crystallinity and microstrain values derived from peak positions (2θ) and full width at half maximum values

| Sample | 2θ | FWHM (deg.) | Crystallite size (nm) | Degree of Crystallinity (%) | Microstrain | Particle size (nm) |
|---|---|---|---|---|---|---|
| HA | 31.78 | 0.2667 | 32.36 | 72.87 | 0.0041 | 127.38 |
| HASA-1%wt | 31.76 | 0.3040 | 28.39 | 49.21 | 0.0047 | 359.46 |
| HASA-5%wt | 31.82 | 0.4454 | 19.38 | 15.65 | 0.0068 | 250.70 |
| HASA-20%wt | 31.90 | 0.7161 | 12.06 | 3.76 | 0.0109 | 172.96 |
| HASA-33%wt | 31.94 | 0.8347 | 10.34 | 2.38 | 0.0127 | 161.01 |
| HASA-50%wt | 31.90 | 0.9119 | 9.47 | 1.82 | 0.0139 | 109.98 |
| 2HASA-5%wt | 31.68 | 0.4019 | 21.47 | 21.30 | 0.0062 | 261.61 |
| 2HASA-20%wt | 31.78 | 0.4956 | 17.41 | 11.36 | 0.0076 | 216.9 |
| 2HASA-33%wt | 31.86 | 0.7700 | 11.21 | 3.03 | 0.0118 | 184.63 |
| 2HASA-50%wt | 31.94 | 0.8882 | 9.72 | 1.97 | 0.0135 | 142.48 |

**Appendix 111:** Elemental composition of HA from XRF result

| Element | % |
|---|---|
| P | 24.805 |
| Ca | 42.665 |
| O | 32.112 |
| Ti | 0.007 |
| Fe | 0.008 |
| Sm | 0.006 |

**Appendix IV:** MTX release data from HA and HA-sodium alginate nanocomposite

| | Time (hr) | 1 | 2 | 5 | 11 | 23 |
|---|---|---|---|---|---|---|
| **HA** | Conc. (mg/ml) | 0.2473±0.0067 | 0.2335±0.0037 | 0.1450±0.0088 | 0.1444±0.0032 | 0.0813±0.0053 |
| | Qty (mg) | 4.95±0.13 | 5.91±0.11 | 5.30±0.23 | 5.02±0.16 | 4.48±0.14 |
| | %Cum.release | 70.20±1.89 | 83.82±1.52 | 75.26±3.23 | 73.38±2.25 | 72.87±3.9 |
| **HASA-1%wt** | Conc.(mg/ml) | 0.2360±0.0037 | 0.1926±0.0025 | 0.1364±0.0022 | 0.1045±0.0037 | 0.0770±0.0058 |
| | Qty(mg) | 4.72±0.07 | 5.03±0.03 | 4.87±0.04 | 4.72±0.08 | 3.89±0.14 |
| | %Cum.release | 78.03±1.22 | 83.17±0.53 | 81.69±0.65 | 80.25±1.34 | 79.11±2.32 |
| **HASA-5%wt** | Conc.(mg/ml) | 0.1524±0.0022 | 0.1378±0.0032 | 0.1192±0.0032 | 0.0677±0.0010 | 0.0442±0.0011 |
| | Qty (mg) | 3.05±0.04 | 3.52±0.07 | 3.83±0.04 | 3.40±0.02 | 3.27±0.02 |
| | %Cum.release | 65.39±0.93 | 75.48±1.59 | 82.27±0.81 | 72.97±0.52 | 70.17±0.49 |
| **HASA20%wt** | Conc.(mg/ml) | 0.1013±0.006 | 0.0877±0.0017 | 0.0579±0.0018 | 0.0430±0.0019 | 0.0310±0.0010 |
| | Qty (mg) | 2.03±0.01 | 2.26±0.03 | 2.10±0.04 | 2.09±0.05 | 2.07±0.04 |
| | %Cum.release | 59.22±0.34 | 66.12±0.97 | 61.47±1.31 | 61.26±1.38 | 60.49±1.16 |
| **HASA-33%wt** | Conc.(mg/ml) | 0.1160±0.0028 | 0.0853±0.0028 | 0.0423±0.0008 | 0.0322±0.0046 | 0.0221±0.0022 |
| | Qty(mg) | 2.32±0.06 | 2.29±0.04 | 1.85±0.02 | 1.80±0.10 | 1.82±0.07 |
| | %Cum.release | 68.22±1.67 | 67.23±1.27 | 54.45±0.49 | 54.13±2.83 | 53.55±2.05 |
| **HASA-50%wt** | Conc.(mg/ml) | 0.1567±0.0020 | 0.1174±0.0019 | 0.0714±0.0014 | 0.0554±0.0012 | 0.0384±0.0018 |
| | Qty(mg) | 3.13±0.04 | 3.13±0.05 | 2.80±0.04 | 2.76±0.05 | 2.77±0.07 |
| | %Cum.release | 92.16±1.19 | 91.99±1.41 | 83.41±1.32 | 83.02±1.44 | 81.53±1.98 |

**Appendix V**: Release data of DOX loaded in HA

| Time (hr) | Conc. (mg/ml) | Qty (mg) | % Cumulative release |
|---|---|---|---|
| 1 | 0.0566 ±0.0056 | 3.08 ±0.28 | 64.46 ±6.42 |
| 2 | 0.0618 ±0.0042 | 3.44 ±0.23 | 74.21 ±5.19 |
| 3 | 0.0612 ±0.0048 | 3.63 ±0.27 | 77.82 ±6.12 |
| 5 | 0.0691 ±0.0051 | 4.28 ±0.30 | 87.21 ±6.79 |
| 9 | 0.0600 ±0.0048 | 3.98 ±0.30 | 85.41 ±6.80 |
| 17 | 0.0543 ±0.0029 | 3.83 ±0.22 | 83.05 ±4.92 |

**Appendix VII:** Kinetic and mechanistic models of DOX release from DOX-HA-SA nanocomposites prepared by different loading methods

| MODEL | PARAMETER | METHOD 1 | METHOD 2 | METHOD 3 | METHOD 4 |
|---|---|---|---|---|---|
| Zero Order | $R^2$ | 0.8179 | 0.9336 | 0.9028 | 0.9328 |
| | $R^2$-adj. | 0.7875 | 0.9225 | 0.8866 | 0.9216 |
| | MSC | 1.2031 | 2.2113 | 1.831 | 2.1995 |
| | $K_0$ | 1.124 | 1.308 | 1.027 | 1.195 |
| First Order | $R^2$ | 0.9475 | 0.9742 | 0.9853 | 0.9868 |
| | $R^2$-adj. | 0.9387 | 0.9699 | 0.9828 | 0.9846 |
| | MSC | 2.4469 | 3.1576 | 3.7169 | 3.8302 |
| | $K_1$ | 0.0650 | 0.037 | 0.034 | 0.029 |
| Korsmeyer-Peppas | $R^2$ | 0.8954 | 0.9830 | 0.9875 | 0.9761 |
| | $R^2$-adj. | 0.8605 | 0.9774 | 0.9833 | 0.9681 |
| | MSC | 1.4575 | 3.2772 | 3.5825 | 2.9331 |
| | N | 0.367 | 0.345 | 0.267 | 0.3120 |
| Higuchi | $R^2$ | 0.9307 | 0.9745 | 0.9821 | 0.9776 |
| | $R^2$-adj. | 0.9192 | 0.9703 | 0.9791 | 0.9739 |
| | MSC | 2.1694 | 3.1701 | 3.5217 | 3.3004 |
| | $K_H$ | 10.266 | 11.444 | 9.172 | 10.477 |
| Hixon-Crowel | $R^2$ | 0.9384 | 0.9783 | 0.9715 | 0.9809 |
| | $R^2$-adj. | 0.9281 | 0.9747 | 0.9667 | 0.9778 |
| | MSC | 2.2865 | 3.3311 | 3.0572 | 3.4598 |
| | $K_{HC}$ | 0.0140 | 0.009 | 0.008 | 0.008 |
| Hopfenberg | $R^2$ | 0.9475 | 0.9783 | 0.9852 | 0.9868 |
| | $R^2$-adj. | 0.9264 | 0.9697 | 0.9793 | 0.9815 |
| | MSC | 2.1962 | 3.0821 | 3.4635 | 3.5788 |
| | N | 568.17 | 3.195 | 524.384 | 226.062 |

**Appendix VIII:** Kinetic models of DOX release from HA

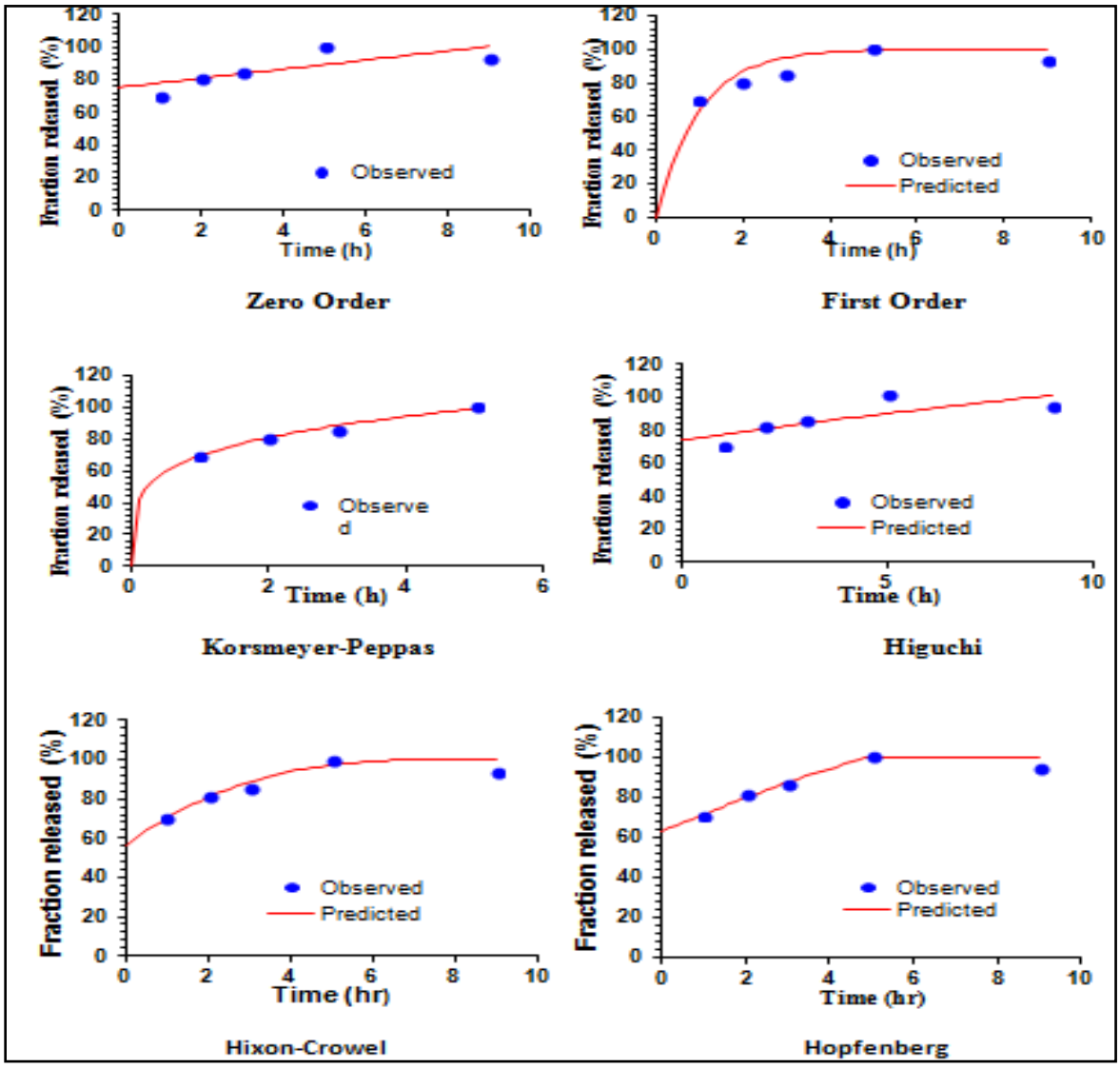

**Appendix IX**: Kinetic models of DOX release from HASA-50%wt